MODELLING SNOWMELT INFILTRATION PROCESSES IN SEASONALLY FROZEN GROUND

A Thesis Submitted to the College of

Graduate and Postdoctoral Studies

In Partial Fulfillment of the Requirements

For the Degree of Master of Environment and Sustainability

In the School of Environment and Sustainability

University of Saskatchewan

Saskatoon

By

SUJATA BUDHATHOKI

PERMISSION TO USE

In presenting this thesis in partial fulfillment of the requirements for a Postgraduate degree from the University of Saskatchewan, I agree that the Libraries of this University may make it freely available for inspection. I further agree that permission for copying of this thesis in any manner, in whole or in part, for scholarly purposes may be granted by the professor or professors who supervised my thesis work or, in their absence, by the Head of the Department or the Dean of the College in which my thesis work was done. It is understood that any copying or publication or use of this thesis or parts thereof for financial gain shall not be allowed without my written permission. It is also understood that due recognition shall be given to me and to the University of Saskatchewan in any scholarly use which may be made of any material in my thesis.

DISCLAIMER

Reference in this thesis to any specific commercial products, process, or service by trade name, trademark, manufacturer, or otherwise, does not constitute or imply its endorsement, recommendation, or favoring by the University of Saskatchewan. The views and opinions of the author expressed herein do not state or reflect those of the University of Saskatchewan, and shall not be used for advertising or product endorsement purposes.

Requests for permission to copy or to make other uses of materials in this thesis in whole or part should be addressed to:

Head of the School of Environment and Sustainability
117 Science Place
University of Saskatchewan
Saskatoon, Saskatchewan S7N 5C8
Canada

OR

Dean
College of Graduate and Postdoctoral Studies
University of Saskatchewan
116 Thorvaldson Building, 110 Science Place
Saskatoon, Saskatchewan S7N 5C9
Canada

ABSTRACT

In cold regions, freezing and thawing of the soil governs soil hydraulic properties that shape the surface and subsurface hydrological processes. The partitioning of snowmelt into infiltration and runoff has important implications for integrated water resource management and flood risk. However, there is an inadequate representation of the snowmelt infiltration into frozen soils in most land-surface and hydrological models, creating the need for improved models and methods. In this research, we test the Frozen Soil Infiltration Model, FroSIn, which is a novel algorithm for infiltration into the frozen soils. The model is applied in a simple configuration to reproduce observations from field sites in the Canadian prairies, specifically St Denis and Brightwater Creek in Saskatchewan, Canada. We demonstrate the limitations of conventional approaches to simulate infiltration in frozen soils, which systematically over-predict runoff and under predict infiltration. The findings show that FroSIn enables models to predict more reasonable infiltration volumes in frozen soils, and also better represent how infiltration-runoff partitioning is impacted by antecedent soil water content.

ACKNOWLEDGEMENTS

To begin with, I would like to extend my sincere gratitude to my supervisor Dr. Andrew Ireson for his unwavering support and guidance throughout my Master's degree. Dr. Ireson's enthusiastic encouragement, suggestions, critical and constructive advice along with valuable feedback has positively affected my academic career and further aided in completion of this research. Special thanks to my committee members, Prof. Lee Barbour, Dr. Chris Kelln, Dr. Helen Baulch and my external examiner Prof. Charles Maule for critically evaluating my research work. I would also like to acknowledge Dr. Karl-Erich Lindenschmidt for being the chair in absence of Dr. Helen Baulch during my defence. This research work would not have been completed successfully without their active guidance and contribution.

I would also like to mention and thank the funding organizations, Natural Sciences and Engineering Research Council (NSERC), Changing Cold Region Network (CCRN), CREATE for Water Security and the Canada Excellence Research Chair in Water Security, School of Environment and Sustainability for providing the financial support to complete this degree programme.

I am particularly grateful to Dr. Garth van der Kamp for providing his valuable insights along with the necessary dataset for this research. I am also thankful to Branko Zdravkovic, Rosa Brannen and Amber Peterson for providing essential information and data from the field sites. It is indeed a great pleasure to be a part of 'School of Environment and Sustainability' and 'Global Institute for Water Security' and would like to thank all the staffs and my friends, especially Prabin, Apurba, Razi, Sahar, Lucia and many others who have always supported and helped me during difficult times and created a friendly and enabling environment to further learn and share.

Finally, I would like to thank my family for their constant support, encouragement and best wishes. In addition, I am forever indebted to my husband-cum-mentor, Prabin Rokaya for his continuous love, support and guidance. I am truly blessed to have him in my life.

TABLE OF CONTENTS

PERMISSION TO USE ..... **i**
ABSTRACT ..... **ii**
ACKNOWLEDGEMENTS ..... **iii**
TABLE OF CONTENTS ..... **iv**
LIST OF FIGURES ..... **vi**
LIST OF TABLES ..... **ix**
CHAPTER 1: INTRODUCTION **1**
1.1 Background 1
1.2 Research Objectives 3
1.3 Thesis structure 4
CHAPTER 2: LITERATURE REVIEW **5**
2.1 Cold Region Hydrology 5
2.2 Snowmelt Processes 6
2.2.1 Estimating the rate of snowmelt 6
2.2.2 Behavior and Importance of Snowmelt in Seasonally Frozen Ground 9
2.3 Fundamental Soil Physics 10
2.3.1 The Unsaturated zone: Infiltration and Water Flow 10
2.3.2 Infiltration into a Frozen Soil 13
2.4 Modelling cold region hydrology 17
2.4.1 Hydrological Modelling 17
2.4.2 Snowmelt and Snowmelt Infiltration Models 19
2.5 Research Gaps and Challenges 22
CHAPTER 3: DATA AND METHODS **24**
3.1 Study Sites 24
3.1.1 St. Denis National Wildlife Area (St Denis) 24
3.1.2 Brightwater Creek (BWC) 25
3.2 Research Flow Design 26
3.3 Data Collection 27
3.3.1 Instrumentation 27
3.3.2 Data Retrieval 31
3.4 Snowmelt period, rate and snowmelt partitioning 31
3.5 Log-normal Pore Size Distribution model (LNPSD) 33

3.6 The Modelling Tools 34
3.6.1 Model setup 34
3.6.2 Driving data 35
3.6.3 Initial and boundary condition 35
3.6.4 Saturated hydraulic conductivity 35
CHAPTER 4: RESULTS AND DISCUSSION 36
4.1 Quantifying snowmelt infiltration and runoff based on field based observations 36
4.1.1 Quantifying snowmelt infiltration and runoff at St Denis 36
4.1.2 Field based data observations at Brightwater Creek (BWC) 51
4.2 Establishing Soil Water Characteristic (SWC) and Soil Freezing Characteristic (SFC) Curves 57
4.2.1 Validation of Log-normal Pore Size Distribution model (LNPSD) with van Genuchten model (VGM) for Soil Water Characteristics (SWC) curve 57
4.2.2 Simultaneous fitting of the Soil Water Characteristic (SWC) and Soil Freezing Characteristic (SFC) curves at St Denis 59
4.2.3 Validating the SWC and SFC curves at St Denis 63
4.2.4 Validating the SWC and SFC curve at Brightwater Creek (BWC) 65
4.3 Testing and comparing models for snowmelt infiltration at St Denis 67
4.3.1 Model Setup 67
4.3.2 Driving Data 68
4.3.3 Initial and boundary condition 69
4.3.4 Sensitivity Analysis for saturated hydraulic conductivity 69
4.3.5 Modelling results using Standard Frozen Soil Infiltration Model (SFSIM) 71
4.3.6 Modelling results using Frozen Soil Infiltration Model (FroSIn) 73
4.3.7 Validating and comparing results from observation, SFSIM and FroSIn during snowmelt period 75
4.3.8 Additional FroSIn model insight from Brightwater creek (BWC) 76
CHAPTER 5: CONCLUSIONS 80
REFERENCES 82
LIST OF APPENDICES 94
Appendix A: Model for flow processes in unfrozen soil 94
Appendix B: Standard Frozen Soil Infiltration Model (SFSIM) 101
Appendix C: Frozen Soil Infiltration Model (FroSIn) 104
Appendix D: Tables 106
Appendix E: Figures 108

LIST OF FIGURES

Figure 2-1 Components of energy budget for a snowpack (after Ho, 2002) 7
Figure 2-2 (a) Soil Water Characteristic Curve (SWC) and (b) Hydraulic conductivity curve for different soil textured soil (modified after Van Genuchten, 1980)..... 12
Figure 2-3 Soil Freezing Characteristic (SFC) curve for silt loam soil in the field of Minnesota during winter (Spaans and Baker, 1996)..... 14
Figure 2-4 Conceptual model for classifying the infiltration potential of frozen soils (a) unlimited (b) limited and (c) restricted (modified after Gray et al., 1985) 16
Figure 2-5 Steps in modelling process (Bear and Cheng, 2010) 18
Figure 2-6 Conceptual model for surface and sub-surface hydrological processes (Ireson et al., 2012) 19
Figure 2-7 Conceptual model of freezing soil in FroSIn (Ireson et al. 2017, in prep) 21
Figure 3-1 (a) Map of St. Denis field site location (b) Map of piezometers (red dots) and few major pond locations at St Denis 24
Figure 3-2 (a) BWC sub-basin in Saskatchewan River basin (effective drainage is shown by hatching) and Flux tower location (triangle) and (b) neutron monitoring location (dark blue dots) and HydraProbe and piezometers boreholes locations (red dots) (Pan et al., 2017). 25
Figure 3-3 Research flow diagram..... 26
Figure 3-4 Experimental setup for soil profile data in Uri transect at St Denis..... 29
Figure 4-1 Long term Pond 50 water level (1968-2016) 36
Figure 4-2 Annual Snow Water Equivalent (1994-2016)..... 37
Figure 4-3 Soil freezing depth of three profiles along the Uri transect 38
Figure 4-4 Unfrozen water content and water storage in upslope profile of Uri transect 40
Figure 4-5 Unfrozen water content and water storage in mid slope profile of Uri transect 40
Figure 4-6 Unfrozen water content and water storage in down slope profile of Uri transect..... 41
Figure 4-7 Water table level along Uri transect (2014-2016)..... 41
Figure 4-8 Observed and simulated snowmelt rate and period..... 43
Figure 4-9 Cumulative of observed and simulated snowmelt 43
Figure 4-10 Simulated snowmelt at St Denis (2012, 2014, 2015 and 2016) 44
Figure 4-11 Water level in Pond 50 during the snowmelt period..... 45
Figure 4-12 Snowmelt partitioning into runoff and infiltration..... 47

Figure 4-13 Long-term snowmelt partitioning into runoff and infiltration (received through personnel communication with Garth van der Kamp, December 5, 2016) 48
Figure 4-14 Spatio-temporal variation of water content in shallow vadose zone at different locations 50
Figure 4-15 Annual Snow Water Equivalent at BWC (2007-2016) 51
Figure 4-16 Soil freezing depth of three profile (P1, P2 and P3) 52
Figure 4-17 Unfrozen water content and water storage in P1 profile 53
Figure 4-18 Unfrozen water content and water storage in P2 profile 54
Figure 4-19 Unfrozen water content and storage in P3 profile 54
Figure 4-20 Change in groundwater level along the transect at BWC 55
Figure 4-21 Spatio-temporal variation of water content in shallow vadose zone at BWC 56
Figure 4-22 Fitting LNPSD with VGM for different soil types 58
Figure 4-23 Fitting LNPSD and VGM model for clay at maximum matric potential 59
Figure 4-24 Fitting LNPSD model with observed SWC curve and validating with observed SFC curve 60
Figure 4-25 Fitting LNPSD model with observed SFC curve and validating with observed SFC curve 61
Figure 4-26 Fitting observed SWC and SFC curve with dual porosity LNPSD model 62
Figure 4-27 Fitting LNPSD model with observed SWC and SFC for upslope profile at St Denis 64
Figure 4-28 Fitting LNPSD model with observed SWC and SFC for midslope profile at St Denis 64
Figure 4-29 Fitting LNPSD model with observed SWC and SFC for downslope profile at St Denis 65
Figure 4-30 Fitting LNPSD model with observed SWC and SFC for P1 profile at BWC 66
Figure 4-31 Fitting LNPSD model with observed SWC and SFC for P2 profile at BWC 66
Figure 4-32 Fitting LNPSD model with observed SWC and SFC for P3 profile at BWC 67
Figure 4-33 Driving data from upslope profile at St Denis for different years (a) 2014 (b) 2015 and (c) 2016 68
Figure 4-34 (a) Sensitivity analysis generating a contour plot for snowmelt runoff ratio (b) Sensitivity analysis inferring to the observed snowmelt runoff ratio 70

Figure 4-35 Simulated results for upslope profile using SFSIM at St Denis 72
Figure 4-36 Simulated results for upslope profile using FroSIn at St Denis 74
Figure 4-37(a) Snowmelt partitioning inferred from observation (b) Snowmelt partitioning based on SFSIM (c) Snowmelt partitioning based on FroSIn 75
Figure 4-38 Driving data for P1 profile at BWC 77
Figure 4-39 Simulated results for P1 profile using FroSIn at BWC 79

LIST OF TABLES

Table 3-1 Data and instrument information from the towers 28
Table 4-1: Surface water balance and partitioning of the snowmelt into runoff and infiltration at St Denis 46
Table 4-2 Fitted parameter values of LNPSD for the retention curves plotted in Figure 4-22 58
Table 4-3 Fitted parameter values of LNPSD at St Denis 62
Table 4-4 Fitted parameter values of LNPSD at BWC 62
Table 4-5 Initial condition data for upslope profile at St Denis 69
Table 4-6 Initial condition data for P1 profile at BWC 77

CHAPTER 1

INTRODUCTION

1.1 Background

The prairie region spans approximately 900,000 km^2 from north-central Iowa in the United States to central Alberta in Canada, and is an important area of agricultural production (Daniel and Staricka, 2000). In Canada, the prairies are located in the provinces of Alberta, Saskatchewan and Manitoba. The Canadian prairies have a cold and semiarid climate with seasonally-frozen ground, and low-angled, undulating topography (Pomeroy et al., 2010). Annual precipitation is approximately 300-400 mm and the majority of the region sees continuous snow cover and frozen soils during the four to five months of winter (Pomeroy et al., 2009). The general topography of the prairies is a hummocky terrain comprising of millions of closed depressions known as 'prairie potholes', 'wetlands' or simply 'ponds'. Closed watersheds around these ponds are known as non-contributing areas, because the water never reaches one of the regional river systems. Surface runoff in the non-contributing areas feeds complexes of ponds, which exchange water by fill and spill processes (Shaw et al., 2012), and feed a terminal pond. Terminal ponds lose water to evaporation and, potentially, to a local ground water flow system (Daniel and Staricka, 2000). Wetlands develop in the depressions around the ponds, and provide ecological services, including biodiversity (Johnson et al., 2010), floodwater storage (Ehsanzadeh et al., 2012) and reduction of sedimentation and nutrient loading (Nachshon et al., 2013). Agriculture is a key land use of the region, and hence the economic prosperity of the region is heavily dependent on water (Pomeroy et al., 2009).

The hydrology of the prairies is vulnerable to changing precipitation states, snowpack persistence, snowmelt rates, and frozen ground states (Fang and Pomeroy, 2007). Recent analyses reported statistically significant 1.5 °C rise in annual air temperature across Canada between 1950-2010 (Vincent et al., 2012). And by 2050, a 2.7 °C rise in annual temperature is expected in north-west

Canada based on the latest projections from the International Panel on Climate Change (Leong and Donner, 2015). As northern regions are more prone to climate warming (Schindler and Smol, 2006), projected future warming can result in significant impacts on hydrological regimes, runoff generation, soil water availability, agricultural productivity, and downstream water resources in the prairies (Barrow, 2009). In recent years, the region has experienced devastating hydrological extreme events. Floods and droughts have occurred in a very short period of time and in close geographical proximity or at the same locations (Pomeroy and Dumanski, 2017). For instance, 2011 and 2014 prairie floods in Canada costed nearly $1 billion economic damage (Pomeroy and Dumanski, 2017) whereas a prolonged drought from 1999 to 2005 on the Canadian prairie resulted in losses of $5.8 billion (Wheaton, 2011).

Given the rapid environmental change the Canadian prairies are experiencing, it is crucial that we advance scientific knowledge on the changing climate and how it will impact our water futures, including an increased ability to predict drought and flood events (Pomeroy and Dumanski, 2017). Only with a better understanding of detailed hydrological processes, it is possible to assess the potential future climate implications (Prudhomme and Davies, 2009) for efficient planning (Miller and Yates, 2006), management (Mango et al., 2011) and adaptation (Salinger, 2005). Understanding snowmelt processes is critical for Canadian prairie hydrology (Gray and Landine, 1988; Hayashi et al., 2016, 2003). The prairies in Canada are subject to seasonally frozen ground, i.e. freezing of the near-surface ground for more than 15 days per year (Zhang et al., 2003). Seasonally frozen grounds experience a seasonal freeze-thaw cycle which influences the physical, chemical and biological processes in the sub-surface (Hayashi, 2013). The thermal and hydraulic interactions between the atmosphere, vegetation, snowpack, and the frozen and unfrozen pore water content in the soil makes these processes complex and difficult to predict (Stähli et al., 1996). Moreover, presence of unfrozen larger pores or 'macropores', formed due to decayed roots, animal burrows and fractures, provides high hydraulic conductivity thus influencing the melt infiltration in the frozen soil (Gray et al., 2001; Hayashi et al., 2003; van der Kamp and Hayashi, 2009). Proper analysis of these snowmelt processes along with study of freeze-thaw phenomenon is of a great importance for various land surface interactions and simulations (Viterbo, 1999).

1.2 Research Objectives

The purpose of the research is to improve our understanding of, and capacity to simulate, snowmelt infiltration and runoff processes in seasonally frozen ground in the prairies. The primary focus of this research is to investigate the partitioning of snowmelt into infiltration and runoff processes. This investigation is important to understand the surface and sub-surface hydrology of the system which generates runoff and maintains soil water storage. The soil thermal properties, while important, are also not addressed in this research as it has been extensively studied elsewhere in the literature.

The specific objectives of the research are as follows:

Objective 1: Quantify snowmelt infiltration and runoff based on field based observation

Observations from the field sites will be analysed to infer how the melting snowpack partitions between runoff and infiltration. Different land covers and soil properties will be assessed from the two field sites (St Denis and Brightwater Creek) in the prairies. This analysis will include analysis of the pattern of soil zero-degree isotherm and assessment of the soil water content and water table response to snowmelt.

Objective 2: Establish Soil Water Characteristic (SWC) and Soil Freezing Characteristic (SFC) Curves

Log-normal Pore Size Distribution (LNPSD) model will be applied to determine the soil hydraulic properties which is related to the pore-size distribution of the soil. The model fit will be assessed by fitting model to the field observed Soil Water Characteristic (SWC) and Soil Freezing Characteristics (SFC) curves. For the SFC curve, a relationship with soil temperature and unfrozen water content will be determined during the winter. During this stage, all soil properties except the saturated hydraulic conductivity, and soil thermal properties, will be obtained.

Objective 3: Test and compare models for snowmelt infiltration

The driving data (soil temperature, precipitation and rain) from Objective 1, along with the model parameters from Objective 2, will be used to simulate infiltration into the frozen soil. The Standard Frozen Soil Infiltration Model (SFSIM) and the Frozen Soil Infiltration (FroSIn) model will be

used for the simulation. The simulation results in terms of runoff, infiltration, storage and drainage will be compared for each model, and where possible, these results will be compared and validated with the observed field measurements.

1.3 Thesis structure

Chapter 2 presents a literature review on snowmelt processes, soil physics and previous work on modelling snowmelt infiltration and runoff processes in frozen ground. The study site, data collection and modelling tools are described in Chapter 3. Chapter 4 presents the results and discussion, and is structured around the three objectives: the first two objectives are based on data analysis, and the third objective involves applying the model. Finally, Chapter 5 summarizes the findings of this thesis.

CHAPTER 2

LITERATURE REVIEW

2.1 Cold Region Hydrology

In the Northern Hemisphere, cold regions are found at high latitude and high altitudes, and are regions where snow plays a dominant role in the water cycle (Rott et al., 2010). In these regions snow usually forms a large portion of the annual precipitation, and is unequally distributed throughout the catchment area (Woo and Marsh, 2005). Cold region hydrology is complex due to the presence of large number of processes and interactions involved, such as snow redistribution, snow ablation, soil freeze-thaw, infiltration and runoff generation over frozen soils (Pomeroy et al., 2007; Fang and Pomeroy, 2010). Zhou et al. (2013) described these complex snow processes as a distinct cold region hydrological behavior, which is exclusive in other temperate hydrological processes.

Snow is a form of precipitation which falls as a porous and crystalline structure when the "air temperature is approximately 0 ℃ or negative" (Pomeroy and Brun, 2001). Pomeroy and Gray (1995) determined that freshly fallen snow has a relatively low density and high albedo, and with the variation in time and densification, the density of the snow increases rapidly. This density, depth, and water equivalent is the most important physical properties of the snow. The Snow Water Equivalent, SWE (mm), is the equivalent depth of water in a snow cover and is calculated using the snow depth (d_s) (mm), average snow density (ρ_s) (kg m^{-3}) and density of water (1000 kg m^{-3}) with the expression,

$$SWE = \frac{\rho_s d_s}{\rho_w} \tag{2.1}$$

Various forms of redistribution occur in the deposited snow due to temperature, wind, water vapor gradient and the settlement of crystals, all of which further influence the characteristics of the snow

cover (Pomeroy and Gray, 1995). Additionally, the topography of the ground also influences the properties of the snow (King et al., 2008). For example, Fang and Pomeroy (2009) found that low aerodynamic surface roughness on snow-covered bare ground resulted larger wind speeds and greater snow distribution compared to the vegetated ground.

2.2 Snowmelt Processes

Much of the present understanding of snowmelt processes and forecasting of snowmelt originated with an in-depth research program piloted by the U.S. Army Corps of Engineers (1956) at Central Sierra Snow Laboratory, California. This research is summarized in a report called "Snow Hydrology" (Dingman, 2015).

2.2.1 Estimating the rate of snowmelt

Estimating the rate of snowmelt is important because of its significance for the surface and sub-surface hydrology. There are two main methods to estimate the snowmelt rate, the Temperature Index Method (TIM) and the energy balance method.

The TIM is a simple method, which only requires the air temperature and is given as,

$$M = M_f(T_a - T_b) \tag{2.2}$$

Here, M is melt rate (mm d^{-1}), M_f is a melt factor (mm $℃^{-1}$), T_a is daily mean and T_b is a base air temperature. T_b is often 0 ℃ but can also be greater or lesser than 0 ℃ depending on the snowpack. The melt factor, M_f, is defined using empirical equations which incorporates all the weather variability, solar radiation and temperature effect of the snowpack. T_a should always be greater than T_b for the positive melt rate.

Snowmelt rate is also calculated by determining the net energy balance method which is a physically based approach (Anderson, 1973). Figure 2-1 shows the significant energy fluxes.

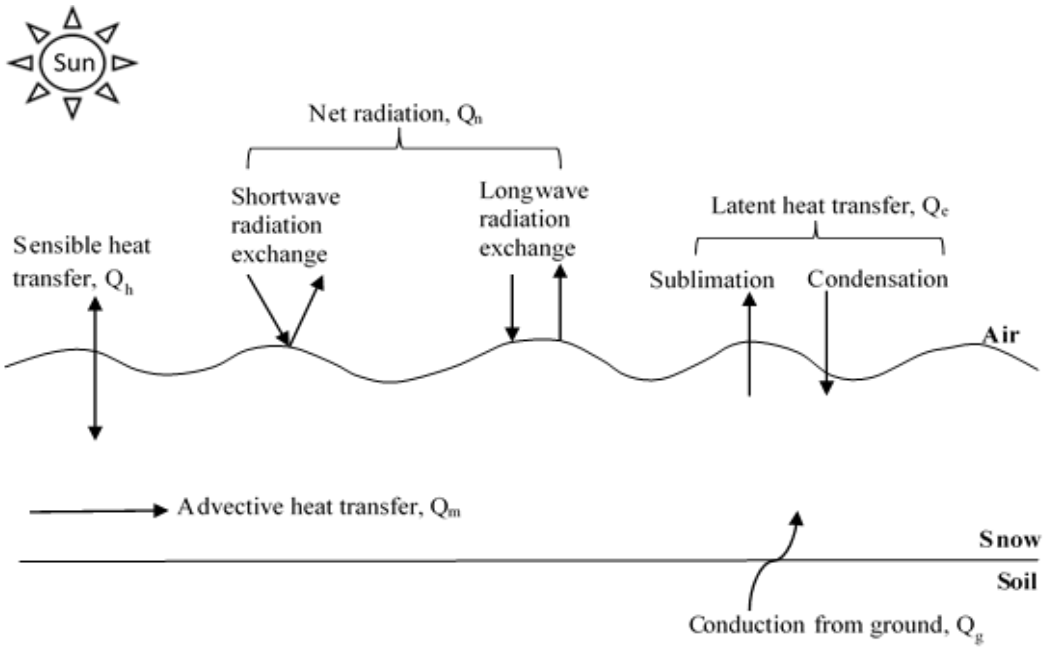

Figure 2-1 Components of energy budget for a snowpack (after Ho, 2002)

The foremost thing to consider in snowmelt is the snowpack energy balance, which is given by:

$$Q_{melt} + \frac{\Delta U}{\Delta t} = \Delta Q \qquad (2.3)$$

where, Q_{melt} (W m^{-2}) is the rate at which energy becomes available for snowmelt, ΔQ (W m^{-2}) is the change in energy flux from both atmosphere and ground and $\frac{\Delta U}{\Delta t}$ is the change in internal energy at time period Δt.

The components of the energy flux are shown below:

$$\Delta Q = Qn + Qe + Qh + Qm + Qg \qquad (2.4)$$

where, all terms are in units of W m^{-2}. Qn is the net radiation transfer flux, Qe and Qh are the latent heat transfer and sensible heat flux from the atmosphere, respectively, which are due to turbulent diffusion. Qm is the advective transfer of heat into the snowpack by melt water and Qg is the net flux of sensible heat, due to conduction with the ground. The snowmelt energy can be calculated, if all of the fluxes listed here, along with the change in internal (stored) energy are measured or

estimated. Helgason and Pomeroy, (2012) pointed out that the measurement of the internal energy is difficult due to the occurrence of phase changes within the melting snow cover. For this reason, in most of the snowmelt equations, the snow cover is assumed to be at isothermal (0 ^{o}C) condition, such that the internal energy is considered zero.

The amount of melt is calculated by coupling the energy balance method with the mass balance of snow cover by using the latent heat of fusion (Gray et al., 1986). The equation is given by;

$$M = \frac{Q_{melt}}{\rho_{w*B*\lambda_f}} \tag{2.5}$$

where, M is the melt (mm day^{-1}), Q_{melt} is the melt energy flux (W m^{-2}), ρ_w is the density of water (~ 1000 kg m^{-3}), B is the thermal quality of snow or the fraction of ice in unit mass of wet snow ≈ 0.95 – 0.97, and λ_f is the latent heat of fusion of ice (344 kJ kg^{-1}).

The snowmelt period of a seasonal snowpack begins to form when the net input of energy fluxes becomes continually positive. This period is usually split up into three distinct phases as described in Dingman, (2015).

Warming phase: The phase during which the absorbed energy raises the average snowpack temperature to isothermal (no vertical temperature gradient within the snowpack) at 0 ℃.

Ripening phase: The phase of the snowpack when the absorbed energy is used to melt the snow, but the meltwater is retained in the pore spaces by surface tension forces. At the end of this phase the snowpack is unable to retain any more liquid water and is said to be “ripe”.

Output phase: The phase where further absorption of energy produces water output, which then appears as runoff, infiltration or evaporation.

The actual melt process may be more complex than this. For example, melting typically occurs at the surface of the snowpack prior to the ripening phase, so that, meltwater may percolate into deeper layers where the snow temperature is below 0 ^{o}C and again refreeze forming an ice layer. This process releases the latent heat, which raises the internal energy of the snowpack, resulting in a continual freeze – thaw cycle (Iwata et al., 2008).

2.2.2 Behavior and Importance of Snowmelt in Seasonally Frozen Ground

Over a large part of the Northern Hemisphere seasonal freezing of the ground results in a transient sub-surface layer with reduced permeability and higher snowmelt runoff (Carey & Pomeroy, 2009). The release of water in these regions, during the snowmelt process is of greater importance to agriculture, hydroelectric power generation, flood control and urban water supply (Male and Granger, 1981).

Snowmelt rate is affected by the continuous freezing and thawing effect. Freezing of the ground occurs when the surface temperature drops below 0 ℃, which sets up temperature gradients from the warmer soil to the colder atmosphere, and results in heat loses from the soil by conduction and radiation (Hayashi, 2013). During early melt season, advection becomes negligible; thus, the net radiation becomes the dominant flux influencing the snowmelt.

Snowmelt in the hill slope dominated terrain shows a distinct melting phenomenon. Pomeroy et al., (2003) determined that, during warm and sunny conditions, snowmelt rates are higher on the south facing slope compared to that of the north facing slope, thus affecting the overall melt rate. The influence of the slope and aspect for these hill slopes as well affects the snow accumulation and melt runoff in the contributing area (Carey and Woo, 1998).

In addition to the hill slope dominated region, another factor influencing snowmelt rate is vegetation. Under the forest canopy, the snow accumulation rate is relatively different from that in the clearings or bare ground (Gelfan et al., 2004; Rutter et al., 2009). In forests in Canada, as much as 60% of cumulative snowfall may be intercepted. The leaf area, tree species and snow load of the initial canopy governs the interception capacities of these forests (Hedstrom and Pomeroy, 1998). Ellis et al. (2010) determined that evergreen needle leaf forest cover strongly influence the energy balance thus affecting the snowmelt rate. Marsh and Pomeroy (1996) further explained that in the forest environment, net radiation is primarily governed by long wave radiation from canopy emission and that energy from the ground surface is typically negligible. Unlike forested areas, the snowmelt rate in the prairies, are highly influenced by snow accumulation in different land cover types (Brannen et al., 2015). Brannen et al. (2015) also found that snowmelt depletion rate is higher in fallow land compared to that in the trees or riparian zones.

The snowmelt infiltration and runoff in the prairies are highly influenced by the antecedent moisture conditions (Ireson et al., 2012). Hayashi et al. (2003) demonstrated that the frozen soil, which retains the antecedent soil water content, acts as water storage and plays an important role in generating higher snowmelt runoff, when the soil is fully saturated. The infiltration process in the frozen soil is also affected by anthropogenic stressors such as land-use change and tillage (Nachshon et al. 2013). For instance, rapid urbanization can significantly reduce the amount of infiltration.

The movement of water in seasonally frozen ground relies heavily on fundamental soil physics and generally occurs on the unsaturated zone (interchangeably vadose zone). The next section details the basic concepts in understanding the theory of water flow in the unsaturated zone.

2.3 Fundamental Soil Physics

2.3.1 The Unsaturated zone: Infiltration and Water Flow

The unsaturated zone is the soil layer of the sub-surface below ground level and above the water table and consists of pores that contain some combination of air, water and in frozen environments, ice. The thickness of the unsaturated zone is highly variable dependent on location, from a few centimeters to hundreds of meters. To understand the fundamental on soil physics we need to understand the basics of infiltration and water flow in this zone.

Horton (1933) describes infiltration as a process by which water enters into the soil and the water flow in the unsaturated zone is driven in response to a gradient in hydraulic head. The hydraulic head, h (m) is defined as the energy of the fluid per unit weight and is equal to the sum of the elevation head, h_z (m) and the pressure head, ψ (m),

$$h = h_z + \psi \qquad (2.6)$$

The pore-water pressure in unsaturated zone is less than the atmospheric pressure, and is caused by surface tension forces resulting in the phenomenon of capillarity. The pressure head is often referred to as matric potential (ψ, with a negative sign) or an equivalent suction pressure (as matric potential, but with a positive sign). Matric potential is a dependent variable of volumetric water content such that the changes in volumetric water content arise changes in matric potential (Horton, 1933). The volumetric water content here defines the volume of water per total volume of soil.

The Soil Water Characteristics Curve (SWC) for any given soil is then defined as the relationship between the volumetric water content (θ) and the matric potential (ψ) (Williams, 1964).

Since whether or not an individual soil pore retains water is a function of the matric potential, as ψ decreases (i.e. becomes more negative) pores begin to empty, starting with larger pores, and then progressing to smaller pores. When a soil dries out, the largest pores are the first to empty, and determines the soil dewatering threshold. This threshold is known as air entry pressure (ψ_a) which further gives rise to capillary fringe when the water content remains constant. The capillary fringe is the region immediately above the water table where all the pores are water filled. The occurrence of the capillary fringe can be understood with the help of capillary tube where the rise in water is caused by the surface tension of the air water interface and the molecular attraction of the liquid and the solid phases. It is generally assumed that the pore space in the soil behaves as a capillary tube and thus follows the capillarity theory (Fetter, 1994), which is given as:

$$\psi_a = \frac{2\gamma cos\alpha}{\rho_w g R} \tag{2.7}$$

Here, ψ_a is the air entry matric potential or air entry pressure, γ is the surface tension of the fluid (kg s^{-1}), $cos\alpha$ is the contact angle of the meniscus with the capillary tube (degrees), ρ_w is the density of the fluid (kg m^{-3}), g is the acceleration due to gravity (m s^{-2}) and R is the radius of the capillary tube (m).

The smaller the radius of the capillary tube, the greater the height of the capillary rise and the more negative the matric potential. Capillarity theory is applied to generate the SWC curve of different textured soil. Figure 2-2 (a) shows the SWC for three different soil types. Coarse grained soil (such as sand) is unable to retain pore water at higher matric potential values due to its larger pores, whereas, finer grained soil, with smaller pores (such as clay) remain saturated at higher matric potential values and hence develops a thicker capillary fringe (van Genuchten, 1980).

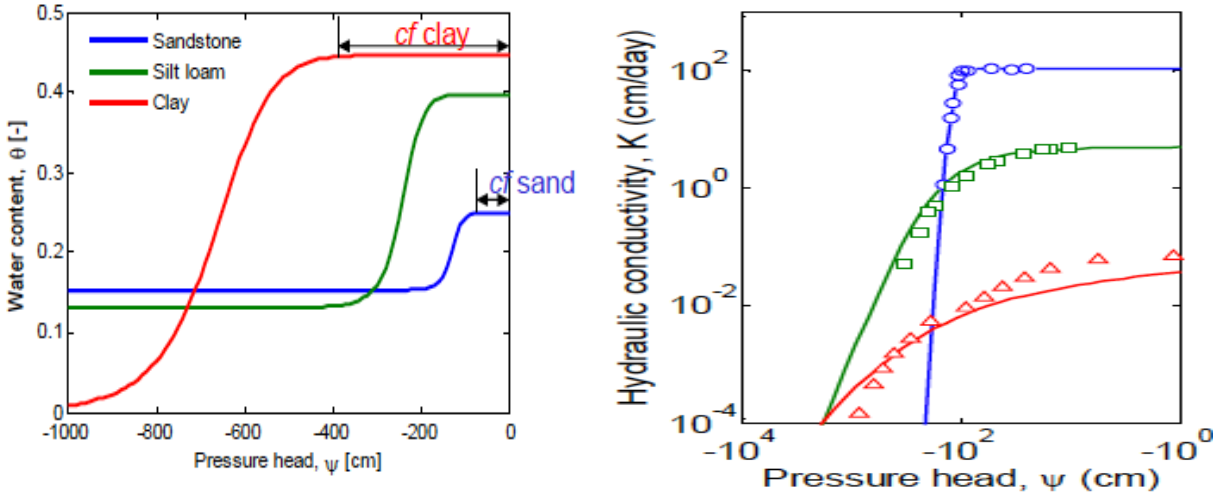

(a) (b)

Figure 2-2 (a) Soil Water Characteristic Curve (SWC) and (b) Hydraulic conductivity curve for different soil textured soil (modified after Van Genuchten, 1980)

Flow in porous media is driven by a gradient in hydraulic head, described above, but is also resisted by friction forces in the tortuous pathways that exist in the media. The concept of hydraulic conductivity (K) was originally introduced by Darcy (1856) for saturated porous soil. Hydraulic conductivity (K) is the rate with which water moves through the soil pores under a potential gradient unit (dh/dx=1) (Dingman, 2015). In a saturated soil, the hydraulic conductivity is a constant term as all the pores are completely filled with water. In unsaturated soils the concept of K was further detailed by Richards (1931). The volumetric water content decrease with the larger most conductive pores draining first as the suction develops. The loss of water from these pores results in a rapid reduction in hydraulic conductivity and is thus a function of the pressure head (ψ). Figure 2-2 (b) shows the K(ψ) relationship of different textured soil. Fine textured soil (clay) has comparatively low hydraulic conductivity compared to coarse textured soil (sand) as clay possess high porosity but low hydraulic conductivity. It is also difficult to measure the K(ψ) relationship directly as $\theta(\psi)$, as it involves a complex movement of unfrozen water into the soil pore space and the measurement greatly relies on the field and laboratory experiments (Hillel, 1998).

2.3.2 Infiltration into a Frozen Soil

Infiltration into a frozen soil is an important yet complex hydrological phenomena and is much more complicated than infiltration in an unfrozen soil due to complex phase change mechanism (Zhao et al., 1997; Ireson et al., 2012; Stähli et al., 1999).

In frozen soil, as the temperature drops, the phase change of pore water lowers the freezing point of water. The freezing point is defined as the temperature at which ice starts to form in the soil pores (usually at 0 ℃). However, due to various chemical impurities and presence of solutes the freezing point of soil can be further depressed below 0 ℃ and the phenomenon is known as freezing point depression (Hansson et al., 2004; Pomeroy and Brun, 2001; Williams, 1964).

As the temperature drops below 0 ℃ in the soil, water freezes first in the larger pores and then progressively in the smaller pores, resulting in more unfrozen water (interchangeably liquid water content) in the smaller pores (Spaans and Baker, 1996). Here, the unfrozen water content is a function of specific surface area of the soil and the freezing point depression (Anderson and Tice, 1973). The specific surface area of finer grained soil (e.g. clay) is higher than that of the coarser grained soil (e.g. sand) thus causing higher unfrozen water content of clay at temperature below freezing point of water compared to that of the sand.

Miller (1980) further determined the relationship of unfrozen water content with decreasing soil temperature. This relationship is known as Soil Freezing Characteristic (SFC) curve, which is considered equivalent to the Soil Water Characteristic (SWC) curve of unfrozen soil as both the curves describes the water retention properties in soil (Koopmans and Miller, 1966; Spaans and Baker, 1996). Particularly, when the soil is frozen, the unfrozen water occurs in small soil pore space and the condition is considered similar to drying of unfrozen soil (Hayashi, 2013). Additionally, Liu et al. (2012) performed laboratory experiments on the soils of Ohio, USA and determined reasonable agreements between the equivalency of SFC and SWC curves.

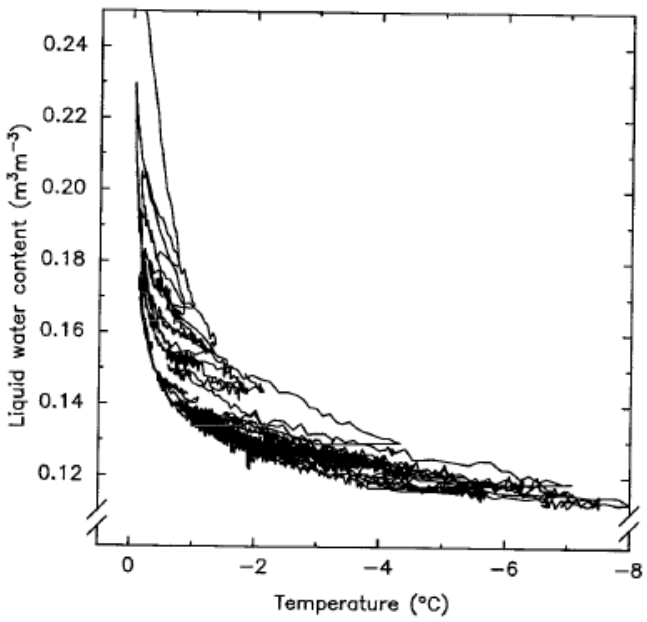

Figure 2-3 Soil Freezing Characteristic (SFC) curve for silt loam soil in the field of Minnesota during winter (Spaans and Baker, 1996)

Figure 2-3, shows the SFC curve during winter (December - March) measured with the Time Domain Reflectometry (TDR) in silt loam soil in the field of Minnesota. The scanning curves in the SFC show considerable hysteresis due to significant freezing and thawing effect in the soil (Spaans and Baker, 1996).

The equilibrium relationship between the unfrozen water, the temperature and the pressure for the SFC curve is given by the Generalized Clausius- Clapeyron Equation (Edlefsen and Anderson, 1943, p.42), given by,

$$\frac{\mathrm{d}P_w}{\mathrm{dT}} = \frac{L_f}{\mathrm{T}V_w} \tag{2.8}$$

where, $\mathrm{d}P_w$ is the change in pressure of liquid water (Pa), dT is the change in temperature (K), L_f is the latent heat of fusion (J kg^{-1}), T is the freezing point temperature (taken as 273.15 K or 0 ℃) and V_w is the specific volume of liquid water (m^3 kg^{-1}). The equation also relates to the freezing point depression of the liquid water at temperatures close to 0 ℃ as the pressure in the ice phase is assumed to be constant in equation 2.8.

Equation 2.8 is further formulated to find the unfrozen water matric potential (ψ) in freezing condition (Dall'Amico et al., 2011), given by,

$$\psi(T) = \frac{L_f}{g} * \frac{T - T_m}{T_m} \quad (2.9)$$

where,$\psi(T)$ is the pressure which is a function of temperature (Pa), L_f is the latent heat of fusion (taken as 3.34×10^5 J kg^{-1}), T_m is the freezing point temperature of pure water (taken as 273.15 K), g is acceleration due to gravity (9.8 m s^{-2}) and T is the observed temperature of the soil.

The reduction in the infiltration rate is due to the presence of ice content in the larger pores which reduces the hydraulic conductivity (Hayashi, 2013). The hydraulic conductivity of frozen soil decreases abruptly as ice starts to form in larger pores in frozen soil, forcing the unfrozen water to flow through smaller pores during the spring melt condition (Kane, 1980). Kane, (1980) as well found a relationship between antecedent water content and snowmelt infiltration rate and determined that soils with lower antecedent water content showed higher infiltration rate and vice-versa during the spring melt condition. The infiltration rate is also affected due to higher amount of infiltration and refreezing of this infiltration during winter. The higher water content and refreezing results into the freezing induced suction (due to a drop in water potential with temperature) which results in an upward movement of the freezing front (Harlan, 1973; Stähli et al., 1999). Silty soil has optimal properties for migration of water to the freezing front as they possess moderate capillarity and hydraulic conductivity for optimal flow, compared to clay, which possess high capillarity but low hydraulic conductivity resulting in low flow.

The viscosity of water is also temperature dependent and increases with colder temperature thus reducing the hydraulic conductivity of the colder saturated soil. For example, wet soil has higher hydraulic conductivity and heat capacity than the dry soil (Kane, 1980).

The temporal and spatial variation of snow cover also greatly influence snowmelt infiltration, as snow insulates the soils and prevents further freezing. A paired-plot experiment performed by Iwata et al. (2010) in Northern Japan demonstrated this function of snow cover. The experiment was conducted in two soil plots- a control plot and treatment plot. The control plot was covered with snow whereas there was no snow in the treatment plot. In the freezing temperatures, the frost

depth in the control plot and treatment plot was observed to be 0.11 m and 0.43 m respectively. Thus, during the snowmelt period, snowmelt infiltration with no surface runoff was observed in the control plot but there was reduced infiltration and some runoff in the treatment plot, in absence of snow cover and higher frost depth.

The infiltration in frozen soil is a distinct function of antecedent water content, soil texture and heat transport mechanism (Gray et al., 2001; Hayashi et al. 2003). Gray et al. (1985) and Granger et al. (1984) identified three distinct categories of snowmelt infiltration in the Canadian prairies (Figure 2-4): Unlimited, Limited and Restricted infiltration.

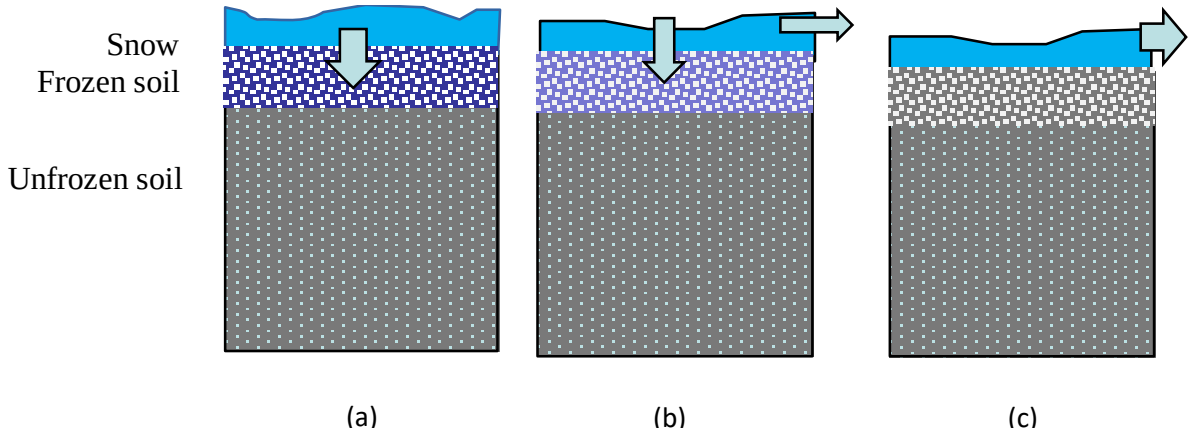

Figure 2-4 Conceptual model for classifying the infiltration potential of frozen soils (a) unlimited (b) limited and (c) restricted (modified after Gray et al., 1985)

Unlimited infiltration occurs in the presence of 'macropores' that could be produced by land-use disturbance, fracturing, worm holes or animal burrows. Here the infiltration rate is equal to the rate of snowmelt and/or rainfall. The case example is seen in the St. Denis National Wildlife Area (St Denis), Canada where the infiltration exceeds the runoff due to presence of these 'macropores' even when the soil is frozen (van der Kamp & Hayashi, 2009).

The occurrence of limited infiltration depends on the initial soil saturation along with the amount of snow cover and ice content in shallow soil. It occurs when the soil is not fully saturated before freeze up and 10% to 90% of melt water can infiltrate through the frozen soil (Hayashi et al., 2003).

Restricted infiltration occurs when the ice on the surface or within the shallow soil impede the infiltration such that snowmelt may sublimate, ponds or goes as runoff. It happens when the soil becomes saturated before freeze up.

Limited or restricted infiltration contributed to the widespread snowmelt flooding in the Canadian prairies in 2011, when high antecedent soil water content caused by the summer rainfall of 2010, resulted in 'limited or restricted infiltration' in frozen soil (during the spring snow melt), leading to high runoff generation.

Watanabe et al. (2013) as well performed a soil column laboratory experiment using silt loam and found three analogous phases of infiltration in frozen soil. They are normal infiltration, slow infiltration and no infiltration. The experiment was based on antecedent water content, temperature and frost depth.

Additionally, the infiltration rate is also indirectly affected by the latent heat (fusion and vaporization) and flow of water vapor during snowmelt which further determines the thermal properties (heat capacity, thermal conductivity) of frozen soil (Ireson et al., 2012). And Hayashi (2013) concluded the relationship between thermal properties along with soil hydraulic properties to be an important factor in determining the infiltration rate in frozen soil.

2.4 Modelling cold region hydrology

2.4.1 Hydrological Modelling

Bear and Cheng (2010) (pg. 29) defines model as "a selected simplified version of a real system and phenomena that takes place within it, which approximately simulates the system's excitation-response relationships that are of interest". The development of computer models to simulate the hydrological processes has received considerable international attention (Zhou et al., 2013).

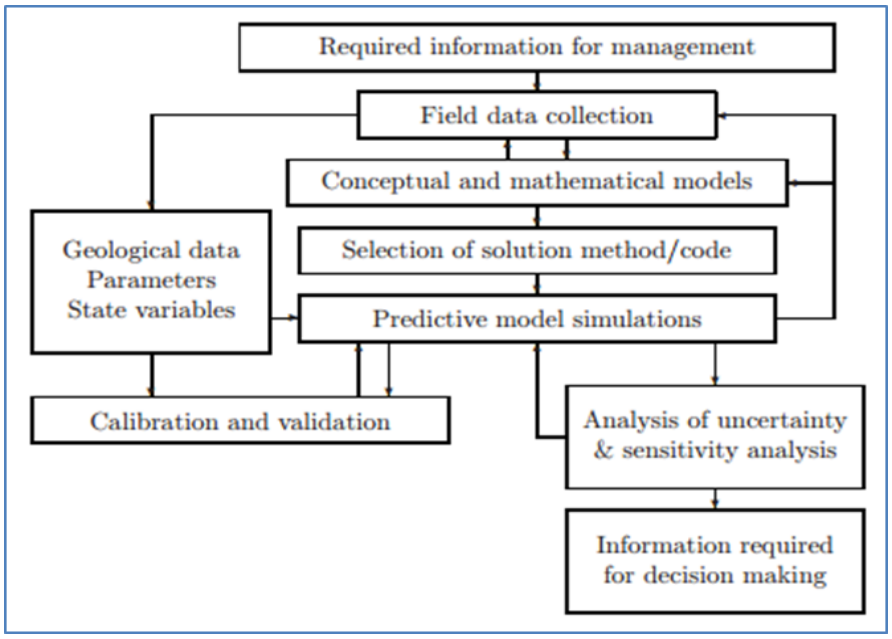

Figure 2-5 Steps in modelling process (Bear and Cheng, 2010)

A hydrological model is a mathematical model which represents the hydrologic processes (such as precipitation, snowmelt, interception, evapotranspiration, infiltration, sub-surface flow, surface flow) and accounts for interactions between these processes (Islam, 2011). Figure 2-5 shows the steps in the hydrological modelling. Based on the assumptions made during the model development, hydrological model can be classified as empirical, conceptual and physically based model (Devia et al., 2015). Empirical models (data driven model) are based on mathematically relating observed response to observed input, conceptual model (parametric) uses hydrologic processes related in observation of catchment, represented by simplified mathematical relationships; whereas in physically based model mass, momentum and energy conservation can be represented with detailed physical processes. Corominas et al. (2013) illustrates that physically based hydrological models (MIKESHE, SWAT and TOPMODEL) have been commonly used to simulate both the saturated and unsaturated flow of water.

In some cases, it may be necessary to conceptualize the physics of a system to develop a conceptual but physically- based model. Ireson et al. (2012) developed such conceptual summary of the surface and sub-surface hydrogeological processes in semi-arid, seasonally frozen ground in Canada (Figure 2-6).

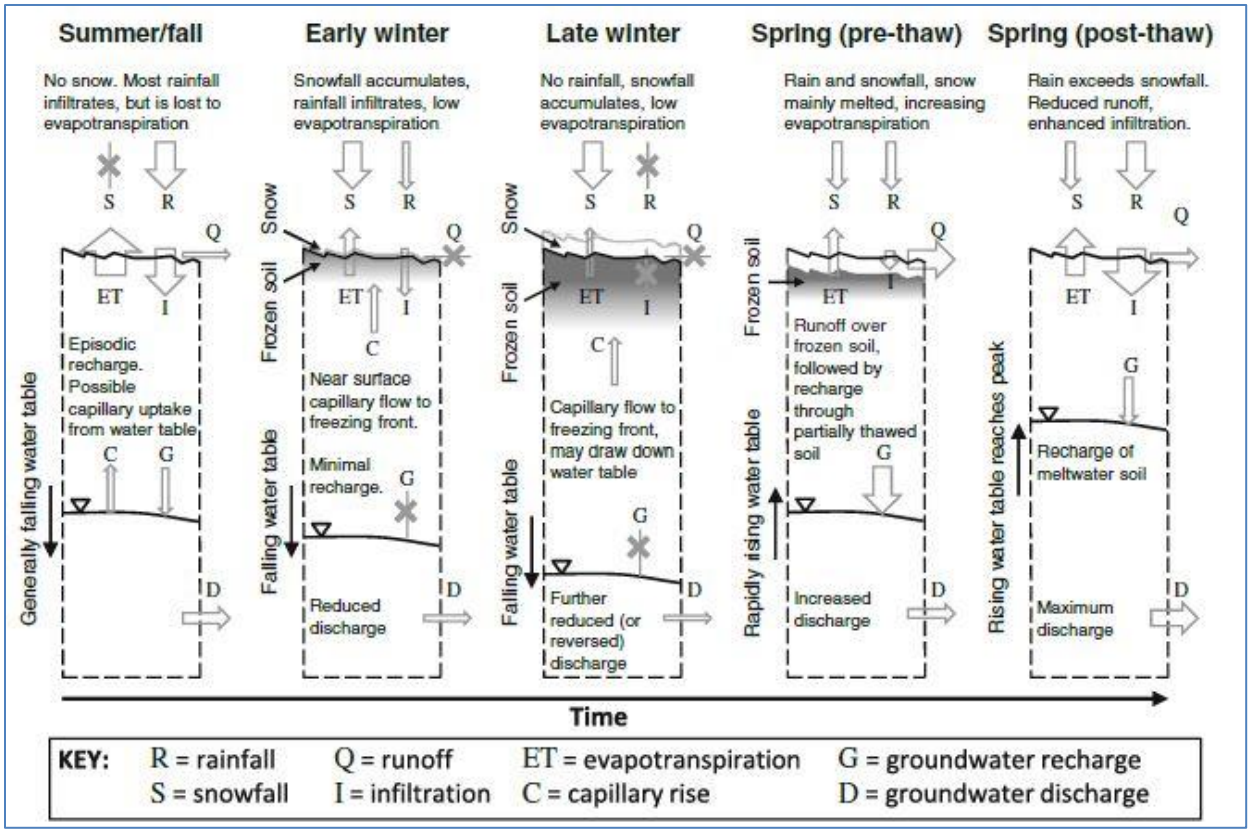

Figure 2-6 Conceptual model for surface and sub-surface hydrological processes (Ireson et al., 2012)

2.4.2 Snowmelt and Snowmelt Infiltration Models

The laboratory experiments and empirical relationships described above are restricted in representing natural field behavior and measuring physical quantities (like mass and phase change) during spring snowmelt, thus indicating the need for developing numerical and mathematical models in simulating these complex processes (Zhao et al., 1997). Most of the computer simulation models like HBV (Bergstrom, 1976), Snowmelt Runoff Model (SRM) (Martinec and Rango, 1986), HYMET (Tangborn, 1984) and SHE (Bøggild et al., 1994), rely on the Temperature Index Method (TIM) for snowmelt modelling. Anderson, (1968) became an early supporter of performing snowmelt simulation using an energy balance approach. Since, then various models have been developed based on his approach. Some of them include EBSM (Gray and Landine, 1988), SNTHERM (Jordan, 1991), CRHM (Pomeroy et al., 2007) and Snobal (Marks et al., 1999).

The Snowmelt Runoff Model (SRM) developed by Martinec and Rango, (1986) is used to model the snowmelt rate from TIM, with no melt condition if the temperature is <0^{o}C (Hock, 2003). The melt factor for the melting period is considered as a time series rather than a fixed parameter. The current version of the model uses temperature, precipitation, and allows for evapotranspiration losses. With the growing number of satellite platforms, the model has the functionality of processing and transmitting the digital snow cover data as a real time input in SRM. Abudu et al., (2012) presented a review paper on using SRM in data sparse mountainous watershed in northwestern China and found that model accuracy was relatively acceptable for snowmelt even in the absence of hydro-meteorological data. Kustas et al. (1994) further detailed the effect and presence of cloud as a dominating factor in estimating the snowmelt rates using the SRM model.

Similarly, the US Army Cold Regions Research and Engineering Laboratory Model (SNTHERM) was developed for determining snowmelt processes along with melt infiltration. The model solves a numerical solution of mass and heat transfer equation, modelling the effects like ice formation, snow ablation, redistribution and metamorphosis of the snow. The model considers snowmelt to be drained by the gravity effect but does not consider the influence of vegetation and the spatial distribution of snow in the model (Suzuki, 2013). Most of the modern Land Surface Models (LSM)(like- CLASS, Verseghy, (1991)), uses Utah Energy Balance Snow Accumulation and Melt model (UEB) (Tarboton and Luce, 1996) for the prediction of rapid snowmelt rates and are driven by inputs like air temperature, vegetation, precipitation, wind speed, humidity and radiation but lack the detailed representation of phase change related with internal energy. These LSM are typically used to predict of snowmelt in open as well as forested environment at a point scale. The Cold Region Hydrological Model (CRHM) (Pomeroy et al., 2007) is a modular object oriented modelling system developed particularly for cold region hydrological processes, where the algorithms are applied as a Hydrologic Response Unit (HRU) and snowmelt infiltration is determined using Zhao and Gray (1999) parametric equations.

However, the theory of heat flow in seasonally frozen soil is more complex and has been given much attention in various snowmelt models (Kurylyk and Watanabe, 2013). The mathematical models have been a central focus incorporating the coupled mass and energy transport into the frozen soil. Harlan (1973) is typically credited with developing the first hydrodynamic based model of coupled water and energy transport in frozen porous soil. Dall'Amico et al. (2011),

Hansson et al. (2004) and Lundin (1990) developed models based on coupled mass and heat transport which was implemented in GeoTOP, HYDRUS and GeoStudio (coupled SEEP/W and TEMP/W) respectively. Similarly, Tao & Gray (1994) developed a numerical model for simulating infiltration in unsaturated, frozen soil. Zhao and Gray (1999) and Zhao et al. (1997) proposed a physically based numerical model based on local volume averaging formulation of transport phenomena in porous media. Simultaneous Heat and Water (SHAW) (Flerchinger and Saxton, 1989) is a physically- based model based on finite difference approach which simulates the physics of a one dimensional frozen soil model using conduction and convection as a heat transport. The model was successfully evaluated for the effects of residue and tillage management on the frozen soil of Nez Perce Prairies in Eastern Washington and was considered useful for the tillage- residue management options for various agricultural purposes.

SOIL model (Stähli et al., 1999) uses two water conducting flow domain for successfully integrating the unfrozen air-filled larger pores and reproducing reasonable soil water storage in the sandy soil in central Sweden. The Frozen Soil Infiltration Model (FroSIn) which was chosen for this research also allows infiltration into the unfrozen air-filled pores in frozen soils, using a novel algorithm for determining the soil hydraulic conductivity in frozen conditions. The model was presented in 2014 American Geophysical Union meeting in San Francisco (Ireson, 2014).

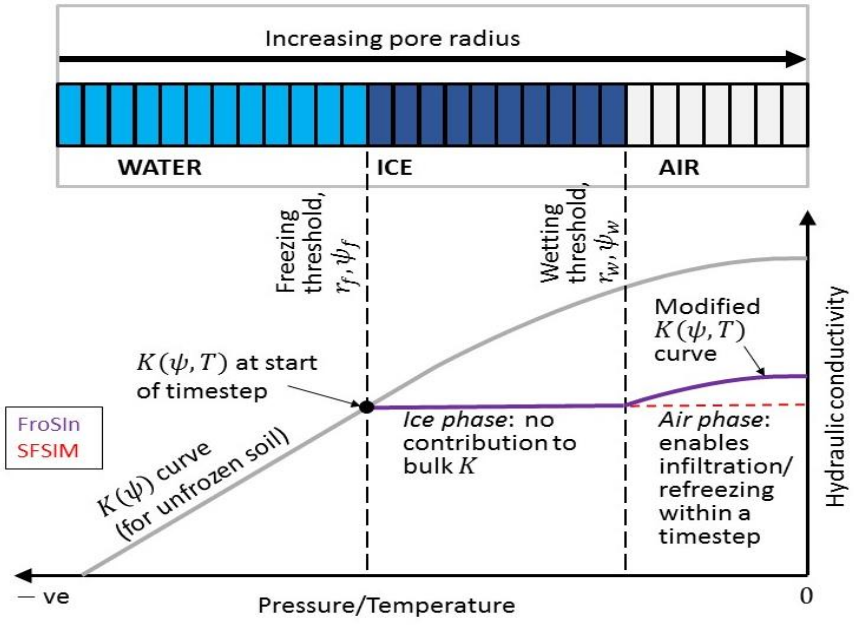

Figure 2-7 Conceptual model of freezing soil in FroSIn (Ireson et al. 2017, in prep)

Figure 2-7 shows the conceptual model of freezing soil in FroSIn. The figure also shows the hydraulic conductivity curve for unfrozen soil and Standard Frozen Soil Infiltration Model (SFSIM) for comparison purpose. The gray line is the unfrozen hydraulic conductivity showing that as the pressure reduces in the soil pores the hydraulic conductivity reduces. In addition, when a partially saturated soil is frozen, the largest pores are the first to freeze and then progressively the smaller pores freeze, which creates a block of ice in the pores and results in no hydraulic conductivity. This is represented by the flat red dotted-line in the figure and most of the conventional model (like SFSIM) uses this formulation in their model, which restricts infiltration into the frozen soil. In FroSIn there is a unique relationship between water content and pressure during unfrozen conditions and between temperature and pressure during frozen conditions. Capillary theory allows us to define a pore radius wetting threshold, r_w, from the soil matric potential, ψ, in unfrozen conditions, and this determines the total (liquid and solid) water content. The Generalized Clausius-Clapeyron Equation (Edlefsen and Anderson, 1943, p.42) gives us an equivalent matric potential as a function of soil temperature (when $T < 0°C$) (see Eqn 3.5). This relationship has no soil dependent parameters, and predicts a linear relationship between T and ψ, such that $\psi = 0$ m when T = 0°C, and $\psi = -124$ m when T = −1°C. From this pressure an equivalent pore radius is found, again from capillary theory, that determines the freezing threshold, r_f. The pore space is partitioned into water ($r < r_f$), ice ($r_w \leq r < r_f$) and air ($r \geq r_w$) (Figure 2-7). In FroSIn, the air phase maintains its hydraulic conductivity, such that water can infiltrate into the air-filled pores. The K curve is recalculated at set time intervals (here 12 hours) to account for the ice phase.

2.5 Research Gaps and Challenges

- Major limitations exist in forecasting streamflow and ground water discharge from snowmelt as the existing snowmelt models lack the capability to accurately quantify snowmelt into infiltration and runoff over frozen soils (Granger et al., 1984; Zhang et al., 2003).
- Modelling snowmelt infiltration in frozen ground is challenging due to thermal and hydraulic interactions of frozen soil (Stähli et al., 1996). In particular, the relationship between the hydraulic conductivity (K) and the matric potential (ψ) in frozen unsaturated condition is difficult to measure.

- Most of the standard infiltration models mentioned in section 2.4.2 (such as SHAW, GeoTOP, Hydrus, GeoStudio) (except SOIL and FroSIn) do not incorporate the infiltration into unfrozen air-filled pores in frozen soil, which provides rapid movement of liquid and pollutants during the spring snowmelt.

CHAPTER 3

DATA AND METHODS

3.1 Study Sites

The two study sites used in this study are located in the prairie regions, which has seasonally frozen environment that provides an ideal opportunity to understand infiltration processes in frozen soils. The study sites are briefly described below.

3.1.1 St. Denis National Wildlife Area (St Denis)

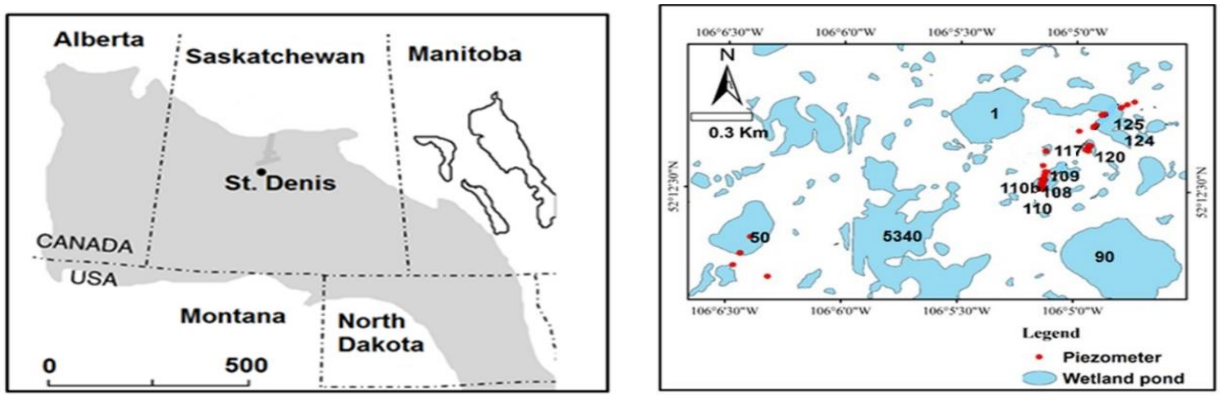

(a) (b)

Figure 3-1 (a) Map of St. Denis field site location (b) Map of piezometers (red dots) and few major pond locations at St Denis

The St Denis field site is located approximately 40 km east (106° 5' 36" W, 52° 12' 34" N) of Saskatoon, Saskatchewan, Canada comprising of 3.85 km^2 (385 ha) and containing numerous wetlands (Garth van der Kamp and Hayashi, 2009). The topography of St Denis is dominated by clay rich (20%-30%) glacial till (Hayashi et al., 2003). The top few meters (5-6 m) is composed of highly conductive macro pores and fractures which gives high hydraulic conductivity of 0.864

m/d- 0.00864 m/d and then hydraulic conductivity generally decreases with soil depth (0.00864 m/d- 0.0000864 m/d) (Hayashi et al., 1998; van der Kamp and Hayashi, 2009).

St Denis has two major land uses: grassland and cultivated land. The total porosity of top 15 cm of cultivated land and grassland is 54.5% and 61.8% respectively (van der Kamp et al., 2003). Monthly mean temperatures are -19 ℃ in January and 18 ℃ in July with mean annual precipitation (1967-1996) as 358 mm with 74 mm of snowfall occurring from November to April (van der Kamp et al., 2003). Hayashi (2013) reported that the soil at St. Denis is affected by cold winter which freezes the soil to considerable depths, eventually affecting both the hydrological and ecological processes.

Watershed of Pond 50 at the St Denis: Pond 50 is located to the west (Figure 3-1, b) of the St Denis. It is a small closed pond which drains the snowmelt from upland and typifies various other ponds in the area. The land use of the area is grassland with the watershed area of 1430000 m^2 (Garth van der Kamp, personal communication, March 17, 2017). At watershed of pond 50, the study focusses on partitioning the snowmelt into infiltration and runoff based on the changes in snowmelt volumes in the pond. For the research, pond 50 was chosen as a reference pond as its watershed lies entirely within the study area thus receiving all the melt water during spring.

3.1.2 Brightwater Creek (BWC)

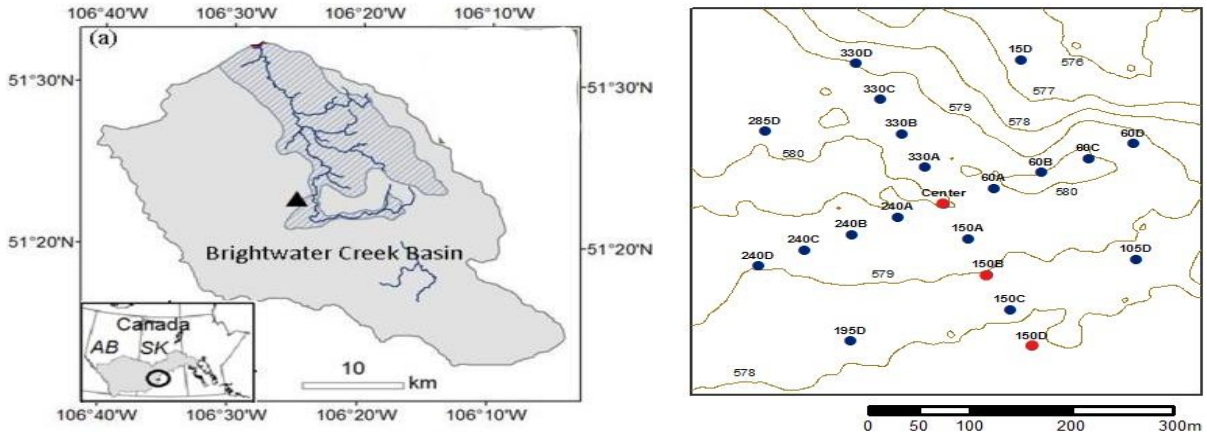

(a) (b)

Figure 3-2 (a) BWC sub-basin in Saskatchewan River basin (effective drainage is shown by hatching) and Flux tower location (triangle) and (b) neutron monitoring location (dark blue dots) and HydraProbe and piezometers boreholes locations (red dots) (Pan et al., 2017).

The BWC field site (51° 22' 54" N, 106° 24' 57" W) lies within a gauged sub-basin of the Brightwater Creek watershed (basin overall area of 900 km^2 and effective drainage area of 282 km^2), which is a sub-basin of the South Saskatchewan River Basin located in the prairies in central Saskatchewan (Figure 3-2). The mean annual precipitation is about 330 mm, falling typically 66 mm as snow. The mean temperature in January is -12.9 ℃ and in July is 18.8 ℃. The study area is located within a ~700 ha grazing pasture and measures an area of 250000 m^2. The climate is semi-arid with a gently undulating landscape and the soil texture of the site ranges from loam to clay loam (Pan et al., 2017).

3.2 Research Flow Design

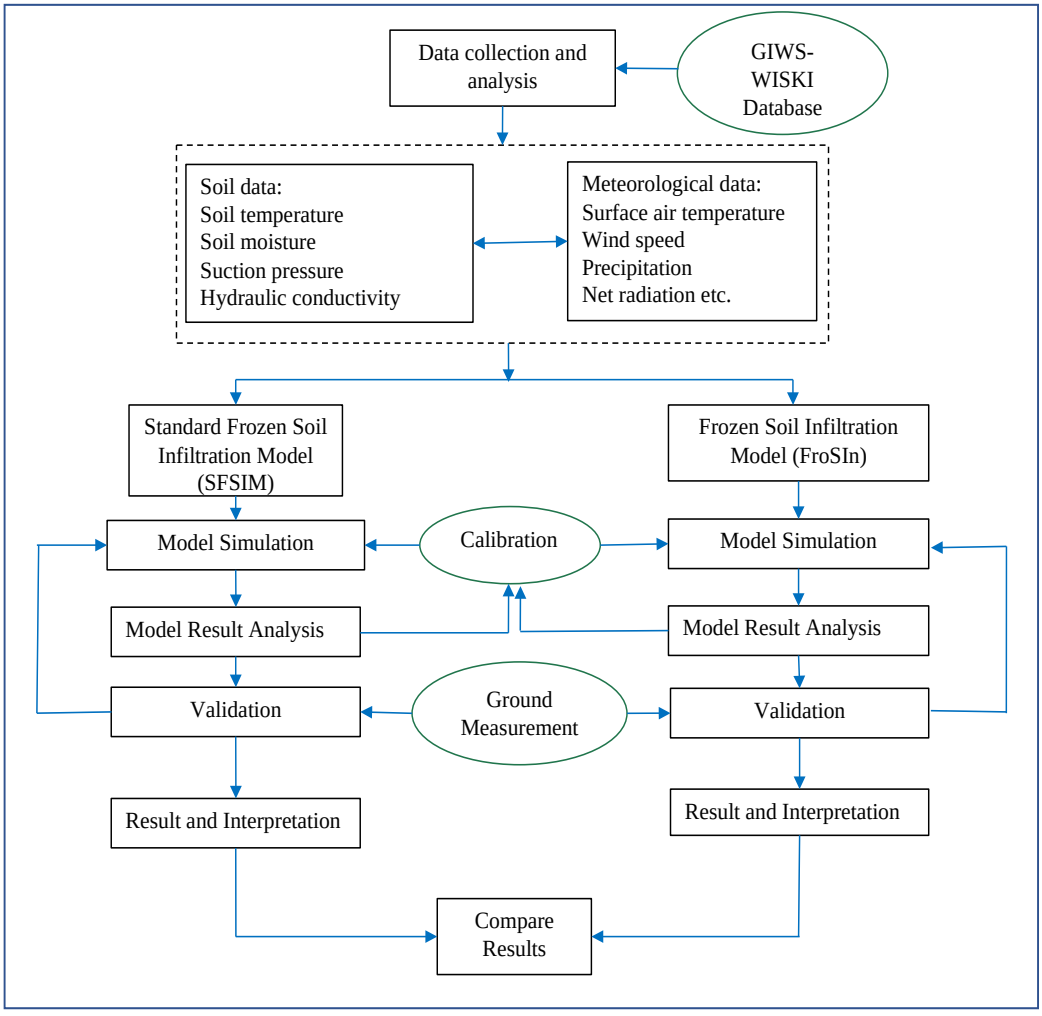

Figure 3-3 Research flow diagram

Figure 3-3 shows the research flow design consisting of several steps. The first step is the data collection and analysis (soil data and meteorological data) from the WISKI database. Both first objective (i.e. to quantify snowmelt infiltration and runoff based on field based observation) and second objective (i.e. to establish the SWC and SFC curve) are performed in the data analysis section. In particular, at St Denis, pond 50 information will be used for snowmelt partitioning. The third objective will be achieved by comparing two different models Standard Snowmelt Infiltration Model (SFSIM) and Frozen Soil Infiltration Model (FroSIn). The next step governs model simulation and calibration. After that, both models will be validated with observation from the study site. Lastly, the results from each model will be compared and interpreted with one another.

All the three research objectives are inter linked with each other and are expected to be fulfilled with the above research flow diagram.

3.3 Data Collection

3.3.1 Instrumentation

A variety of instrumentation was used to acquire the soil and meteorological data from the field sites. The soil data for model parametrization were identified as soil temperature (℃), soil volumetric water content (m^3 m^{-3}) and soil matric potential (kPa). The meteorological data (precipitation (mm), air temperature (℃), relative humidity (%), atmospheric pressure (kPa), incoming short and longwave radiation (W m^{-2}) and wind speed (m s^{-1})) were determined to simulate the snowmelt rate and period for the model. A brief introduction to the instruments, along with their specifications and experimental design, is summarized below:

St Denis

The hourly meteorological data from St Denis is observed from a 10 m mast tower and a 10m scaffolding tower. The mast tower is located on the slope of Pond 50 at an elevation of 554 masl and the scaffolding tower is located 200 m north of Pond 1 at an elevation of 560 masl.

The land cover near the mast tower is perennial grass and the scaffolding tower is annual crops. These annual crops include wheat, barley and flax seed. The evapotranspiration from the site was estimated from the latent heat flux data available from the eddy covariance sensors on the scaffolding tower. As described by Brannen et al. (2015), at St Denis, the eddy covariance method

was used for the energy balance closure considering the wind speed (m/s), air temperature ($°C$) and water vapor density (g cm^{-3}). The wind speed was measured with the 3-D ultrasonic anemometer and the water vapor density was measured with the open path gas analyzer. The mean and covariance of the data were collected from the data logger and the corrections on the eddy covariance measurements was based upon 2-D coordinate rotation (Baldocchi et al., 1988), air density fluctuations (Webb et al.,1980), sonic path length, high frequency attenuation and sensor separation (Horst, 1997; Massman, 2000).

Table 3-1 Data and instrument information from the towers

Tower	**Height (m) (above ground level)**	**Instrument type**
10 m mast tower		
Wind Speed (m/s)	10	RM Young 5103-10
Wind Direction(degrees)	10	RM Young 5103-10
Air temperature/Relative humidity (%)	2	Vaisala HMP series
Barometric Pressure(kPa)	2	MetOne or Setra SBP270
Global Solar Radiation (W/m^2)	1	LiCor Li200X
Precipitation (mm)	0.5	Texas Electronics TE525M tipping bucket rain gauge
10 m scaffolding tower		
Wind Speed(m/s)	2	Met One 14A
Wind Direction(degrees)	10	NRG
Air temperature /Relative humidity (%)	1.5	Vaisala HMP series
Air temperature /Relative humidity (%)	10	Vaisala HMP series
All component Radiation(W/m^2)	10	Kipp and Zonen CNR4
Fluxes (C, λE and H)	10	CS CSAT3 and EC150
Precipitation (mm)	10	Texas Electronics TE525M

The data along with the instrument from towers are listed in Table 3-1. All the sensors are connected to a Campbell Scientific CR 1000 data logger. The data from mast tower were logged

from 1989 to date and that from the scaffolding tower were logged from 2011 to date. The required data for simulation were collected from the scaffolding tower and the gaps in the data were filled based on the mast tower wherever applicable.

Similarly, the soil data was measured in the cultivated land between ponds 107 and 108a which is named as Uri transect (Figure 3-4). The Uri transect has three soil profiles (namely upslope, midslope and downslope) connecting ponds 107 and 108a at St Denis. Figure 3-4 shows the experimental layout of the Uri transect.

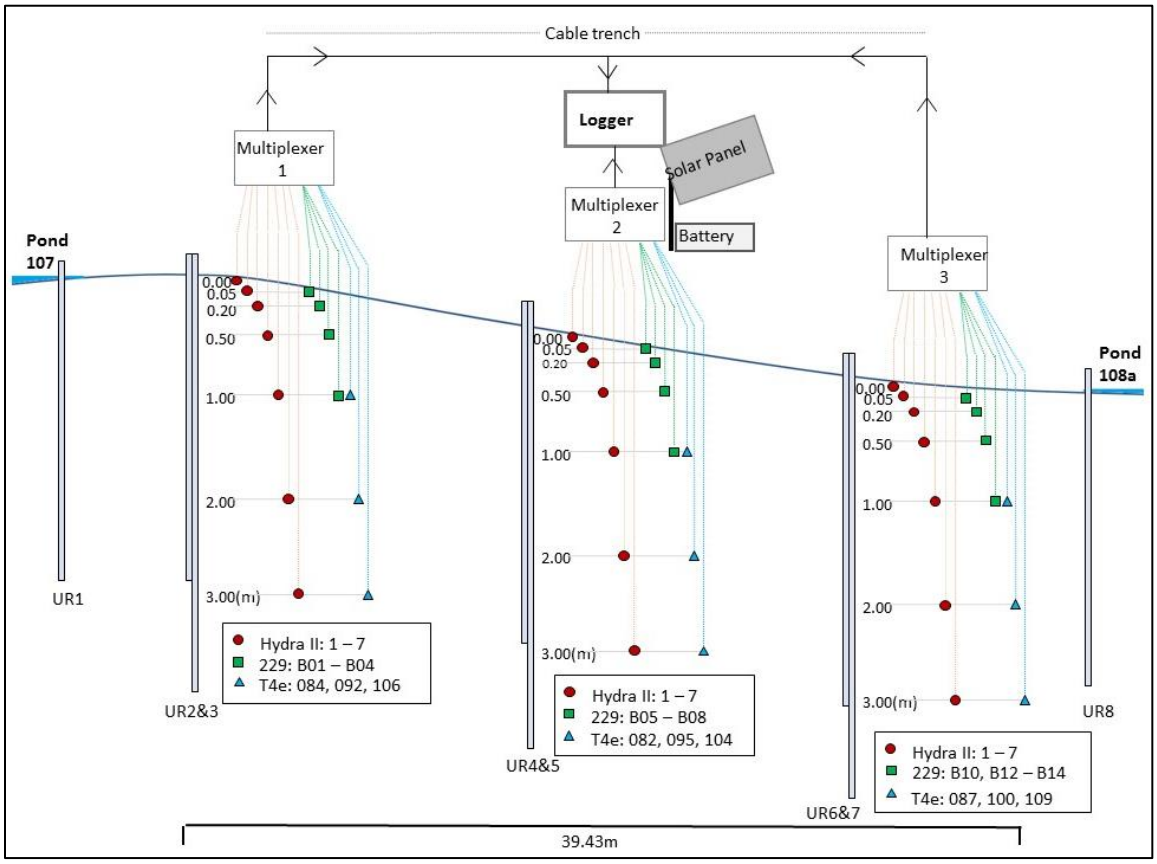

Figure 3-4 Experimental setup for soil profile data in Uri transect at St Denis

HydraProbe (Hydra II) is a sensor which measures the soil volumetric water content and soil temperature at depths of 5 cm, 20 cm, 50 cm, 100 cm, 200 cm and 300 cm in three soil profiles. The water content is measured by measuring the soil dielectric constant, using an impedance method, and then relating this to the volumetric water content via a calibrated relationship (Stevens Water Monitoring Systems Inc, 2007). It is not completely clear whether the signal from the

instrument can be interpreted in frozen conditions, but Spaans and Baker (1995), suggests that since the dielectric constant of ice is so much lower than that of liquid water, these instruments likely give a reasonable measure of the liquid water content. This will be discussed further when interpreting the observations.

The soil matric potential (suction pressure) is measured using heat dissipation sensors (229 probes, Campbell Scientific) at the depths of 5 cm, 20 cm, 50 cm and 100 cm. The heat dissipation sensors (-10 kPa to -2500 kPa) is a porous block sensor which measures pressure of dry soil. Because of the pressure range limitation of the 229 probes, tensiometer (T4e, Decagon Devices) (+100 kPa to -85 kPa) was used to measure the pressure of wet soil at the depth of 100 cm, 200 cm and 300 cm.

Similarly, several deep and shallow piezometer boreholes were used to measure the water table level along the Uri transect. The piezometer boreholes installed along the transect has the shallowest depth of 2.6 m and the deepest depth of 6.8 m. The pressure transducers in the piezometer boreholes are Solinst level loggers, which log the level at half hour intervals. The level data was also corrected for the changes in atmospheric pressure.

Brightwater Creek (BWC)

The precipitation data for BWC was measured using a Geonor T200-B weighing gauge. As described by Pan et al. (2017) the precipitation bias for snow was corrected for under catch using a wind speed-catch efficiency relationship (Smith, 2007), and for the rain a catch efficiency of 95% was assumed. The evapotranspiration was calculated from the latent heat flux data available from the eddy covariance technique for which data is collected from the Campbell Scientific CSAT3 sonic anemometer and a Campbell Scientific KH20 Krypton hygrometer mounted on the scaffolding tower located in the study area (Pan et al., 2017). All other meteorological data (net radiation, relative humidity, pressure etc.) were collected from the scaffolding tower. The instruments were mounted at a height of 4.85m above the ground having a representative measurement fetch of approximately 500 m.

Similarly, the root zone soil water content was measured at 21 locations with 50 m spacing along two perpendicular transects in a crosshair pattern centred on the flux tower (Figure 3-2, b) with a neutron probe model CPN 503DR Hydra Probe (CPN International Inc., Concord, CA) (Pan et al., 2017). Three HydraProbes (Hydra Probe II, Stevens Water Monitoring Systems Inc., USA) was

also installed along the marked red dots (Figure 3-2, b) to measure soil water content and temperature at the depths of 20 cm, 50 cm, 100 cm and 160 cm. The soil profile was named as P1, P2 and P3 for centre, 150B and 150D (Figure 3-2, b) respectively for convenience (Pan et al., 2017). Factory supplied general calibration equation for loam with an accuracy within ± 0.04 cm^3/cm^3 (Seyfried et al., 2005) was used for HydraProbe calibration. Similarly, heat dissipation sensors (229 probes, Campbell Scientific) and tensiometer (T4e, Decagon Devices) were used for measuring the matric potential of the soil at various depths. Three piezometers boreholes along with level loggers (Solinst, Model 3001) were also installed at P1, P2 and P3 location to measure the water table level.

3.3.2 Data Retrieval

The data was retrieved from the Water Information System KIsters (WISKI) platform at the Global Institute for Water Security (GIWS), University of Saskatchewan. WISKI database management[1] uses Campbell Scientific LoggerNet software and .NET modules to handle real time data collection, data processing, storing and reporting from the research area.

The WISKI desktop client was used to access and view data from the database and analyse the data in various modelling environment. The type and characteristics of required data available in the WISKI has been listed in Appendix D (Table D.1 and Table D.2).

3.4 Snowmelt period, rate and snowmelt partitioning

The snowmelt rate determines the required amount of melt water during spring which can then be partitioned into runoff and infiltration. The snowmelt rate was simulated using the Energy Balance Snow Melt (EBSM) (Gray and Landine, 1988) module in Cold Region Hydrological Model (CRHM) (Pomeroy et al., 2007). In CRHM the snowmelt rate was calculated based on surface and subsurface energy balance approach and has been widely used to determine snowmelt processes in the prairies (Pomeroy et al., 2002; Shook et al., 2013; Fang and Pomeroy, 2009).

The required meteorological data for CRHM are wind speed, precipitation, incoming longwave and shortwave, relative humidity and air temperature which was extracted from the two field sites

[1] http://giws.usask.ca/documentation/system/GIWS_WISKI.pdf

(St Denis and Brightwater Creek). The simulation from CRHM also determines the tentative melt period which is crucial for spring runoff quantification.

The prairies region lack accurate stream flow discharge measurement (both at St Denis and Brightwater Creek). But at St Denis the ponds could be used as a proxy to partition the snowmelt into infiltration and runoff. The closed basins at St Denis drains snowmelt water and additional precipitation from uplands into the ponds (Hayashi et al., 2016). Pond 50 was used for the runoff calculation based on the area, volume and depth relationship, developed by Hayashi and Van Der Kamp (2000). The runoff was estimated based on the spring time rise in the water volume level into the pond. The area, volume and depth relationship provides an equation to calculate the area, A (m^2) and volume, V (m^3) of the pond based on the depth (m) of the water, which is given as,

$$A = s\left(\frac{h}{h_o}\right)^{\left(\frac{2}{p}\right)} \tag{3.1}$$

where, s is a scaling factor and p is the dimensionless constant which represents the basin shape; h is water level depth and ho is the unit depth (=1).

Similarly, the volume is calculated as,

$$A = s\left(\frac{h}{h_o}\right)^{\left(\frac{2}{p}\right)} \tag{3.2}$$

The runoff (mm) was calculated based on the change in the volume of the pond to that of overall watershed area of the pond. Infiltration (mm) was then calculated solving the surface water balance equation and is given by,

$$\text{Infiltration} = \text{SWE} + \text{rain} - \text{runoff} - \text{evapotranspiration} \tag{3.3}$$

where, SWE (mm) is the overall landscape snow water equivalent estimated by taking a weighted mean by land cover at St Denis, rain (mm) is the rainfall event during the snowmelt period, runoff (mm) is determined from the above area, volume and depth relationship and evapotranspiration is in mm day^{-1}.

Due to lack of discharge measurement at Brightwater Creek snowmelt partitioning was not performed at this site. However, the pattern for zero degree isotherm, soil water content and water table level was assessed for Brightwater Creek.

3.5 Log-normal Pore Size Distribution model (LNPSD)

The Soil Water Characteristic (SWC) and Soil Freezing Characteristic (SFC) curves were established based on the soil particle size distribution model namely, Log-normal Pore Size Distribution (LNPSD) model. The model assume a log normal pore size distribution which may be defined by three parameters (porosity, mean radius, and standard deviation) (e.g. Kosugi, 1994; Shirazi and Boersma, 1984). Such a distribution model was considered which is expected to fit with the observed SWC and SFC data from St Denis and Brightwater Creek.

Before applying the LNPSD model, the model's consistency with the more widely used van Genuchten model (VGM) (van Genuchten, 1980) was checked. In LNPSD model, the equation for SWC curve is based on the log normal pore size distribution (Kosugi, 1994) which is also equivalent to the Kosugi's two parameter model (Kosugi, 1996). The equation is given by,

$$f(\psi) = \frac{(\theta_s - \theta_r)}{(2\pi)^{\frac{1}{2}}\,\sigma(\psi_a - \psi)} . exp\left[- \frac{\left\{ ln\left(\frac{\psi_a}{\psi - \psi_a}\right) - \mu \right\}^2}{2\sigma^2} \right], when\ \ \psi < \psi_a \tag{3.4}$$

$$f(\psi) = 0, when\ \ \psi \geq \psi_a$$

where, $f(\psi)$ is the pore capillary pressure distribution function, θ_s is the saturation moisture content ($m^3\,m^{-3}$), θ_r is the residual moisture content ($m^3\,m^{-3}$), ψ_a is the air entry pressure, μ is the mean and σ is the standard deviation.

For the SFC curve, the equivalent pressure for given temperature was given by the Generalized Clausius Clapeyron Equation (Edlefsen and Anderson, 1943)

$$\psi(T) = \frac{L_f}{g} * \frac{T - T_m}{T_m} \tag{3.5}$$

where, L_f is the Latent heat of fusion (taken as 3.34×10^5 J kg^{-1}), T_m is the freezing point temperature of pure water (taken as 273.15 K), g is acceleration due to gravity (9.8 m s^{-2}) and T is the observed temperature of the soil.

The equation for SWC curve in the van Genuchten model (VGM) is defined by the parametric relationship for effective saturation (S_e) as a function of matric potential (ψ),

$$S_e(\psi) = \frac{\theta(\psi) - \theta_r}{\theta_s - \theta_r} = \left(\frac{1}{1 - |\alpha\psi|^n}\right)^m \quad (3.6)$$

where, θ_r is the residual moisture content ($m^3\ m^{-3}$), θ_s is the saturation moisture content ($m^3\ m^{-3}$), α (m^{-1}) is related to inverse of the air entry suction, and both 'n' and 'm' are dimensionless parameters and related to the pore size distribution.

After validation with the VGM model the LNPSD model was then used to calibrate and validate with the observed SWC and SFC curves for St Denis and Brightwater Creek to determine three required parameters (porosity, mean radius and standard deviation) to run the models.

3.6 The Modelling Tools

The Standard Frozen Soil Infiltration Model (SFSIM) and Frozen Soil Infiltration model, FroSIn (developed by Dr. Andrew Ireson) (Ireson et al., 2017 in prep.), were applied to two field sites (St Denis and Brightwater Creek). The objective was to explore whether the simulation of infiltration into the frozen soils could be improved. The models are briefly described in the literature review section (section 2.4.2) and full description of the models along with the governing equations are provided in the Appendices A, B and C.

The model setup, driving data, initial and boundary conditions and the saturated hydraulic conductivity values were determined for both the models (SFSIM and FroSIn) for each study site. The models were set up with the required data and the simulated results were compared with each other.

3.6.1 Model setup

Both Standard Frozen Soil Infiltration Model (SFSIM) and Frozen Soil Infiltration model (FroSIn) represents a 1D model considering the spatial and the temporal grid size as a control volume. Both

the models were set up with a control volume of soil depth 1.5 m which indicates the unsaturated zone in the study site. The required soil parameter values were determined from the LNPSD model. The analyses were performed for three recent years 2014, 2015 and 2016, focussing more during the snowmelt period (March and April) for both the study sites. An individual run was performed for each year, from October to May, with the observed pressure head in previous fall (October) acting as the initial condition for that particular year. It should also be noted that at this stage of the model run, the effects of plants or different land cover was not incorporated into the model, so the model does not incorporate the changes in the evapotranspiration fluxes.

3.6.2 Driving data

The driving data required for the models are soil temperature, snowmelt and rainfall rates. The soil temperature and rainfall rate were inferred from the observations and the snowmelt period and rates were simulated using Cold Region Hydrological Model (CRHM) for both the study sites.

3.6.3 Initial and boundary condition

The initial condition for the analysis was used as a prescribed pressure head condition during previous fall (October) of a particular year. For example, for 2014 the initial condition for pressure was determined from October 2013 which gives the exact antecedent soil water condition. The upper boundary condition was determined considering equal distribution of observed snowmelt and rainfall flux and a free drainage boundary condition was applied to the bottom of the model.

3.6.4 Saturated hydraulic conductivity

The required saturated hydraulic conductivity (Ksat) for the models was estimated based on the sensitivity analysis of the observed initial water content during fall (October) and saturated hydraulic conductivity parameters taken from the literature (Hayashi et al., 1998; van der Kamp and Hayashi, 2009).

CHAPTER 4

RESULTS AND DISCUSSION

4.1 Quantifying snowmelt infiltration and runoff based on field based observations

4.1.1 Quantifying snowmelt infiltration and runoff at St Denis

This section details the field based data analyses at St Denis to quantify the snowmelt infiltration and runoff. Detailed pond 50 data and other hydrological data are presented with discussion. The overall fluctuations of major variables in vadose zone at St Denis is summarised in Appendix E (Figure E.1).

4.1.1.1 Pond Water Level

The long-term (1968-2016) pond 50 water level data is shown in Figure 4-1. The data shows fluctuations in water level until 2010 with some drastic rise and fall in the pond level. But there was a continuous rise in the water level after 2010 significantly raising the pond water level. Hayashi et al., 2016 found the past two decades to be particularly wet with high pond levels in the study site. However, the pond level was minimal during the drought years in 1990, 2001 and 2002.

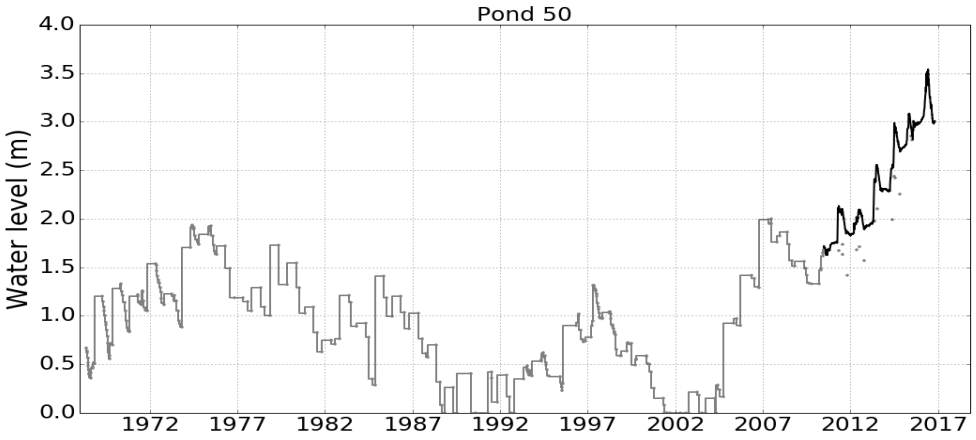

Figure 4-1 Long term Pond 50 water level (1968-2016)

4.1.1.2 Hydrological data

Snow Water Equivalent (SWE)

The long-term snow survey data is available at St Denis which is shown in Figure 4-2. Snow surveys were performed annually in spring, before the snowmelt period (March or April) to determine the Snow Water Equivalent (SWE) at various predetermined transects. The mean SWE from 1994 to 2016 was recorded to be 64.5 mm with the highest SWE of 120 mm recorded in 2013.

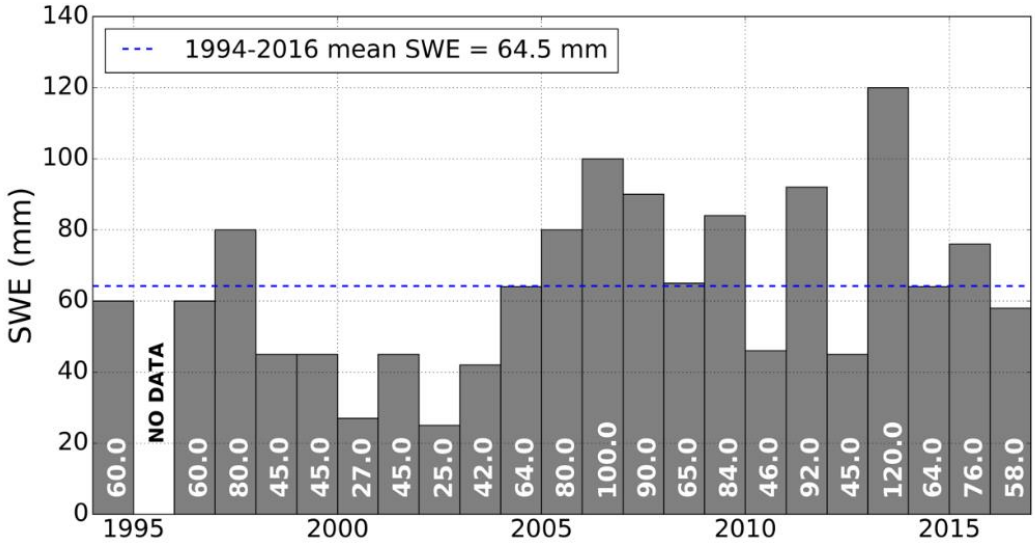

Figure 4-2 Annual Snow Water Equivalent (1994-2016)

Soil freezing and thawing

Contouring the zero-degree isotherm provides a method for tracing the freezing and thawing in the soil profile. Above $0°C$ the soil is thawed and below $0°C$ the soil is partially to fully frozen, due to the freezing point depression. Therefore, the zero-degree isotherm tracks the extent of freezing and thawing of soil during winter.

The depth of zero-degree isotherm (Figure 4-3) was plotted using the soil temperature data from the Uri transect. At St Denis, the soil in mid slope in winter 2013-2014 froze to a maximum depth of approximately 1.2 m. The frozen soil depth in 2013-2014 and 2014-2015 winter were considerably deeper compared to that of 2015-2016 winter. Hayashi et al. (2003) reported the

relationship of deep soil frost as a result of relatively thin snowpack (<0.3 m) insulation during winter on the prairies. The soil at St Denis was dry in 2014-2015 before freeze-up (due to high evaporation in the summer of 2013), but the deep soil freezing was developed due to shallow snowpack (SWE of 64 mm in April 2014) and cold air temperature (~ -24 $°C$) in 2013-2014 winter.

In contrast, in 2015-2016 the soil freeze depth was very shallow (around 0.2 m), which might be the result of low surface air temperature (-10 $°C$) in the consequent winter.

Pan et al. (2017) also found that the difference in the soil frozen depths to be due to the difference in the antecedent soil water content in the prairies. For example, from the observation in the study site, it was noted that 2013 was comparatively wetter than 2014 due to high summer rainfall of 2012 (431 mm), resulting in higher antecedent moisture content and thus higher soil freezing depth in 2013-1014 winter.

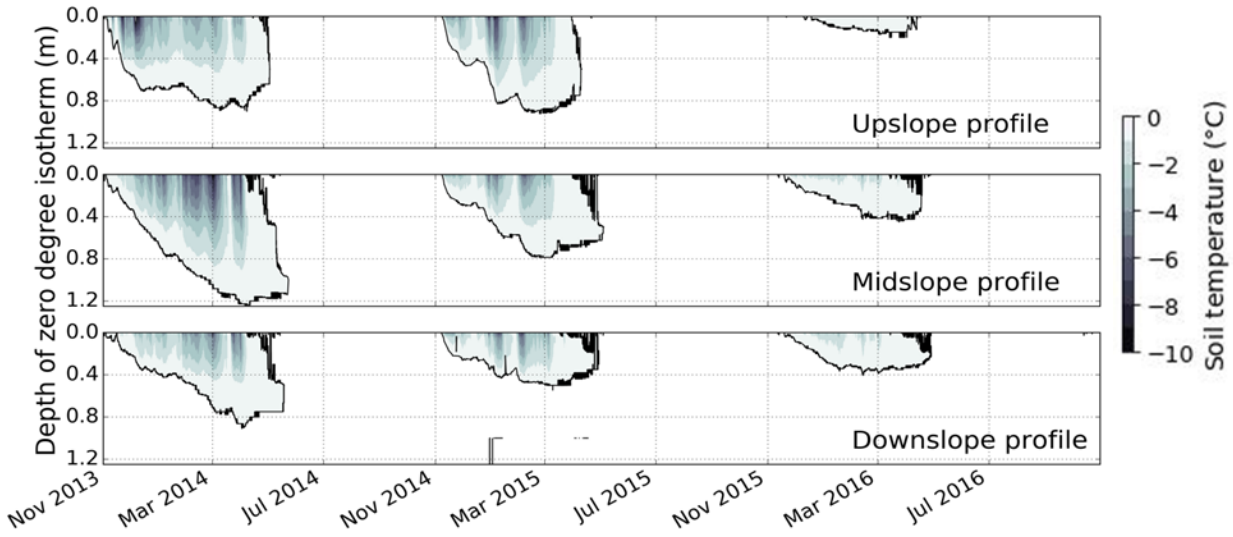

Figure 4-3 Soil freezing depth of three profiles along the Uri transect

Unfrozen water content and water storage

Unfrozen water content of soil along the Uri transect was measured using the HydraProbe sensor and the unfrozen water storage was also determined from the measured water content. Figure 4-4, Figure 4-5, and Figure 4-6 shows the unfrozen water content and water storage at various depths along the three profiles (upslope, midslope and downslope) of the transect.

In all of the shallow readings, every winter there is a large, rapid drop in the unfrozen water, which is caused not by drying, but by freezing of the pore water. This is followed in spring by a similarly rapid rise in unfrozen water content, associated with thawing. It is suggested that dielectric instruments measure unfrozen water content in frozen conditions (Spaans and Baker, 1995), however, they may require further calibration to get the magnitudes correctly. If the instrument is measuring the unfrozen, i.e. liquid water content, then we see rather large, "residual" unfrozen water contents (around 0.10 in the upslope), which is not expected. This could be real if there are salts present in the pore water, which are progressively excluded during freezing. Alternatively, the probes may be reading the pattern of freezing, but not the actual magnitudes. This issue requires further work and is beyond the scope of this research.

The water content from the upslope profile suggests the soil porosity of 0.5-0.6 m^3/m^3 at the greatest in the study site. However, the water content for midslope and downslope profile showed much higher soil porosity (~0.8 m^3/m^3) which indicates data error in both the profiles. This error might be related to instrumentation where the HydraProbe loosens its position in the soil due to presence of rocks or pebbles in course of time and develops a void space which is then filled with water. This leads to inaccurate reading of higher water content from the sensors. This also warrants some careful investigation of HydraProbe for future data analysis and research in the study site.

The unfrozen water storage (S) (m) in the transect was determined based on the relationship of volumetric unfrozen water content (θ) (m^3/m^3) and various soil depths (Δz) (m), as, $S = \theta * \Delta z$. The soil depths were determined based on the measured water content depths and the total water storage was calculated by summing the water storage (S) of various depths. Note, in the storage calculations, we assume that in the winter the HydraProbes are providing reliable measurements of unfrozen water content, and we thus report the total unfrozen storage. In Figure 4-4, for the upslope profile, the general pattern of the water storage implies that in the subsequent winter of 2013-2014 and 2014-2015, the ground froze to maximum depth (~0.9 m) resulting in lower unfrozen water content and thus lower water storage in those winters. And, during spring and summer rain events the water storage rose to maximum (~1.4 m) in 2014 and 2015. Comparably, for 2015-2016 winter the ground froze to minimum depth of 0.4 m, resulting in higher water storage.

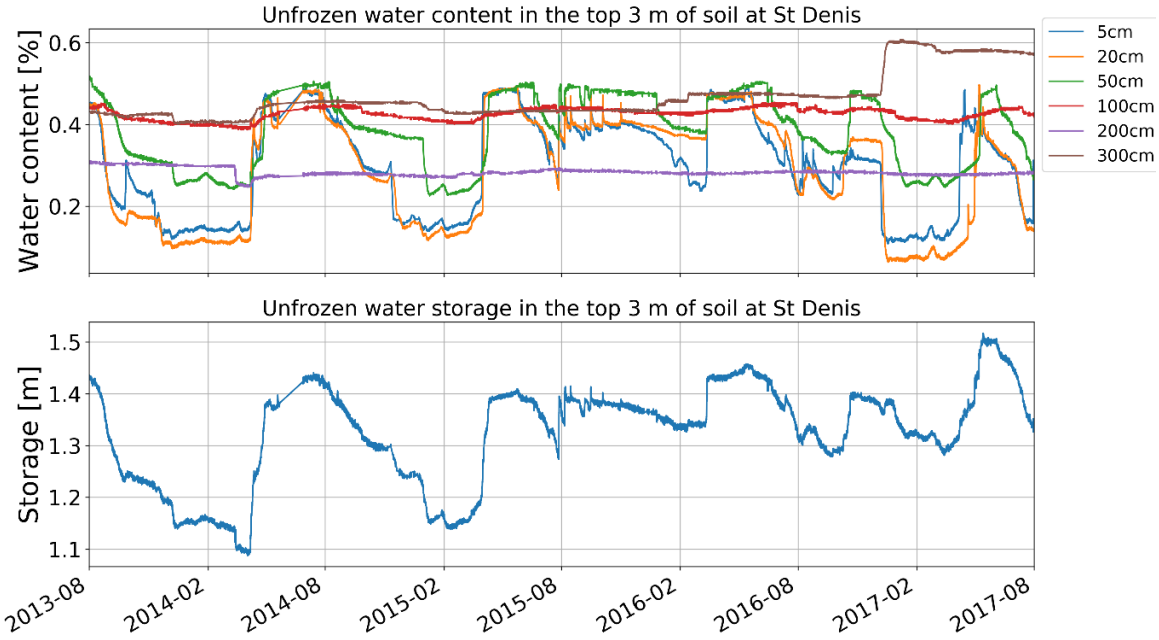

Figure 4-4 Unfrozen water content and water storage in upslope profile of Uri transect

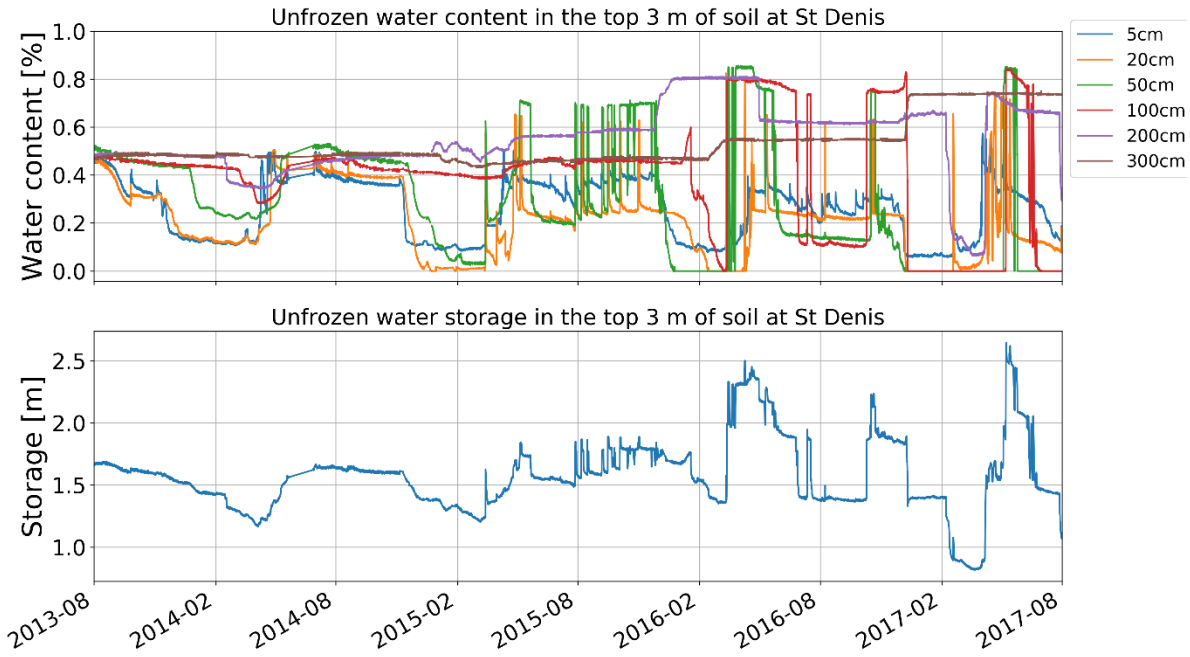

Figure 4-5 Unfrozen water content and water storage in mid slope profile of Uri transect

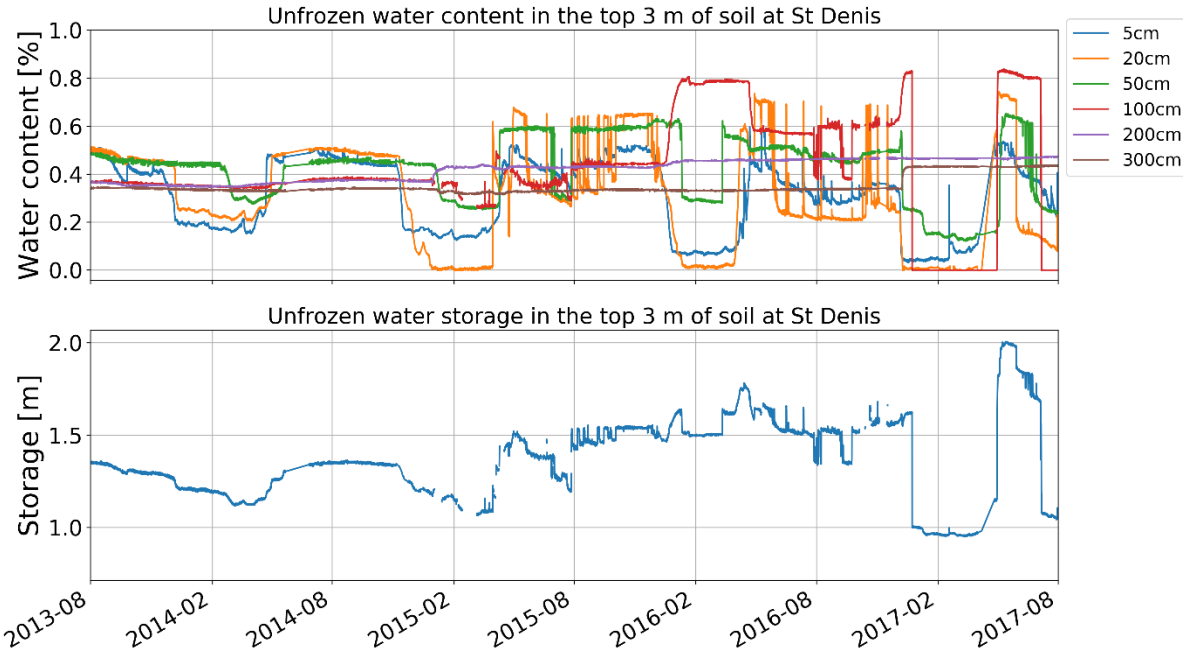

Figure 4-6 Unfrozen water content and water storage in down slope profile of Uri transect

Ground water table

Figure 4-7, shows the change in ground water table in three profiles (upslope, midslope and downslope) along Uri transect. The data was retrieved from October 2013 till date.

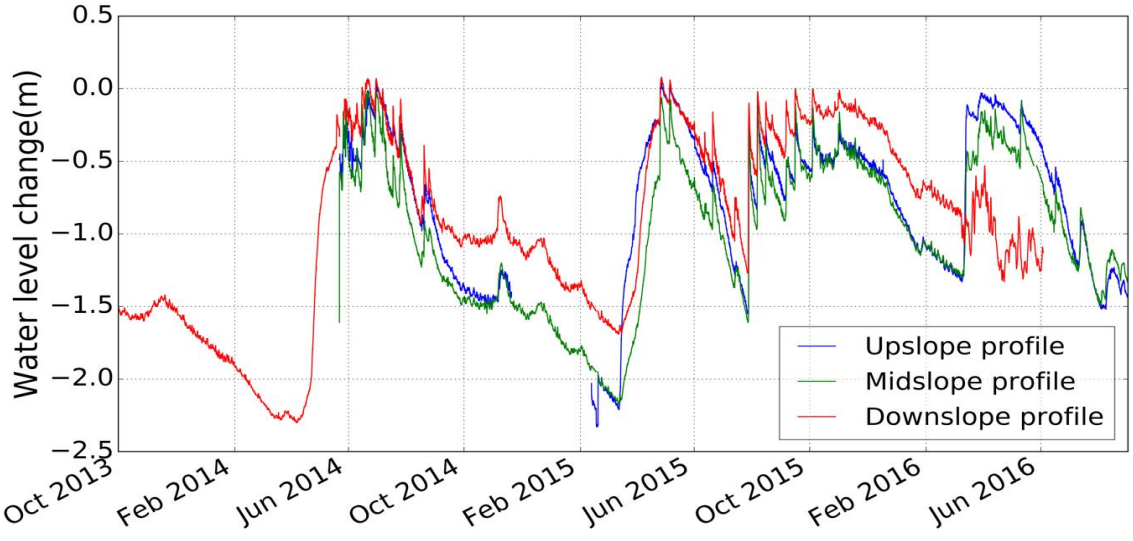

Figure 4-7 Water table level along Uri transect (2014-2016)

The level logger data showed agreeable correlation with each other (with some missing data for upslope and mid slope in 2013 and early 2014). The water table was lowest during the winter of 2013-2014 and 2014-2015 because of deeper soil freezing depth. And, there was a significant rise in the water table during the spring (March, April and May) and summer precipitation (June - July) events in 2014, 2015 and 2016.

It was also noticed that at St Denis depression-focussed recharge has been a major source for the shallow ground water recharge during spring (Hayashi et al., 2003). As described by Hayashi et al. (2003) the infiltration of water through large pores and cracks from partially frozen soil under the pond allowed formation of ground water mound thus resulting in rapid rise of ground water during spring.

4.1.1.3 Quantifying snowmelt rate

The validation of the modelled snowmelt from CRHM was made with the daily snow survey observations taken in 2013 at St Denis by Brannen et al. (2015), who used these data to estimate snowmelt rates. The data was obtained from Brannen. The observed total basin snowmelt in the research was based on the weighted average of the areal fraction of snowmelt at different land cover types (fallow, crop, grass, grass (hayed), wetland vegetation and tress) (Brannen 2015). Whereas, the simulated snowmelt from CRHM was based on the peak SWE of the overall catchment and meteorological data from the scaffolding tower located in the cropland. Figure 4-8, shows the simulated and observed snowmelt period and rate in 2013.

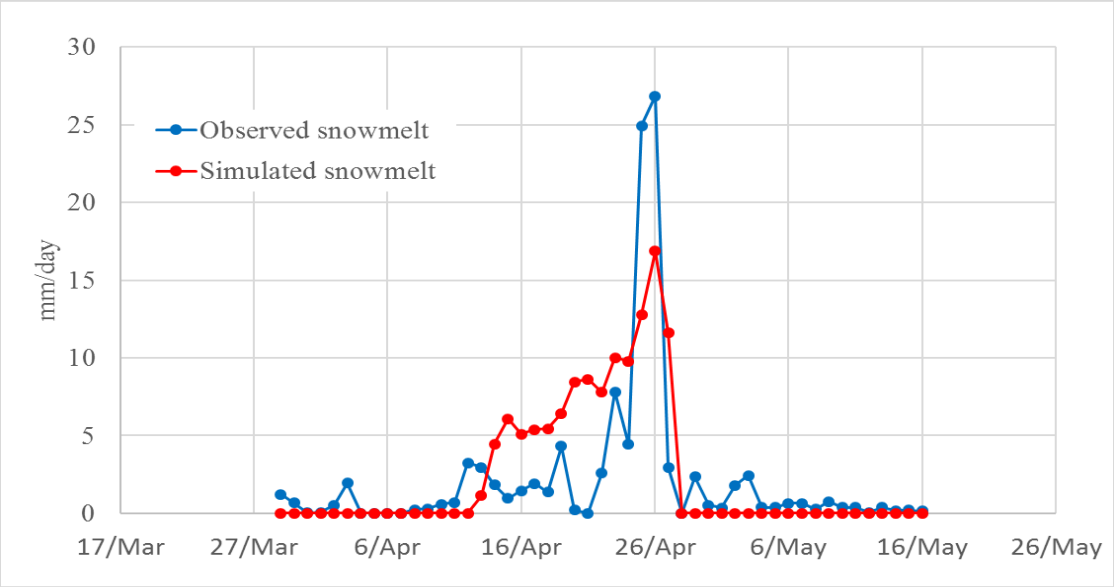

Figure 4-8 Observed and simulated snowmelt rate and period

The simulated snowmelt period fitted quiet well with the observed snowmelt period (11 April- 27 April) with a discrepancy in the peak melt day. There is also small difference in the cumulative total snowmelt (Figure 4-9), which is simply due to the difference in the peak SWE amount used in the CRHM. In CRHM, the SWE value used was the overall landscape estimate at St Denis. However, the observed snowmelt was based on a determined study catchment and was weighted by the areal fraction of different land cover types in the catchment as detailed in Brannen (2015).

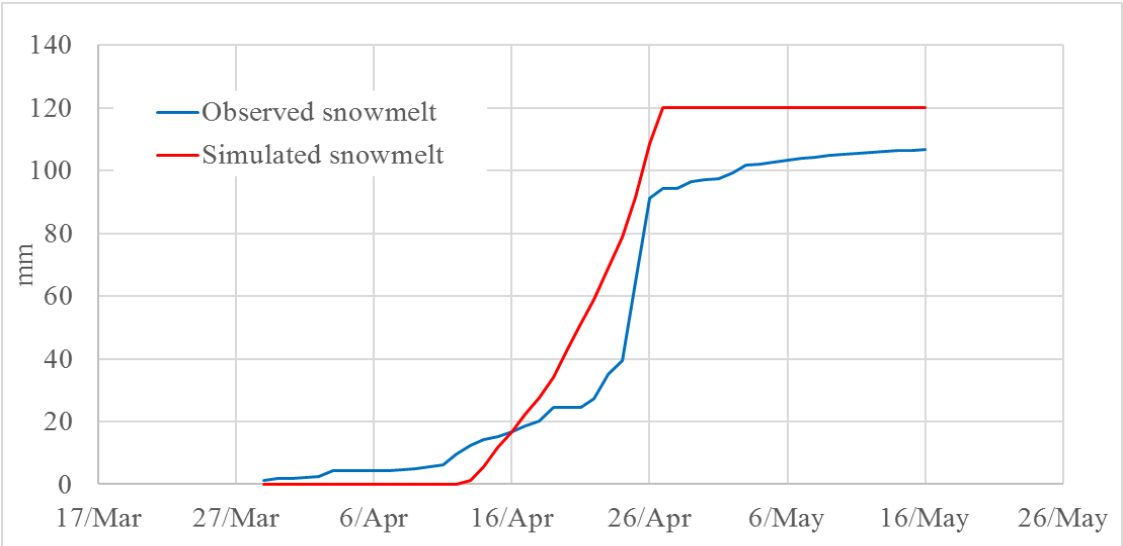

Figure 4-9 Cumulative of observed and simulated snowmelt

Based on this validation with 2013, the snowmelt rate and period was determined for 2012, 2014, 2015 and 2016 (Figure 4-10). It showed that in all years the snowmelt started and ended in the March of that year, except the year 2014, where the snow started to melt only in the beginning of April. This late snowmelt can be explained with the cold air temperature (-15°C to -10°C) till March of 2014.

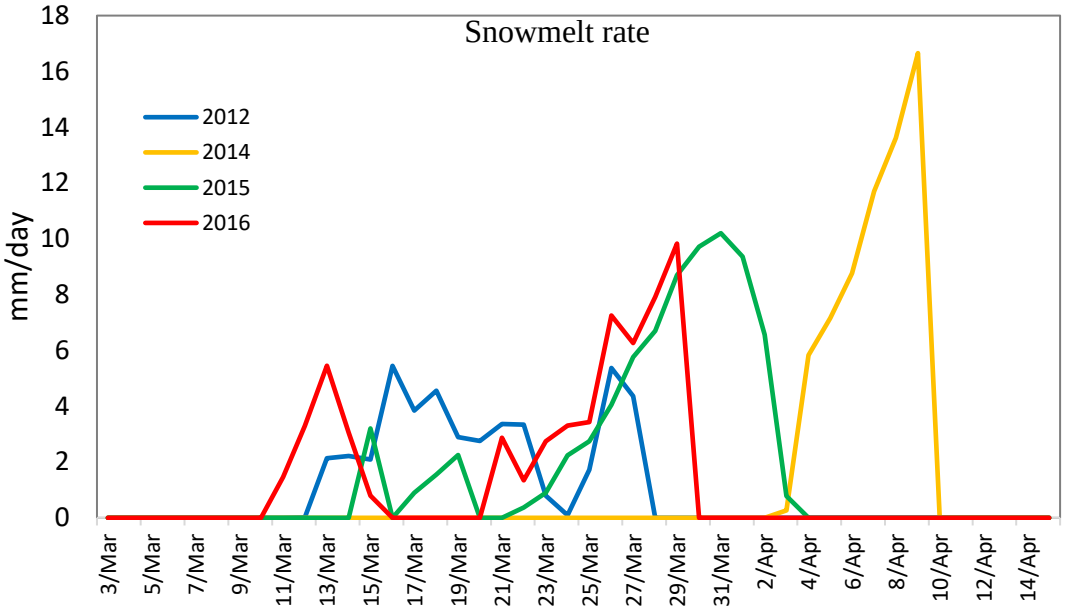

Figure 4-10 Simulated snowmelt at St Denis (2012, 2014, 2015 and 2016)

4.1.1.4 Snowmelt partitioning

Snowmelt partitioning into runoff and infiltration was based on the area, volume and depth relationship (Hayashi and Van Der Kamp, 2000). The runoff travel time for the pond was assumed to be the maximum pond water level taken just before the big rain event. Figure 4-11, shows that there was a rise in the pond water level during the snowmelt period and also during the summer rain event.

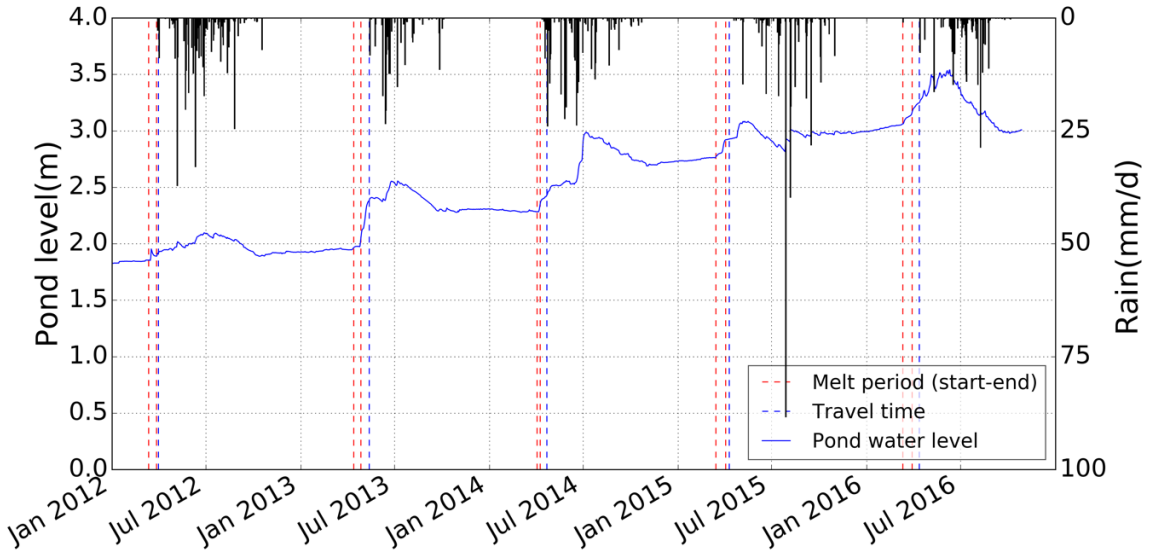

Figure 4-11 Water level in Pond 50 during the snowmelt period

The change in the volume (ΔV) of the pond was determined considering the start and end of the melt period. The snowmelt runoff was then calculated using the change in volume (ΔV) and the total watershed area (WA) of the pond. The basin shape factor 's' and 'p' value for pond 50 was determined as s = 29500, p = 2.45, h_o = 1 and Watershed Area (WA) = 1430000 m^2 (Garth van der Kamp, personal communication, December 5, 2016). The determination of watershed area and basin shape factor uses a LIDAR derived Digital Elevation Model (DEM) of pond 50 with the resolution of 1m and vertical accuracy of 0.15 m as defined by Ehsanzadeh et al.,(2012).

Table 4-1: Surface water balance and partitioning of the snowmelt into runoff and infiltration at St Denis

Snowmelt period		Pond level (m)	Area (A) (m^2)	Volume (V) (m^3)	Change in volume (ΔV)(m^3)	Runoff (mm) ($\Delta V/WA$)	Snowmelt (SWE) (mm)	Rain (mm)	Evaporation (mm/d)	Infiltration (mm) (Snowmelt + Rain-Runoff-Evap.)
Start	2012-03-12	1.85	48867	49928	3232.51	2.26	45	4.7	8.8	38.6
End	2012-03-31	1.92	50265	53160						
Start	2013-04-13	1.96	51237	55476	23265.91	16.27	120	0	24.8	78.9
End	2013-05-13	2.38	59972	78742						
Start	2014-04-03	2.28	57911	72849	8745.25	6.12	64	12.8	21.0	49.6
End	2014-04-22	2.43	60938	81594						
Start	2015-03-15	2.77	67786	103412	10872.64	7.60	76	0	18.0	50.3
End	2015-04-10	2.92	70901	114284						
Start	2016-03-11	3.06	73588	124142	14041.79	9.82	59	0.9	21.64	28.4
End	2016-04-12	3.25	77218	138184						

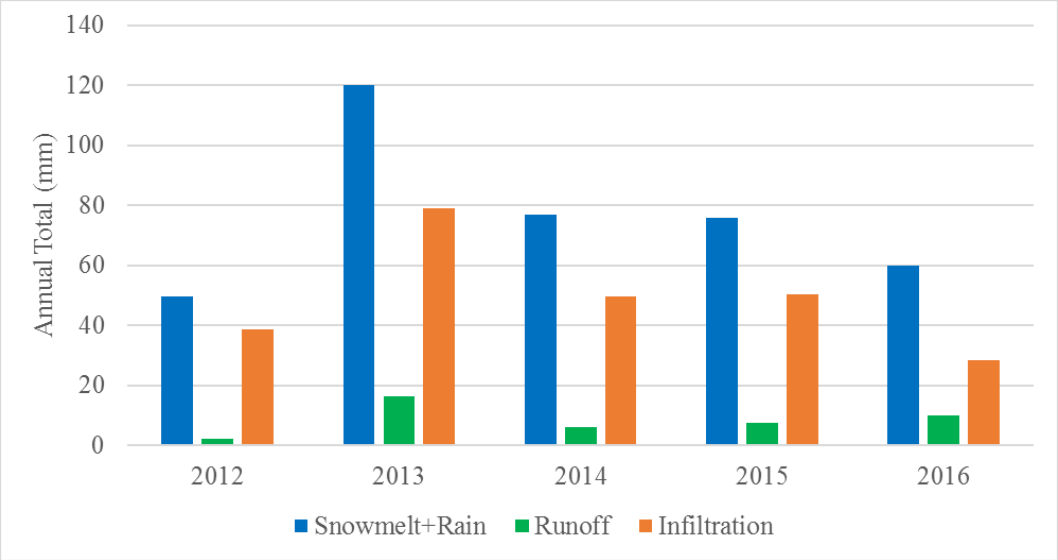

Figure 4-12 Snowmelt partitioning into runoff and infiltration

The partitioning of snowmelt into runoff and infiltration is shown in Figure 4-12. The partitioning was based on the spring snowmelt period taken from

Table 4-1. It was noted that in all years (2012-2016), the runoff generated into the pond ranged between 2.2-16.2 mm. These runoff values were minimum compared to the infiltration (28.6 – 78.9 mm) values, which suggested that the soil at St Denis has high infiltration capacity even when it is frozen. The high infiltration was because of the presence of large pores and cracks which remains air filled during freeze up and creates high hydraulic conductivity during spring snowmelt (Gray et al., 2001).

Garth van der Kamp (unpublished, retrieved through personnel communication, March 17, 2017) has produced similar estimates of runoff for the Pond 50 watershed (Figure 4-13), dating back to 1969, which consistently showed infiltration dominated the study area.

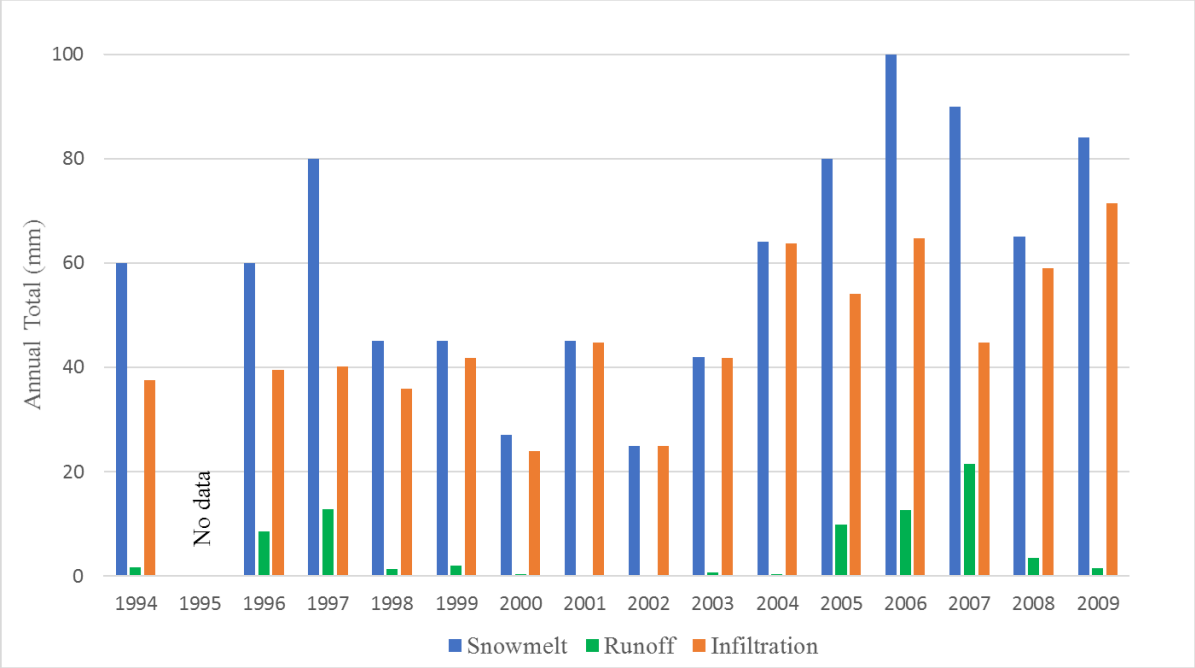

Figure 4-13 Long-term snowmelt partitioning into runoff and infiltration (received through personnel communication with Garth van der Kamp, December 5, 2016)

Hayashi et al., (2003) also performed a detailed study on infiltration of snowmelt in partially frozen soil considering pond 109 and determined that the runoff values (ranged between 6-19 mm) were much smaller than the infiltration values (25-29 mm). They also determined that the lower antecedent soil water content and dry soil during the fall of 1999 produced higher infiltration in the subsequent spring of 2000.

4.1.1.5 Spatio-temporal variation of water content at St Denis

Along the Uri transect at St Denis, the soil water content profiles for pre-freezeup, during melt/thaw and post-thaw conditions are shown in Figure 4-14. The pre-freezeup, during melt/thaw and post-thaw conditions were determined tentatively as October, April and June respectively for different years (2014, 2015 and 2016). For example, for 2014, the pre-freezeup, during melt/thaw and post-thaw water content observations were determined as an average water content of October 2013, April 2014 and June 2014 respectively.

The observations in different profiles showed that the water content noticeably changed up to top 1 m depth of the soil profile, changing less prominently below 1 m. This changes signify the nature

of the fractured clay soil resulting high water content variability for the top soil layer which then lowers in the bottom layer.

It was also noted that in 2014 and 2015 the soil had dry antecedent water content (i.e. pre-freeze up) compared to 2016 in all the profiles. The dry soils in 2014 and 2015 produced less runoff (6.12 m and 7.6 m respectively) compared to 2016 (runoff value of 9.82 m). This runoff value is consistent with the established idea that the infiltration capacity in frozen soils is higher in dry antecedent water content conditions and lower in wet antecedent water content conditions (Gray and Landine, 1988). It is also worthwhile noting that there is much variation in the water content for different depths in different profiles along the transect highlighting the complexity of spatial and temporal variation of water content for accurate soil water storage and water balance in the study area.

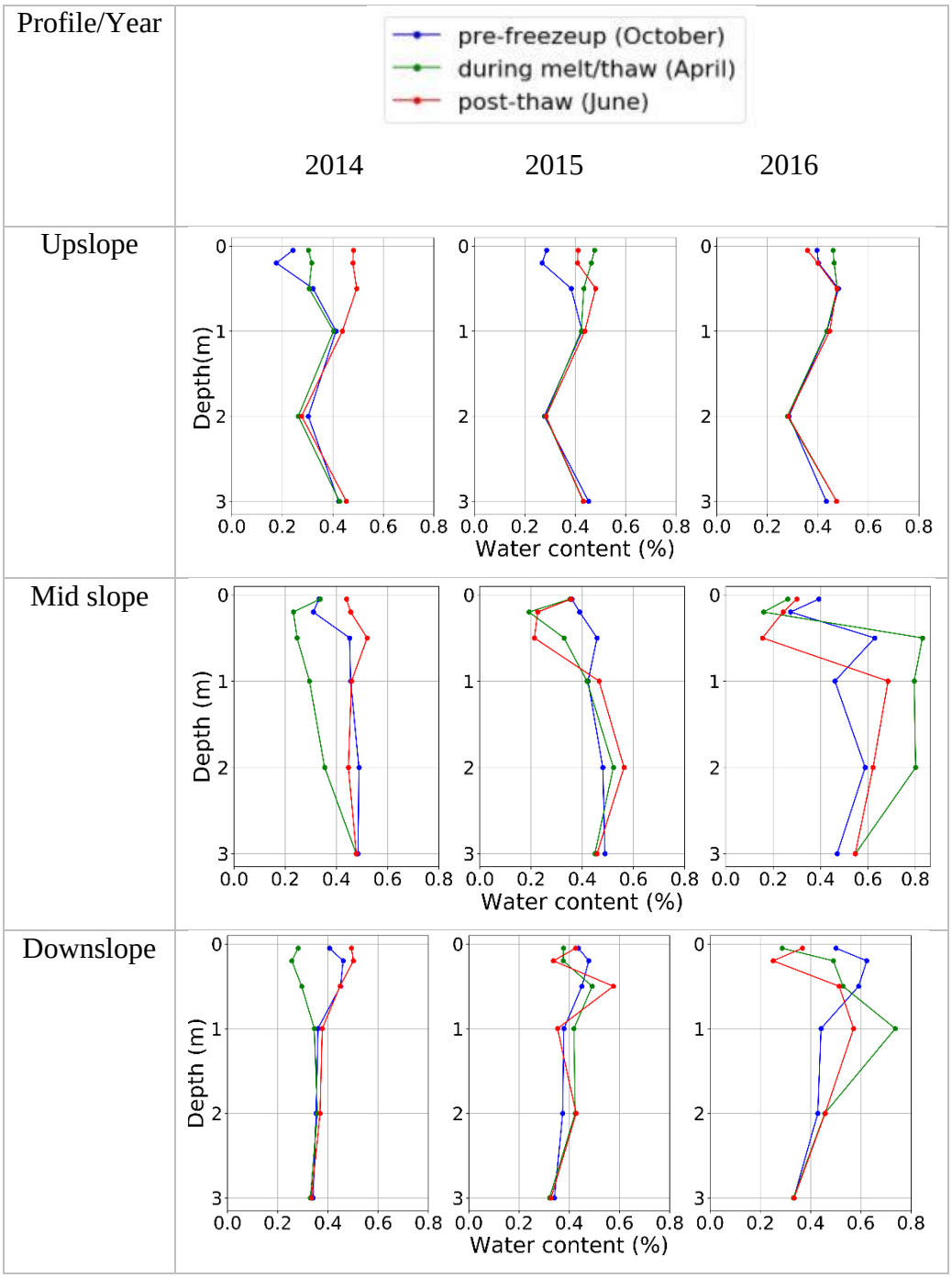

Figure 4-14 Spatio-temporal variation of water content in shallow vadose zone at different locations

4.1.2 Field based data observations at Brightwater Creek (BWC)

Various hydrological data from Brightwater creek (BWC) was plotted and analyzed for insights into the vadose zone hydrological processes. However, due to lack of accurate discharge measurement the snowmelt processes were analysed on qualitative understanding of available hydrological data. The overall fluctuations of major variables in vadose zone at BWC is summarised in Appendix E (Figure E.2).

4.1.2.1 Hydrological Data

Snow Water Equivalent (SWE)

Figure 4-15, shows the Snow Water Equivalent (SWE) recorded at Brightwater Creek (BWC). The snow survey was performed every year before the snowmelt period (March) to determine the SWE and snow depth. There was comparatively less SWE (33.2 mm) in 2015 with highest recorded as 88.5 mm in 2011. The mean SWE (2007-2016) recorded was 62.42 mm.

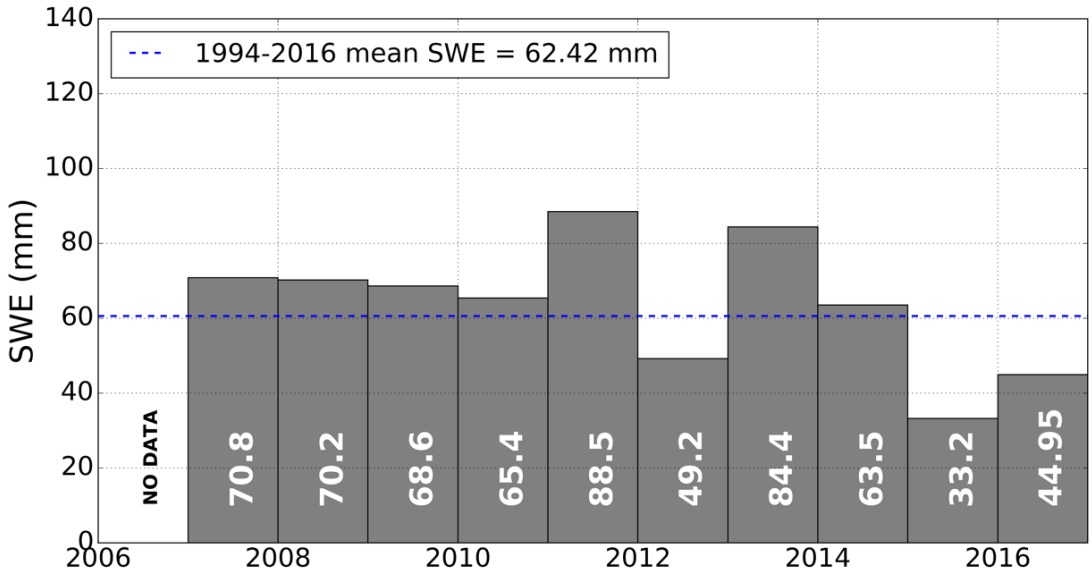

Figure 4-15 Annual Snow Water Equivalent at BWC (2007-2016)

Soil freezing

The depth of zero-degree isotherm was determined along the transect in three profiles (P1, P2 and P3) is shown in Figure 4-16. The soil temperature was measured up to the depth of 1.6 m.

It was observed that the maximum freezing depth measured in the winter of 2013-2014 and 2014-2015 was 1.6 m and the figure also shows that the soil might still be freezing beyond 1.6 m. The deeper soil frost in both the years was due to colder air temperature (~ -15 ℃ to -20 ℃) during winter and might be due to higher antecedent soil water content from the summer rain, in 2013 (rainfall= 207 mm) and 2014 (rainfall= 393 mm). However, the soil freezing depth in the winter of 2015-2016 was comparably low, which was due to less cold air temperature (~ -5 ℃ to -8 ℃) during winter. The SWE recorded in 2015-2016 was 33.2 mm which also provided less insulation resulting in some freezing depth.

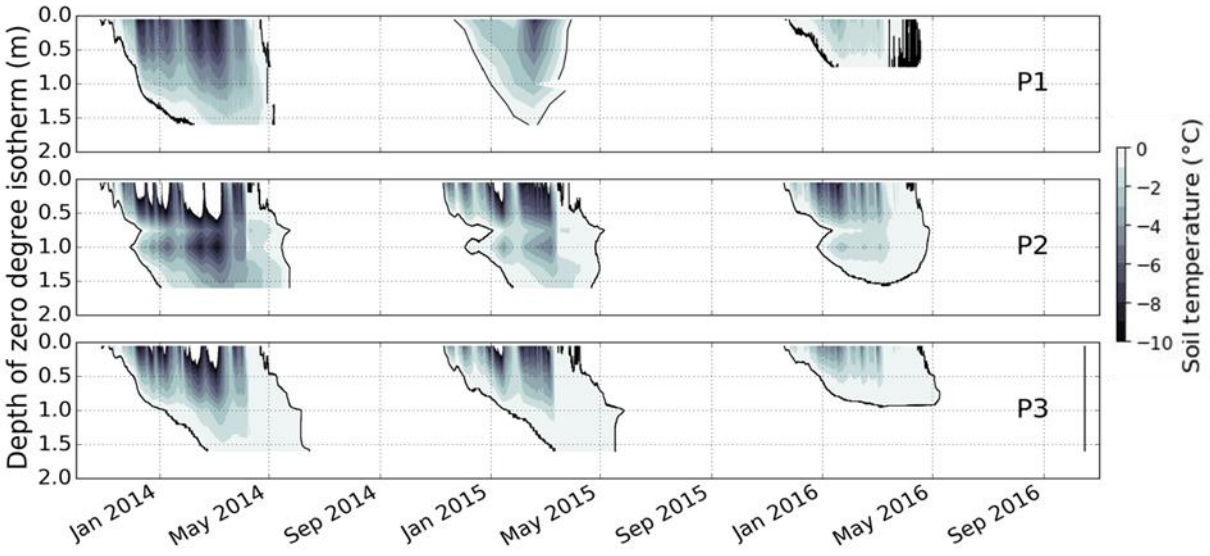

Figure 4-16 Soil freezing depth of three profile (P1, P2 and P3)

Unfrozen water content and water storage

For profile P1, P2 and P3 the unfrozen water content data is available at various soil depths for top 0.5 m, 1.6 m and 1.6 m respectively at BWC. Figure 4-17, Figure 4-18 and Figure 4-19 shows the unfrozen water content and water storage for P1, P2 and P3 profile respectively. The unfrozen water storage of the soil was calculated from the unfrozen water content data as described previously in the St Denis result section. From the water content figures, it was noted that the greatest porosity of the soil at BWC is ~ 0.5 m^3/m^3. It was also noticed an increase in the unfrozen water content after the winter and during the spring, which is due to thawing and snowmelt infiltration during snowmelt period. The volumetric water content measured at various depth also suggested that the soil water content fluctuated greatly in top 1 m of the unsaturated soil profile.

From the unfrozen water storage figures, it was noticed that the calculated water storage was higher for profile P3 compared to other profiles (P1 and P2), which is consistent with the presence of depression focussed recharge phenomenon (Hayashi et al., 2003), where the overlying snow and surface water was collected in the depression, which increased the water storage of underlying soil and also recharged the groundwater. It should also be noticed that the total unfrozen water storage plotted during winter was affected by the storage of frozen water which is not measured by the HydraProbe. Thus, resulting in large swing of water going into the subsequent spring thaw period.

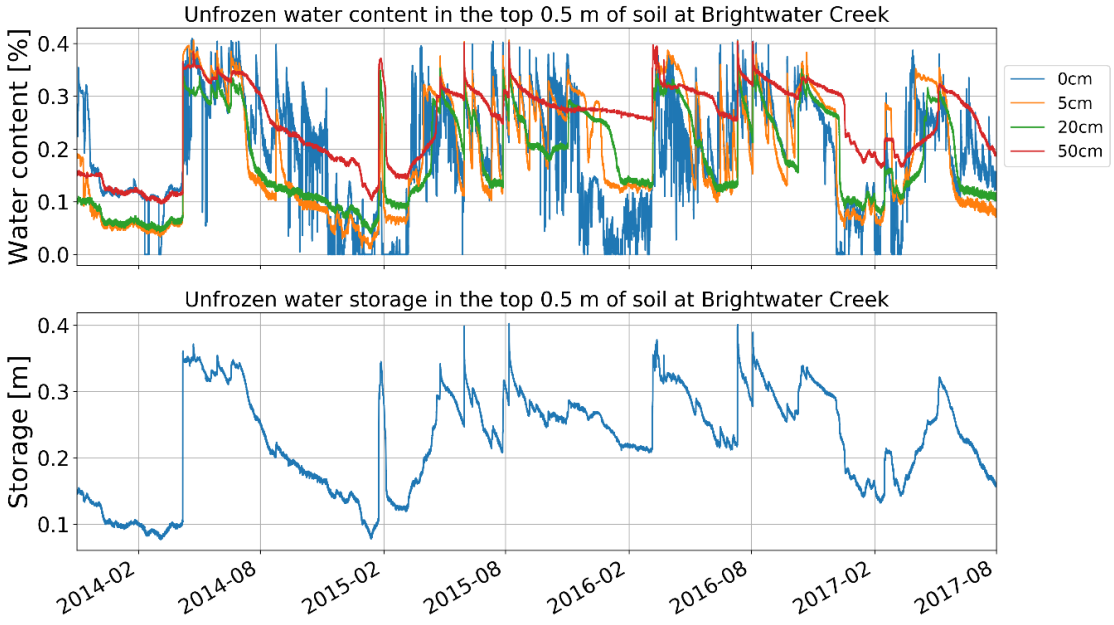

Figure 4-17 Unfrozen water content and water storage in P1 profile

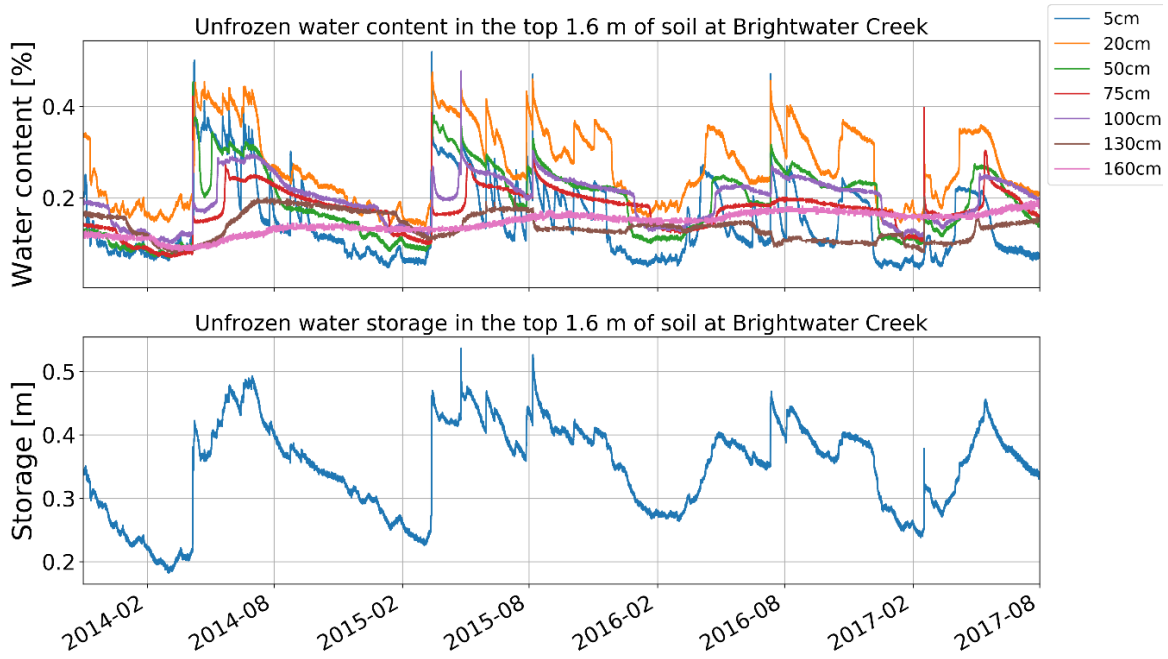

Figure 4-18 Unfrozen water content and water storage in P2 profile

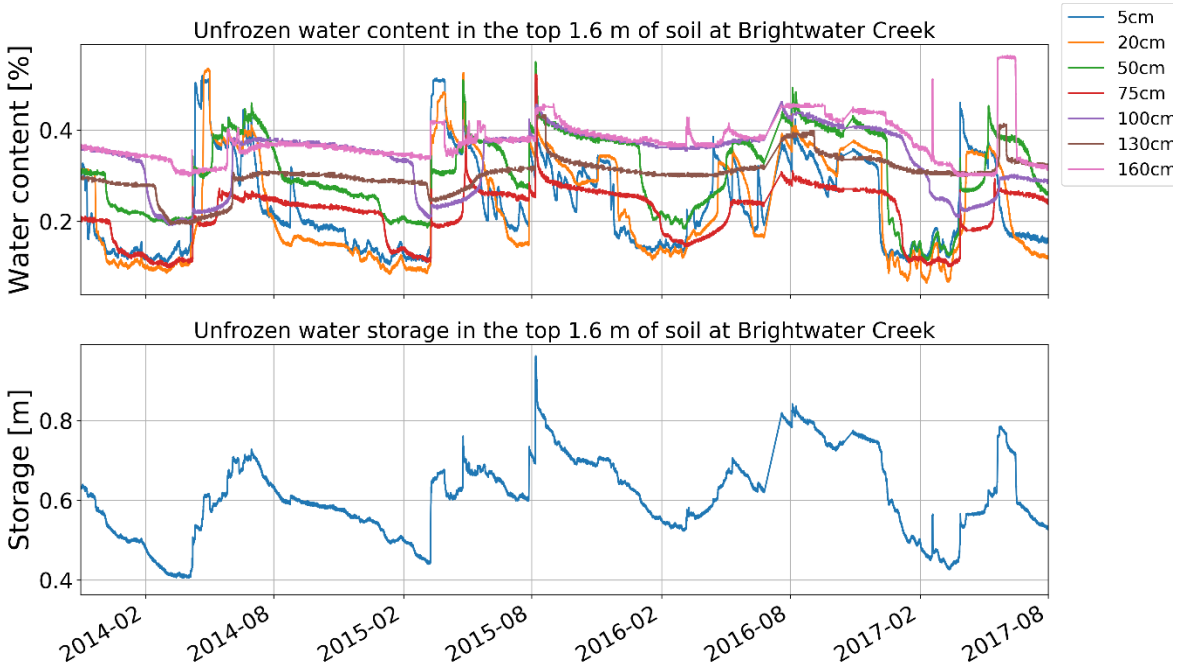

Figure 4-19 Unfrozen water content and storage in P3 profile

Ground water table

The ground water level was collected along the transect from October 2013 onwards. Figure 4-20, shows the changes in the ground water level for various profiles (P1, P2 and P3) at BWC.

The data showed agreeable correlation with each other during all seasons, with some missing data from P3 profile during the winter of 2016. The water table level for P3 increased significantly than P1 and P2 during the spring snowmelt and peaked during the summer suggesting the behaviour of depression focussed recharge mechanism in the study area as discussed by (Pan et al., 2017).

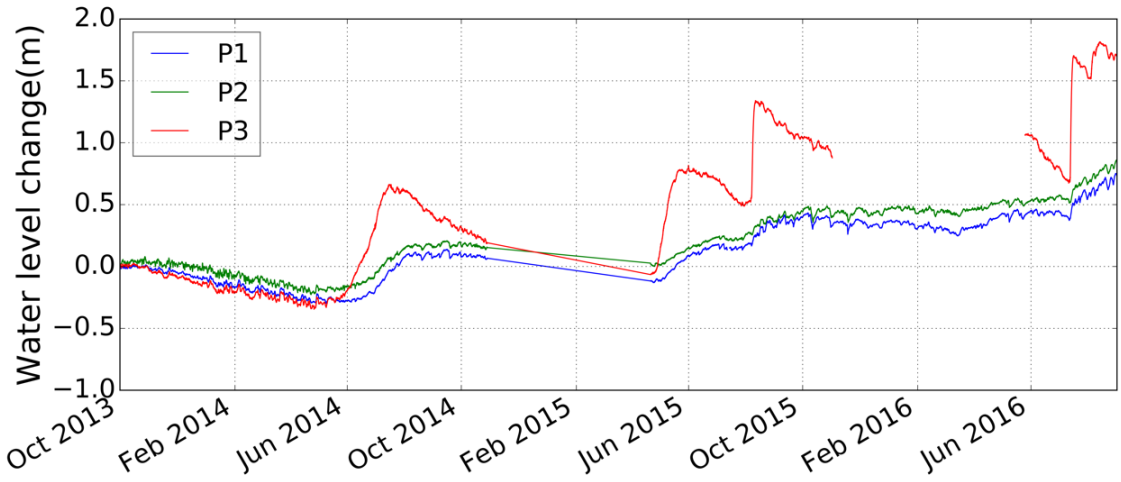

Figure 4-20 Change in groundwater level along the transect at BWC

4.1.2.2 Spatio-temporal variation of water content at BWC

Figure 4-21, shows the water content at various profiles and depths for the pre-freeze-up, during melt/thaw and post-thaw period taken in October, April and June respectively. The observation showed higher antecedent soil water content for profile P1 compared to P2 and P3 in the pre-freeze-up period. It was also noticed that there was variation in the water content values during melt/thaw and post-thaw period in these profiles for different years.

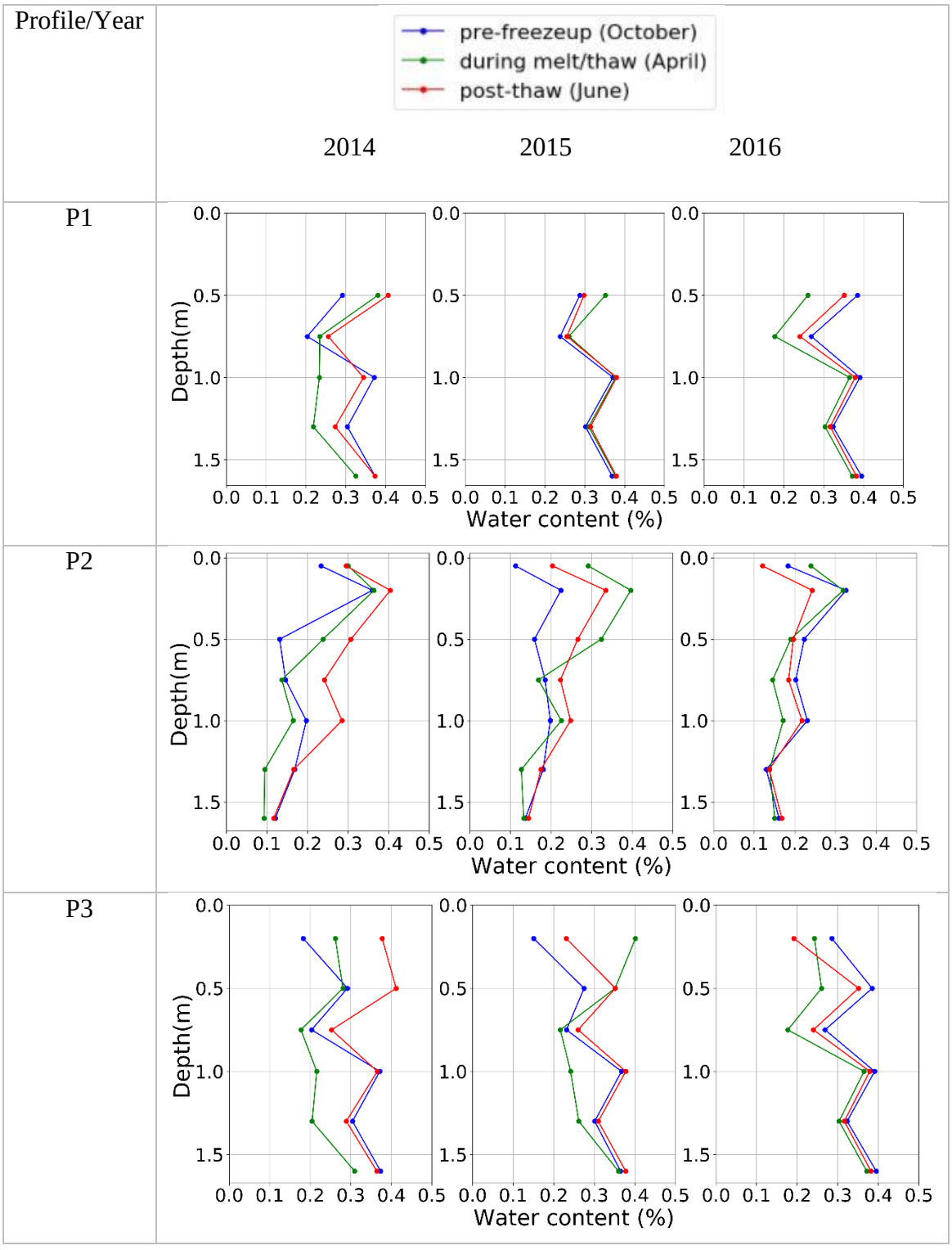

Figure 4-21 Spatio-temporal variation of water content in shallow vadose zone at BWC

4.2 Establishing Soil Water Characteristic (SWC) and Soil Freezing Characteristic (SFC) Curves

This section discusses the second objective of fitting the Soil Water Characteristics (SWC) and Soil Freezing Characteristics (SFC) curves under unfrozen and frozen conditions with results and discussion from the study sites.

4.2.1 Validation of Log-normal Pore Size Distribution model (LNPSD) with van Genuchten model (VGM) for Soil Water Characteristics (SWC) curve

The equivalency of the LNPSD with that of the VGM model for SWC curve was determined by fitting the VGM with six example soil types (Hygiene sandstone, Silt LoamGE3, Guelph Loam drying, Beit Netofa Clay, Touchet Silt Loam and Guelph Loam wetting) (van Genuchten, 1980) using the LNPSD model. The fitting of the models was performed by minimizing the Root Mean Squared Error (RMSE), calculated based on the differences of water content (θ) between two models (Table 4-2). The residual water content (θr) was rescaled to zero in both the models, which signifies there is no residual water content in the pore space of the soil and the saturation water content(θs) is the relative water content. Figure 4-22 shows the SWC curve for above mentioned soils fitted using LNPSD model.

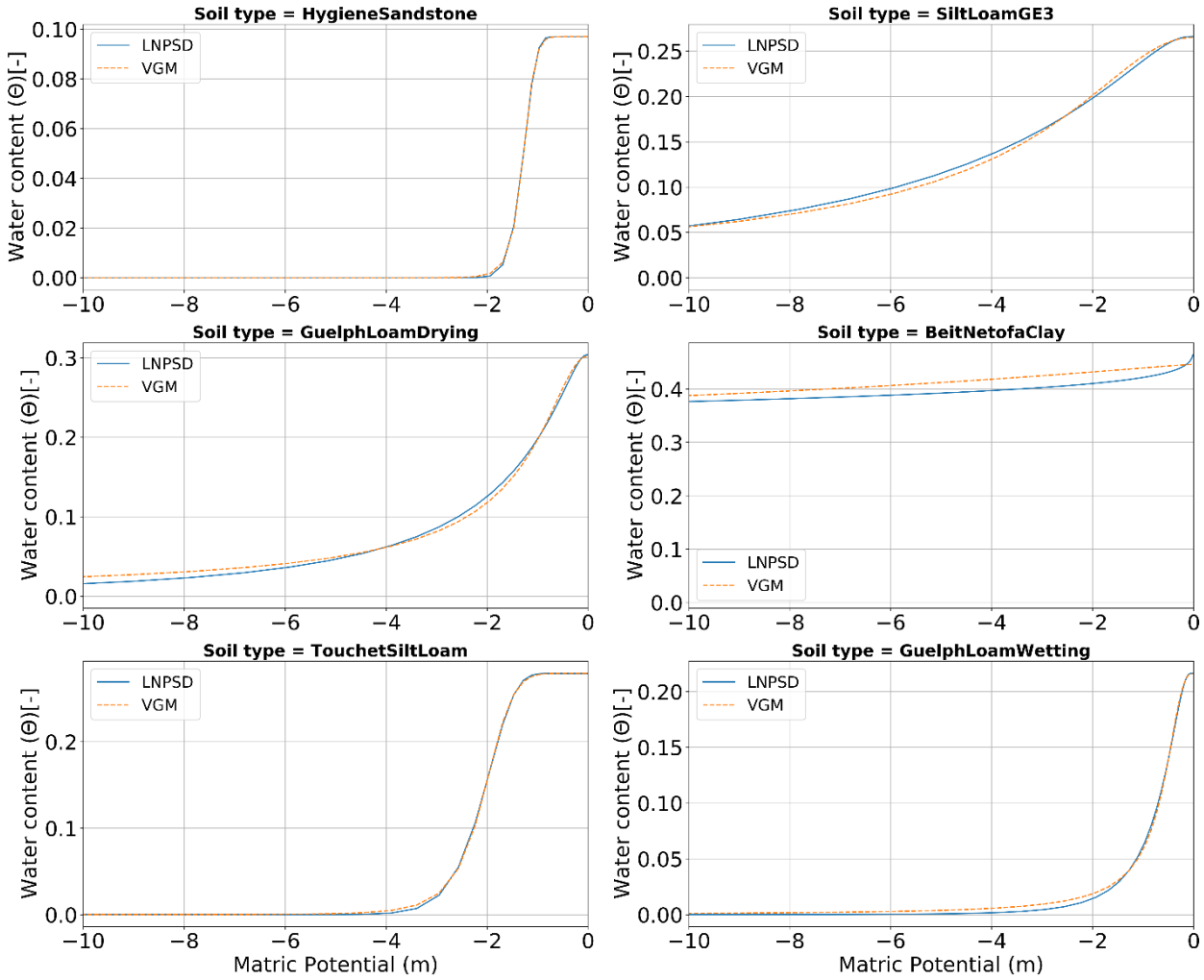

Figure 4-22 Fitting LNPSD with VGM for different soil types

Table 4-2 Fitted parameter values of LNPSD for the retention curves plotted in Figure 4-22

Soil type	Soil porosity (n)	Log mean pore radius (lr_m)	Log standard deviation of pore radii (lr_s)	RMSE
Hygiene sandstone	0.09	-4.93	0.07	0.0002
Silt Loam G.E. 3	0.26	-6.49	0.48	0.0033
Guelph loam (drying)	0.30	-6.12	0.49	0.0039
Beit Netofa Clay	0.46	-144.23	5.23	0.028
Touchet Silt Loam	0.27	-5.17	0.11	0.0007
Guelph loam (wetting)	0.21	-5.09	0.32	0.0016

It was noted that the LNPSD model fitted agreeably with the VGM for all six soil types except clay. The fitting for clay was poor at lower matric potential (Figure 4-23). It is well known that the clay has smaller pore size so it retains more water at higher matric potential. So, there may be limitation to fit the clay using the LNPSD model. Moreover, it was also observed that the residual water content for clay in VGM did not converge to zero even at maximum matric potential which might need further research.

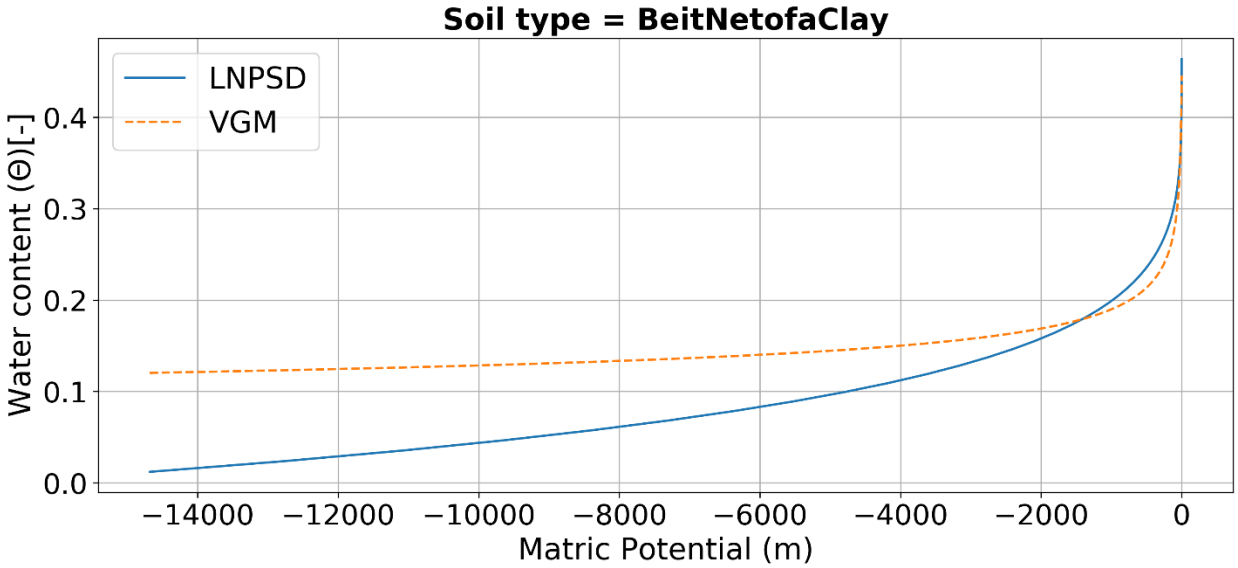

Figure 4-23 Fitting LNPSD and VGM model for clay at maximum matric potential

4.2.2 Simultaneous fitting of the Soil Water Characteristic (SWC) and Soil Freezing Characteristic (SFC) curves at St Denis

The observed SWC curve (i.e. the red dots in Figure 4-24) was determined using the summer water content data (August-October) and the observed SFC curve (i.e. the blue dots in Figure 4-24) was determined using the winter unfrozen water content data (November-January). The depth of water content observation was 5 cm. It was noticed that there was a high residual water contents during the frozen condition. Moreover, it was also noted that the freezing process in SFC curve continued from where the drying process ended, which makes the initial water content of SFC similar to that of the final water content of SWC.

The LNPSD model describes the SWC and SFC curves with a single set of parameters, and it was attempted to identify these parameters for both curves with the observations from the upslope

profile at St Denis. Extreme outliers were removed from the observations for the fitting purpose. The fitting between the observed and the modelled SWC and SFC curves was achieved by minimizing the Root Mean Squared Error (RMSE).

In ideal situation, both the SWC and SFC curves should be defined with the same parameters such that the fitted parameters values with one curve can be used to validate the other. The LNPSD model was first calibrated to the SWC curve (showing an excellent fit) and validated with the SFC curve (Figure 4-24). But fitting to the SFC curve resulted poor performance. The curve fitted to SWC losses water content way to quickly under the frozen condition.

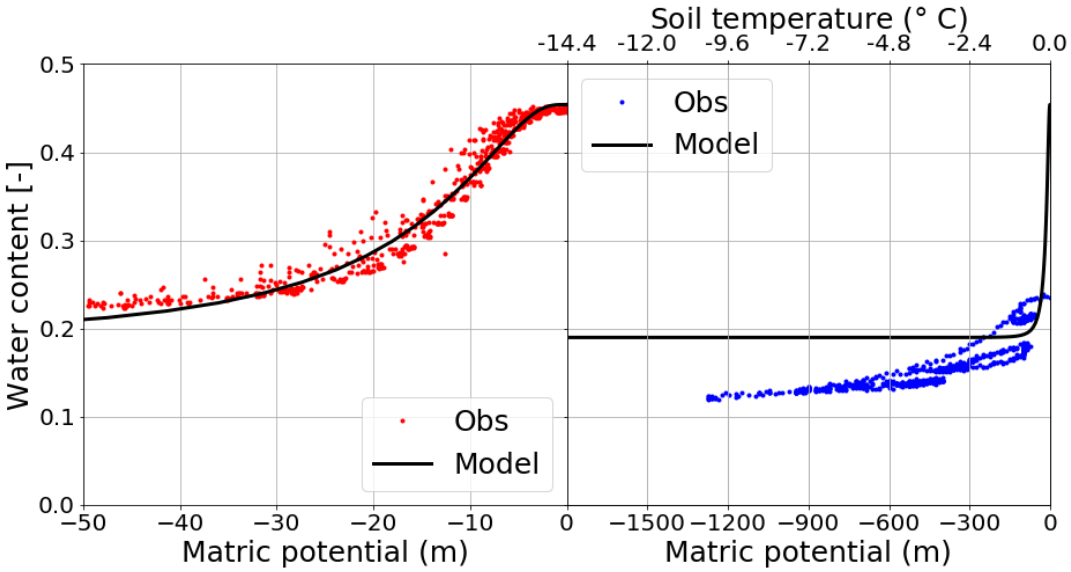

Figure 4-24 Fitting LNPSD model with observed SWC curve and validating with observed SFC curve

Alternatively, fitting was performed with the SFC curve minimizing the RMSE error and found a good agreement but again the parameter validation failed when used with the SWC curve (Figure 4-25). This time, the curve fitted to the SFC did not wet up enough during drying condition. So, it was concluded that fitting could not be performed for both curves simultaneously with a single set of parameter values at same time.

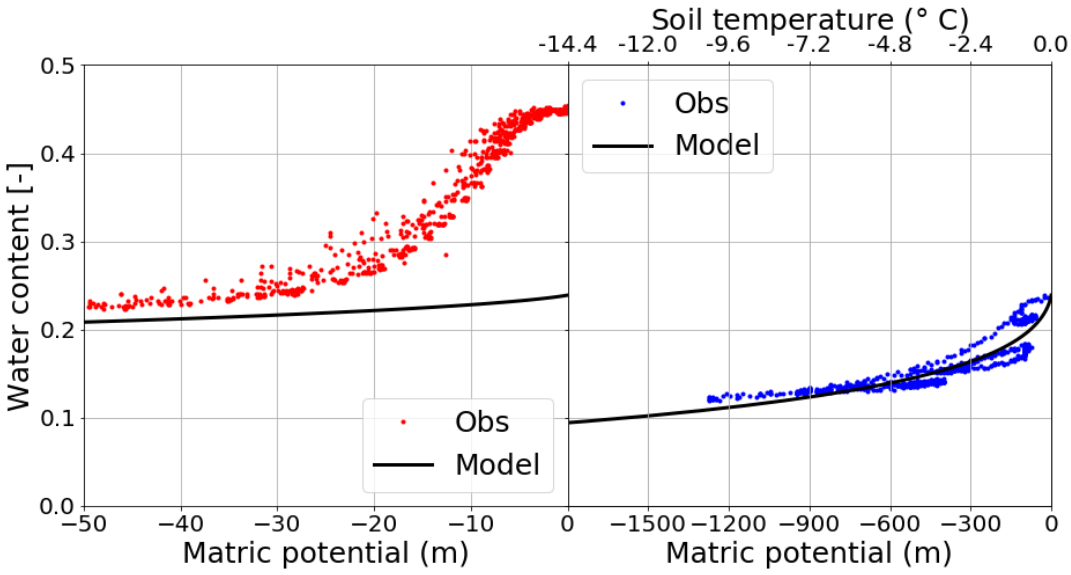

Figure 4-25 Fitting LNPSD model with observed SFC curve and validating with observed SFC curve

To solve this issue, the concept of dual continuum media in LNPSD model was introduced where the parameter value fits the SWC curve (affected by larger pores) and also fits the SFC curve (affected by smaller pores) simultaneously (Figure 4-26). The range of the equivalent matric potentials during the freezing (based on the Generalized Clausius –Claperyron Equation, Edlefsen and Anderson, 1943), was also much lower than the range of the potentials during drying. The fitting ultimately results in two sets of parameters that fits both curves simultaneously. The parameters determined for soil pore size distribution at St Denis on log scale are detailed in Table 4-3.

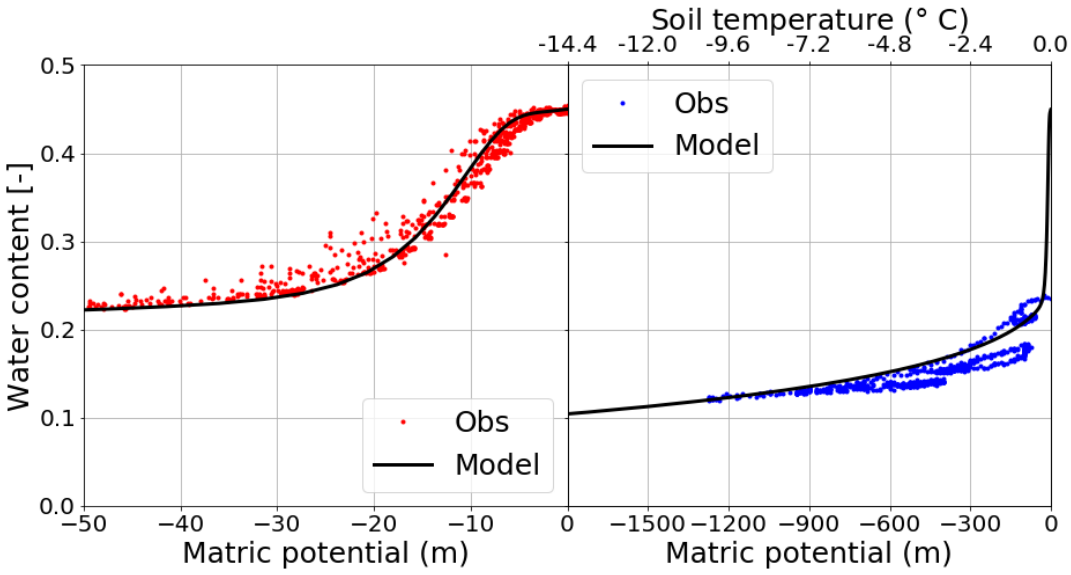

Figure 4-26 Fitting observed SWC and SFC curve with dual porosity LNPSD model

Table 4-3 Fitted parameter values of LNPSD at St Denis

Soil domain	Soil porosity (n)	Log mean pore radius (lr_m)	Log standard deviation of pore radii (lr_s)	RMSE
Large pore-size	0.2	-6.1	0.2	0.012
Small pore-size	0.25	-17	1.36	0.01

Likewise, the LNPSD model was used for fitting the observed SWC and SFC data at Brightwater Creek (BWC) for 2013 and different sets of parameter values were obtained. The parameters determined for the soil pores size on log scale are detailed in Table 4-4.

Table 4-4 Fitted parameter values of LNPSD at BWC

Soil domain	Soil porosity (n)	Log mean pore radius (lr_m)	Log standard deviation of pore radii (lr_s)	RMSE
Large pore-size	0.08	-5.8	0.235	0.01
Small pore-size	0.36	-24.25	1.96	0.07

4.2.3 Validating the SWC and SFC curves at St Denis

The volumetric water content [-], the matric potential, ψ (m) and the soil temperature (℃) was retrieved from the three profiles (upslope, mid-slope and downslope) of Uri transect at St Denis. The water content was plotted against matric potential to produce Soil Water Characteristic (SWC) curve and the water content was plotted against soil temperature for the Soil Freezing Characteristic (SFC) curve.

The LNPSD model with the determined parameter values from Section 4.2.2 (Table 4-3) was used to fit with the observed SWC and SFC curves for all three profiles at various depths (5, 20, 50 and 100 cm) and years (2013, 2014, 2015 and 2016). Figure 4-27, Figure 4-28 and Figure 4-29 demonstrates the fitting performed on the observed SWC and SFC curves at various depths and years. The solid black line is the water content value from the model fit and the colored dots are the observed water content values in different years. The variation in the water content value in different years might be attributed to hydrological variation and heterogeneity associated with the study area. For example, different rate of precipitation, evaporation, infiltration, soil type and so on.

It was observed that for most of the years and soil profiles, there was a good agreement between the modelled and the observed water content. However, some poor fit was also noticed in some profiles and years which pointed out that it was not possible to fit all the observations perfectly with the same set of parameter value. But, considering the overall fitting it was decided to use the same parameters value for the snowmelt infiltration models for the third objective of this research.

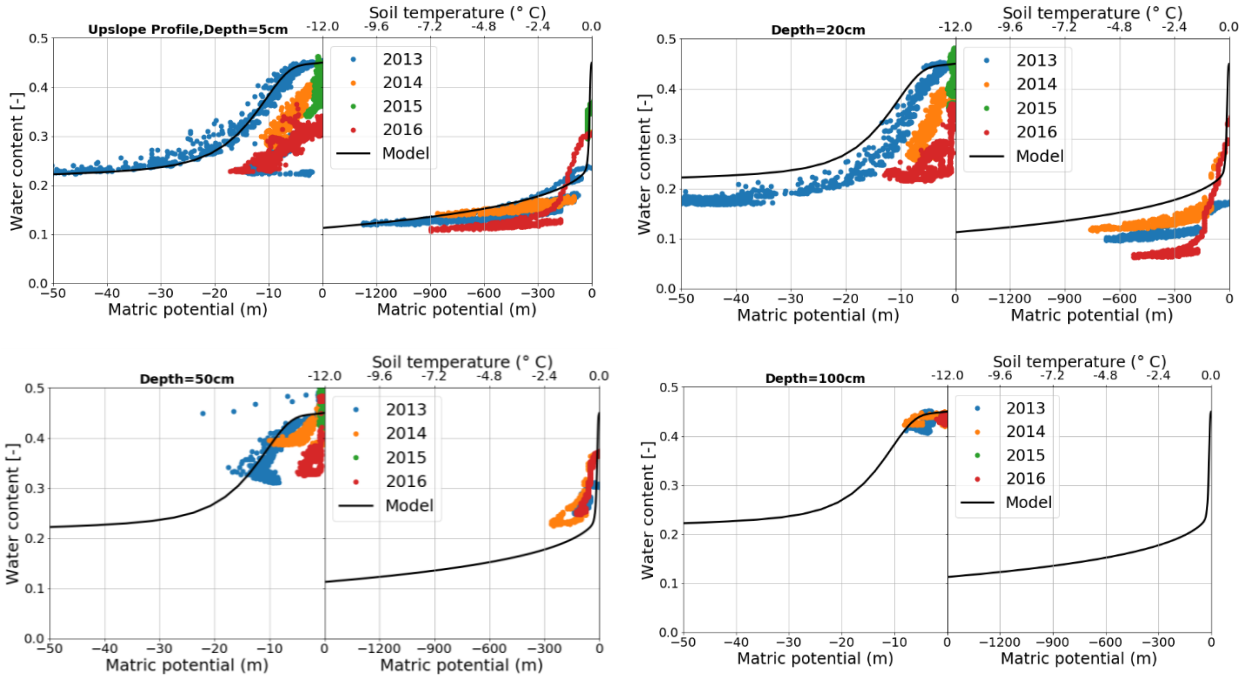

Figure 4-27 Fitting LNPSD model with observed SWC and SFC for upslope profile at St Denis

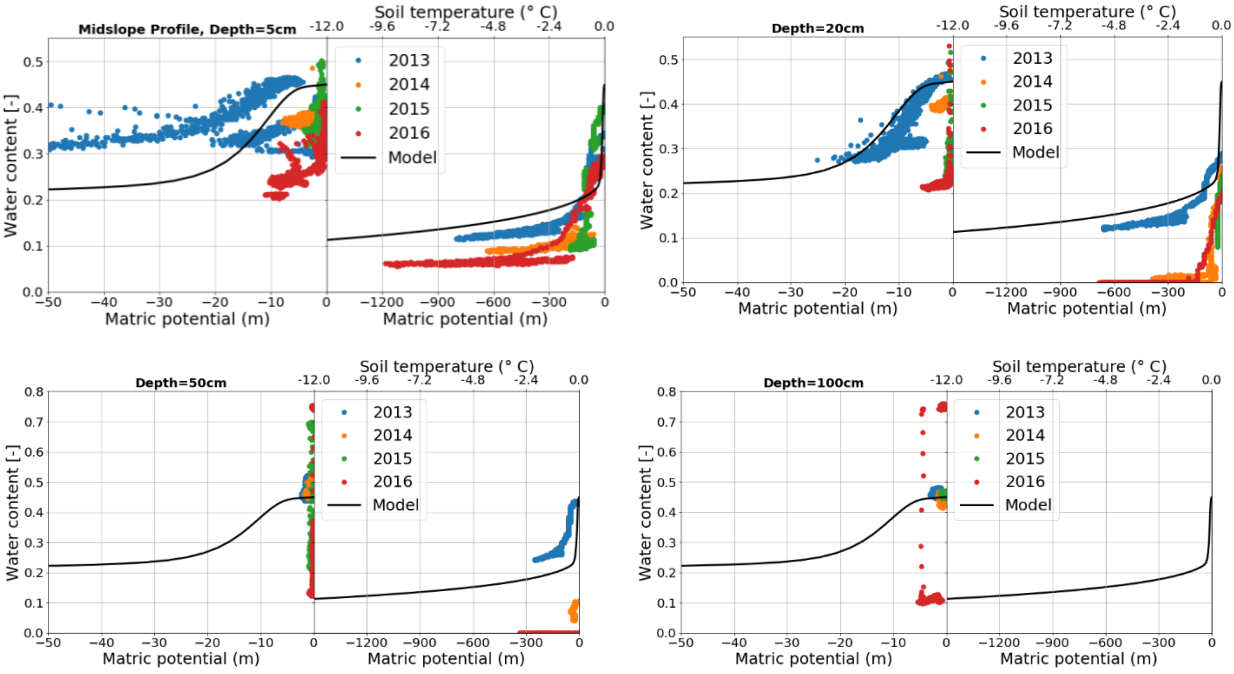

Figure 4-28 Fitting LNPSD model with observed SWC and SFC for midslope profile at St Denis

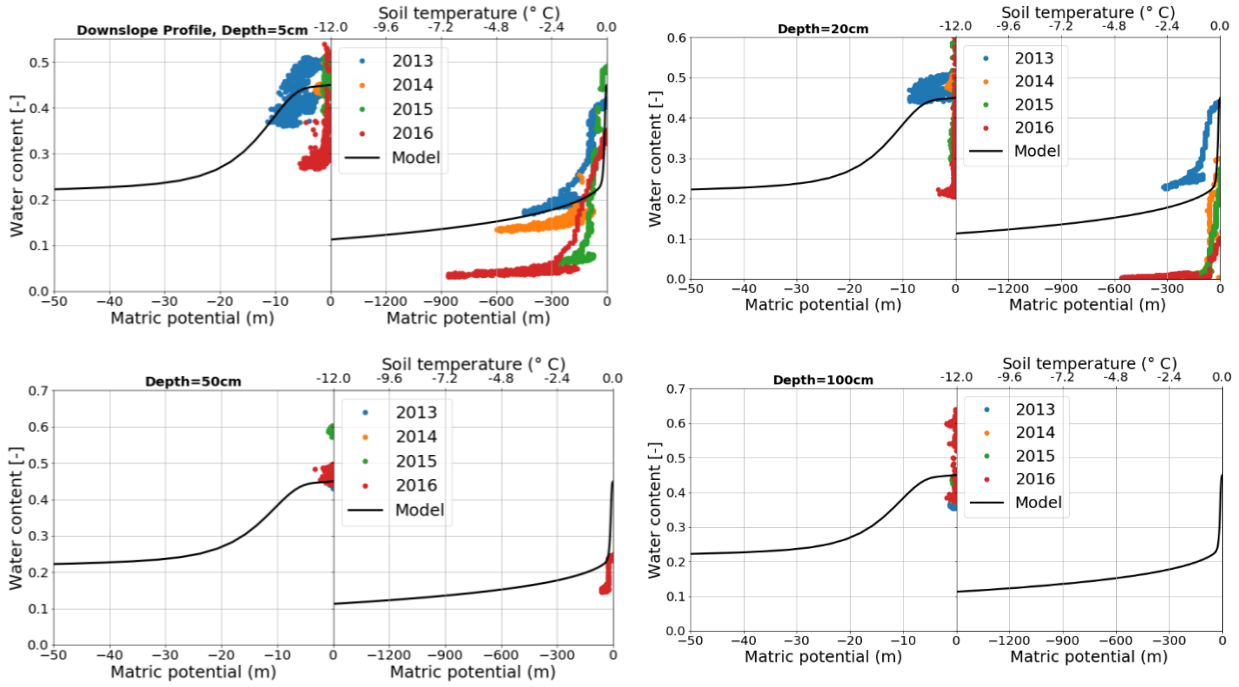

Figure 4-29 Fitting LNPSD model with observed SWC and SFC for downslope profile at St Denis

4.2.4 Validating the SWC and SFC curve at Brightwater Creek (BWC)

The LNPSD model was also fitted with the observed SWC and SFC for three profiles (P1, P2 and P3) along the transect at BWC. The model parameters were taken from Section 4.2.2 (Table 4-4). Figure 4-30, Figure 4-31 and Figure 4-32 shows the fitting performed at different profiles, depths and years. For the P1 profile, the observed water content data was only available for the top 50 cm and for P1 and P2 profile the data was available up to the depth of 160 cm. It was observed that for most of the years and soil profiles at BWC, there was a good agreement between the modelled and the observed water content with certain exceptions in some profiles and depths.

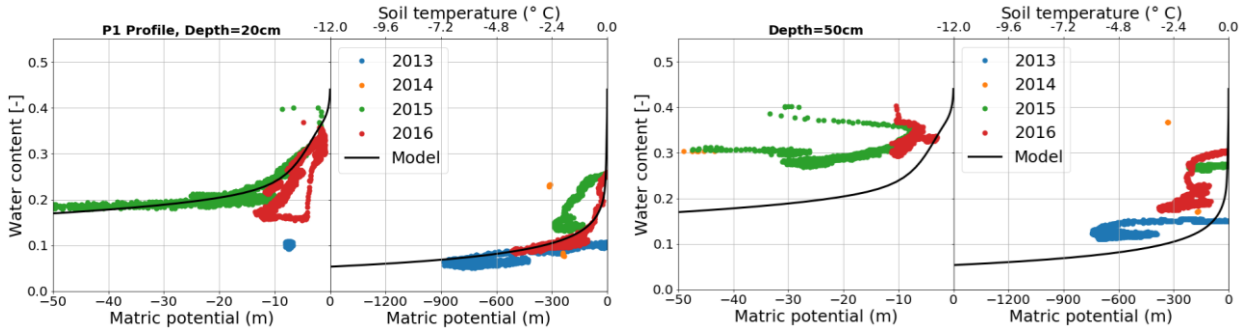

Figure 4-30 Fitting LNPSD model with observed SWC and SFC for P1 profile at BWC

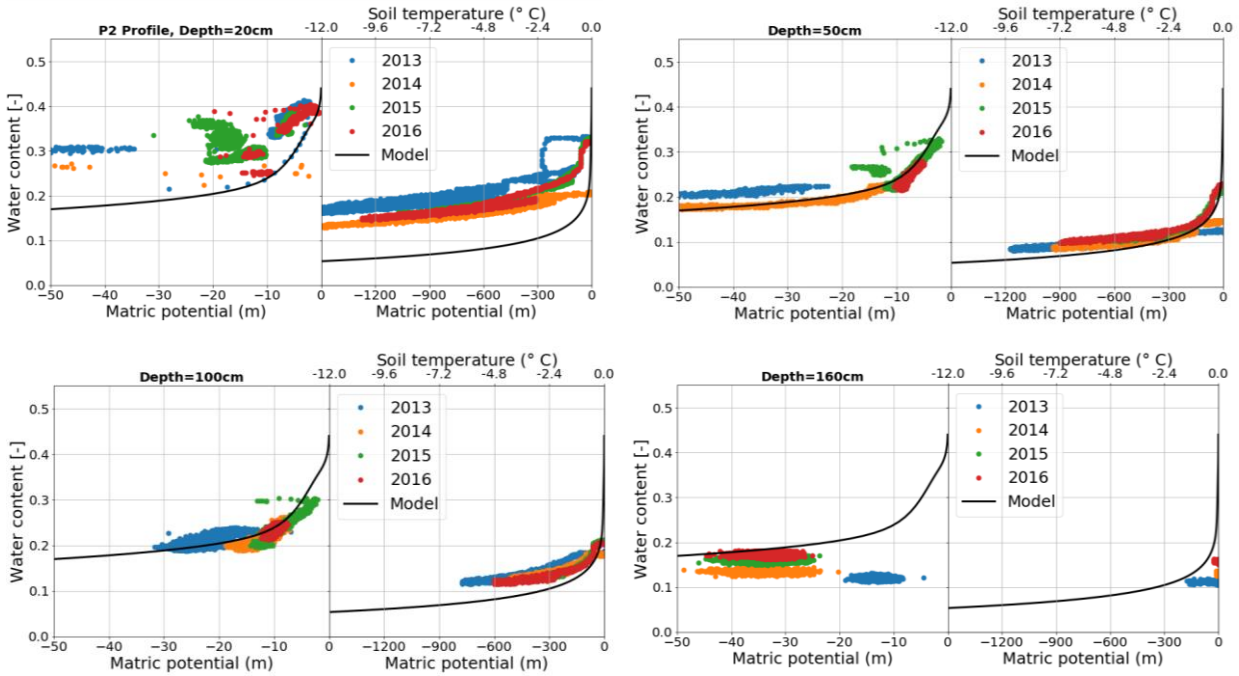

Figure 4-31 Fitting LNPSD model with observed SWC and SFC for P2 profile at BWC

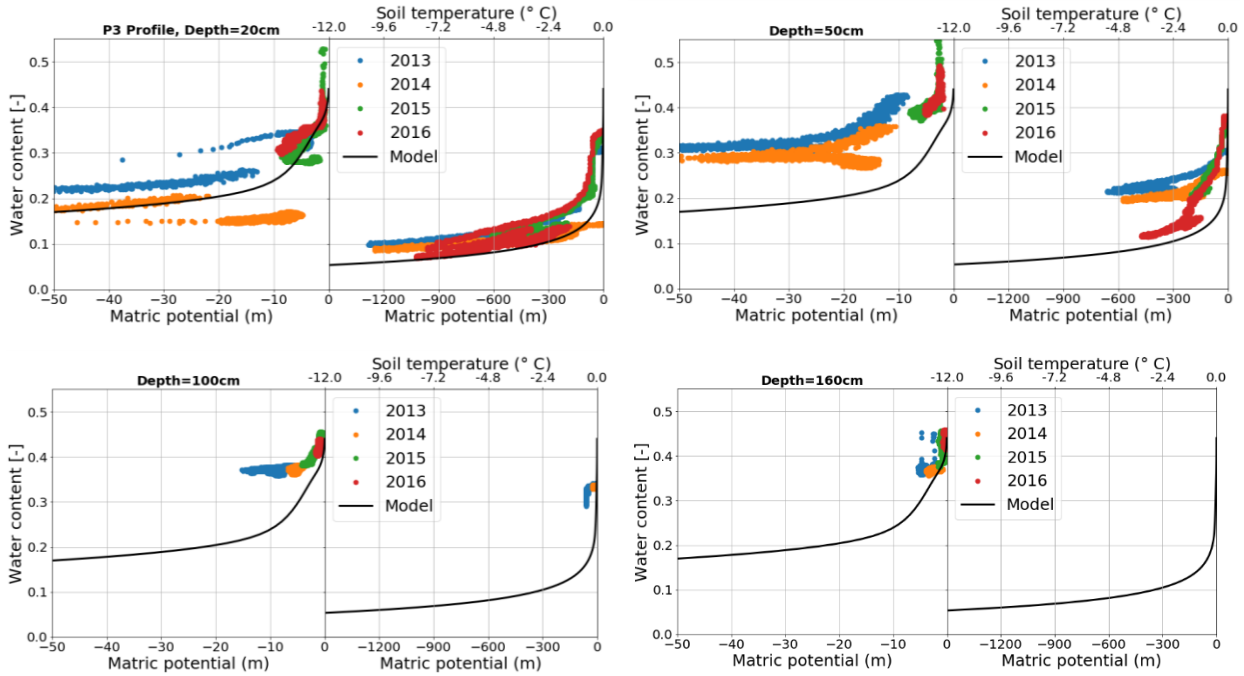

Figure 4-32 Fitting LNPSD model with observed SWC and SFC for P3 profile at BWC

4.3 Testing and comparing models for snowmelt infiltration at St Denis

This section details the third objective of validating and comparing models for snowmelt infiltration with field data at St Denis and BWC. The simulation for snowmelt infiltration was performed using the Standard Frozen Soil Infiltration Model (SFSIM) and the Frozen Soil Infiltration model (FroSIn). As described in section 2.4.2, the SFSIM uses a conventional approach which do not account for infiltration into the larger air-filled pores, whereas, FroSIn accounts for air-filled, ice-filled and liquid-filled pores in frozen soil and simulates infiltration into the larger air-filled pores.

The model setup, driving data, initial and boundary conditions and the saturated hydraulic conductivity values are kept same in both the models (SFSIM and FroSIn). The models were set up with the required data and the simulated results were compared with each other.

4.3.1 Model Setup

Both the models were set up considering a 1.5 m depth of the soil and the fitted soil parameter values from Table 4-3 and Table 4-4. The analyses were performed for years 2014, 2015 and 2016, focussing more during the snowmelt period (March and April).

4.3.2 Driving Data

The driving data required for the models are soil temperature, snowmelt and rainfall rates. The soil temperature and rainfall rate were inferred from the observations and the snowmelt period and rates were simulated using Cold Region Hydrological Model (CRHM). Figure 4-33, shows the driving data (snowmelt, rain and soil temperature) from the upslope profile at St Denis.

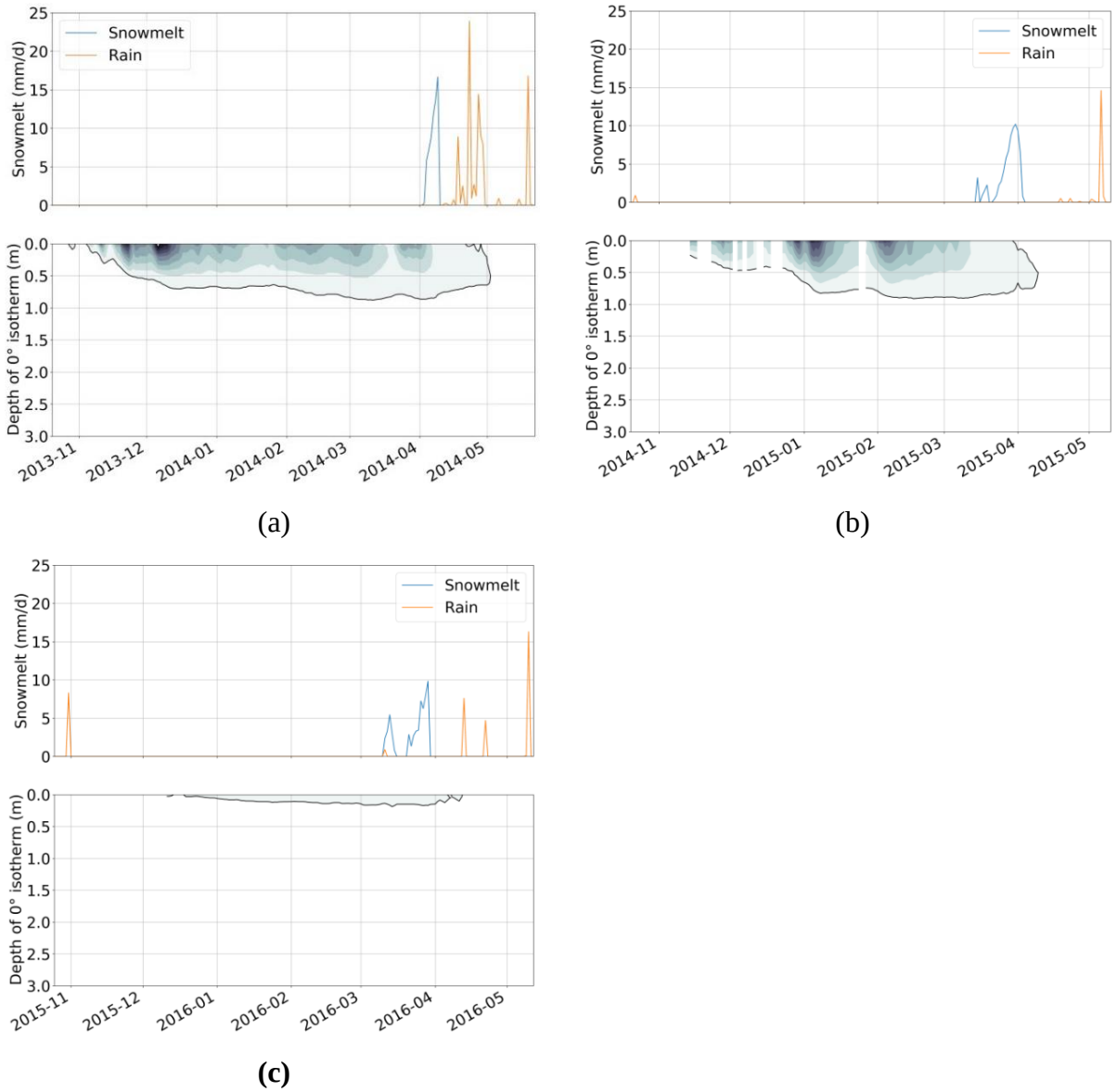

Figure 4-33 Driving data from upslope profile at St Denis for different years (a) 2014 (b) 2015 and (c) 2016

4.3.3 Initial and boundary condition

The initial condition for the analysis was used as a prescribed pressure head condition during previous fall (October) of a particular year. Table 4-5 summaries the initial condition data for upslope profile at St Denis. The upper boundary condition was determined considering equal distribution of the observed snowmelt and rainfall flux and the bottom boundary condition was a free drainage boundary condition.

Table 4-5 Initial condition data for upslope profile at St Denis

Year	2014	2015	2016
Initial condition date	2013-10-31	2014-10-31	2015-10-31
Depth (cm)	Pressure (ψ) (m)	Pressure (ψ) (m)	Pressure (ψ) (m)
5 cm	-13.15	-7.85	-0.34
20 cm	-42.98	-6.96	-0.29
50 cm	-9.21	-1.87	-0.09
100 cm	-3.77	-0.74	-0.32
200 cm	-0.058	0.423	1.63

4.3.4 Sensitivity Analysis for saturated hydraulic conductivity

The required saturated hydraulic conductivity (Ksat) for the models was determined based on the sensitivity analysis of the initial water content and saturated hydraulic conductivity parameter. The analyses were performed on the model by generating a contour plot of the snowmelt runoff ratio with different Ksat parameter and initial water content values as shown in Figure 4-34 (a). The initial water content values are based on the observed range of water content during fall (October) and the Ksat parameter values are estimated from the literature (van der Kamp and Hayashi, 2009).

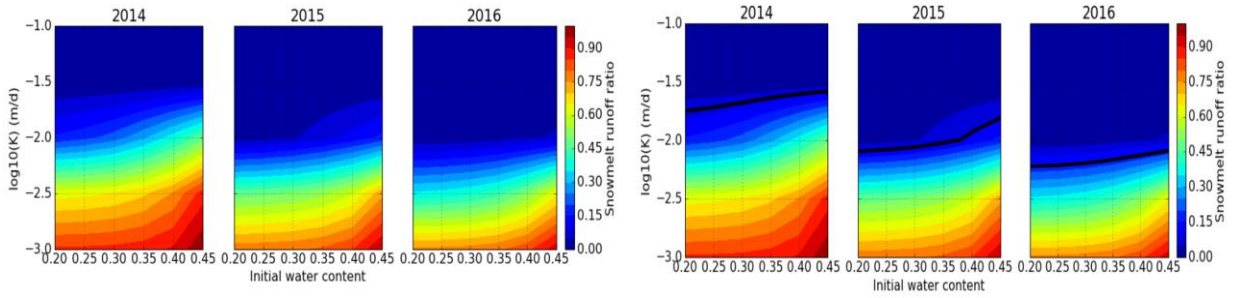

Figure 4-34 (a) Sensitivity analysis generating a contour plot for snowmelt runoff ratio (b) Sensitivity analysis inferring to the observed snowmelt runoff ratio

Figure 4-34 (a) shows a relationship between Ksat and initial water content to determine the snowmelt runoff ratio during spring. A low Ksat (~ log10 (-3) = 0.001 m/d) with high water content (~0.45) produced a lot of runoff ratio (~ 0.9) during spring as more water turns into ice and there is less infiltration. However, a high Ksat (~ log10 (-1.5) = 0.031 m/d) produced no runoff as all the water infiltrates into the frozen soil. This figure suggested the primary dependence of the runoff ratio with the Ksat and the initial water content.

Figure 4-34 (b) shows the sensitivity analysis inferring to the observed snowmelt runoff ratio from Table 4-1. The runoff ratio determined at St Denis for 2014, 2015 and 2016 was 0.09, 0.1 and 0.163 respectively. These numbers were plotted in the contoured plot, as a solid black line. The observed runoff ratio suggested that in all years the runoff was low. There was most runoff in 2016 and least in 2014 which is consistent with the observation of having dry antecedent water content in 2014 and wet antecedent water content in 2016 (see section 4.1.1.5).

Further, the sensitivity analysis result from Figure 4-34 (b) proposed that there was no single Ksat value which intersect all the lines, suggesting variable value for Ksat each year. But given the uncertainty in the observed runoff estimation from St Denis (i.e. if the observation was not from the Uri transect) that was not too concerning and thus the Ksat was somewhere in between the plotted solid lines and was chosen as ~ 0.01 m/d (= log10 (-2)). The general pattern of the sensitivity analysis with the runoff ratio gave the confidence in the behaviour of the model and choosing Ksat as 0.01 m/d as the model input parameter.

4.3.5 Modelling results using Standard Frozen Soil Infiltration Model (SFSIM)

The modelling results for upslope profile at St Denis using SFSIM is detailed in Figure 4-35. The figures summaries the change in different fluxes (snowmelt, rain, runoff, infiltration and drainage) and changes in storage for three years (2014, 2015 and 2016). The model was run from October till May for each year.

From the overall surface water balance in each year, it was noticed that the model systematically overestimated runoff compared to infiltration for all three years. These results were expected from the SFSIM as the model does not account for infiltration into the unfrozen air-filled pores during snowmelt period thus all the snowmelt water goes into runoff during spring.

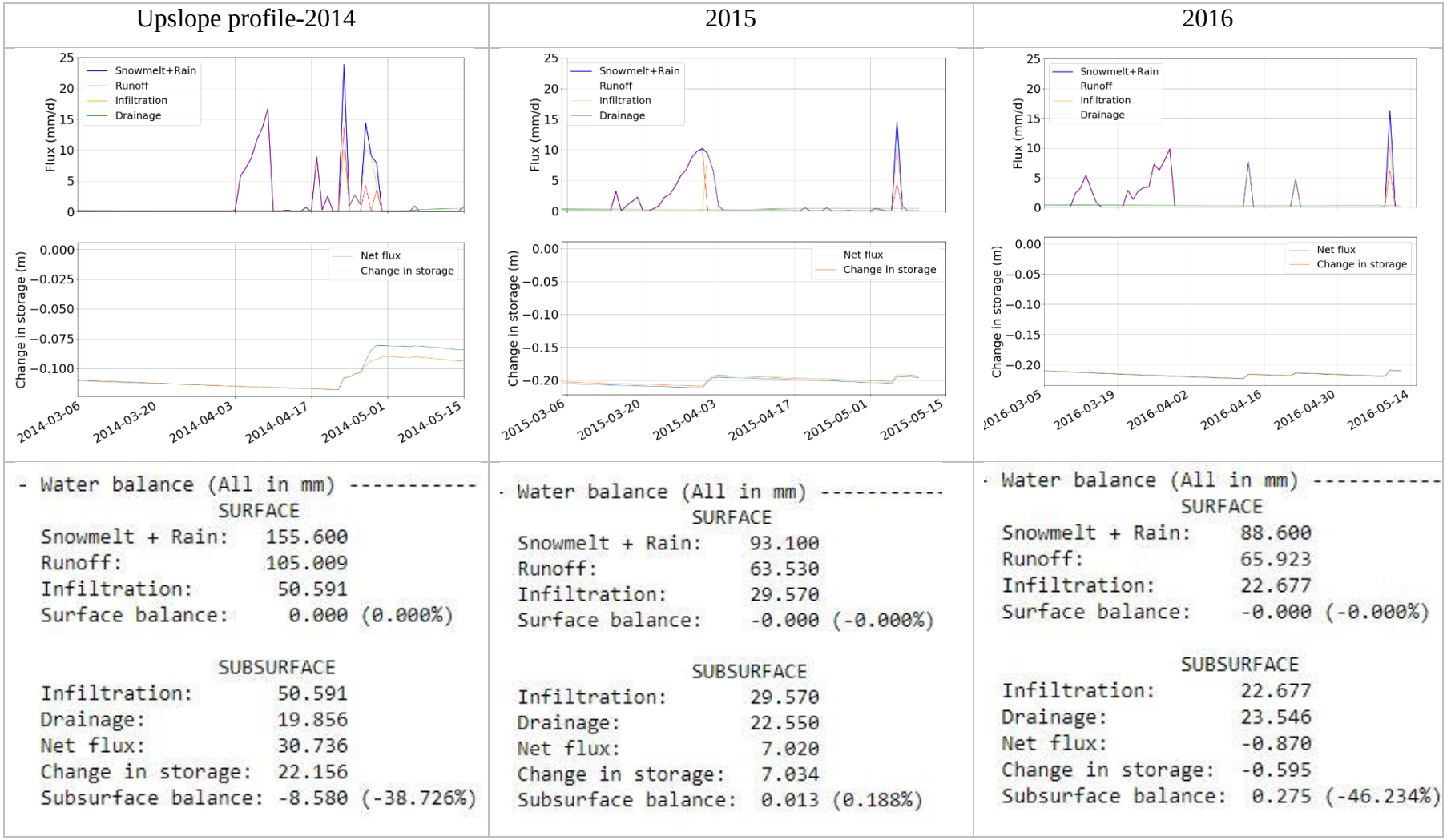

Figure 4-35 Simulated results for upslope profile using SFSIM at St Denis

4.3.6 Modelling results using Frozen Soil Infiltration Model (FroSIn)

The modelling results for upslope profile at St Denis using FroSIn is detailed in Figure 4-36. The model was run from October till May for each year (2014, 2015 and 2016) and the figures summaries the change in different fluxes (snowmelt, rain, runoff, infiltration and drainage) and change in storage in those years.

From the surface water balance, it was noticed that there were greater infiltration rates compared to runoff for all the three years. These results suggested that the model was helpful to predict more reasonable infiltration into the unfrozen air-filled pores.

(Note: The modelling results from FroSIn for other profiles (midslope and downslope profiles) are in the Appendix E, Figure E.3 and E.4)

Upslope profile-2014	2015	2016
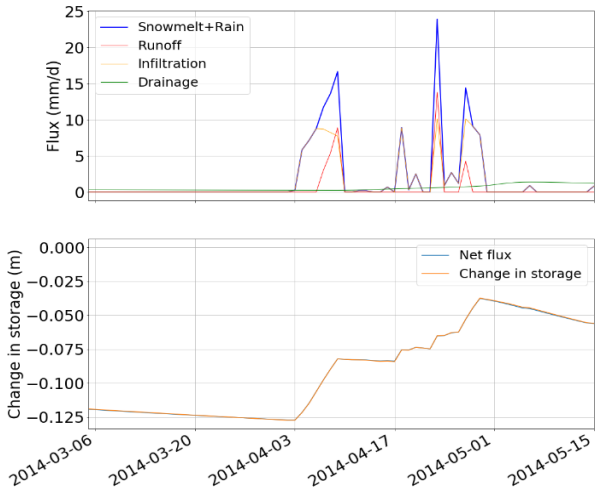	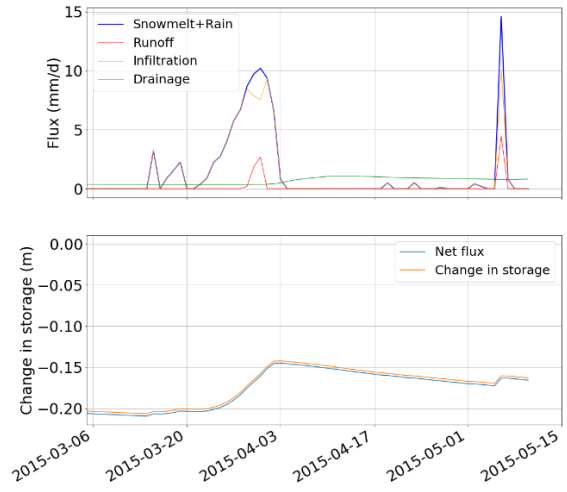	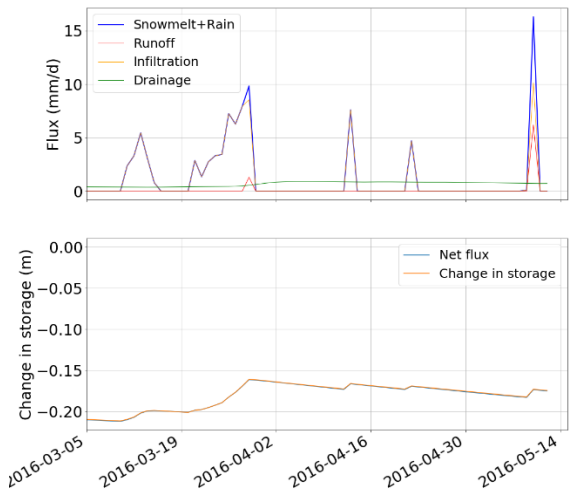
- Water balance (All in mm) ---------- SURFACE Snowmelt + Rain: 155.600 Runoff: 42.029 Infiltration: 113.571 Surface balance: 0.000 (0.000%) SUBSURFACE Infiltration: 113.571 Drainage: 50.297 Net flux: 63.273 Change in storage: 63.594 Subsurface balance: 0.321 (0.505%)	- Water balance (All in mm) ---------- SURFACE Snowmelt + Rain: 93.100 Runoff: 9.244 Infiltration: 83.856 Surface balance: -0.000 (-0.000%) SUBSURFACE Infiltration: 83.856 Drainage: 45.963 Net flux: 37.893 Change in storage: 38.287 Subsurface balance: 0.394 (1.029%)	- Water balance (All in mm) ---------- SURFACE Snowmelt + Rain: 88.600 Runoff: 7.476 Infiltration: 81.124 Surface balance: 0.000 (0.000%) SUBSURFACE Infiltration: 81.124 Drainage: 47.145 Net flux: 33.979 Change in storage: 34.494 Subsurface balance: 0.515 (1.493%)

Figure 4-36 Simulated results for upslope profile using FroSIn at St Denis

4.3.7 Validating and comparing results from observation, SFSIM and FroSIn during snowmelt period

Considering the snowmelt period from

Table 4-1, snowmelt partitioning into runoff and infiltration was performed for 2014, 2015 and 2016. The validations of the model results were based on the inferred observation from Pond 50 runoff analysis (Figure 4-12). The results from SFSIM and FroSIn was then compared with each other, and, also with the field observation.

Figure 4-37 (a) (b) and (c) are the snowmelt partitioning inferred from the observation, the SFSIM and the FroSIn respectively during the snowmelt period of 2014, 2015 and 2016.

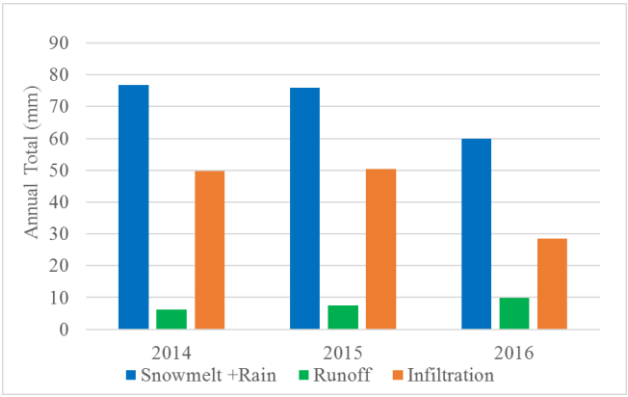

(a)

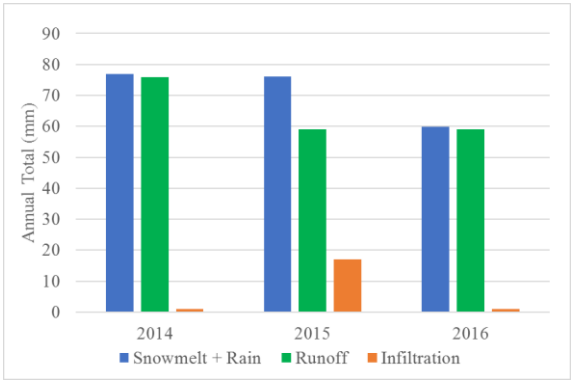

(b)

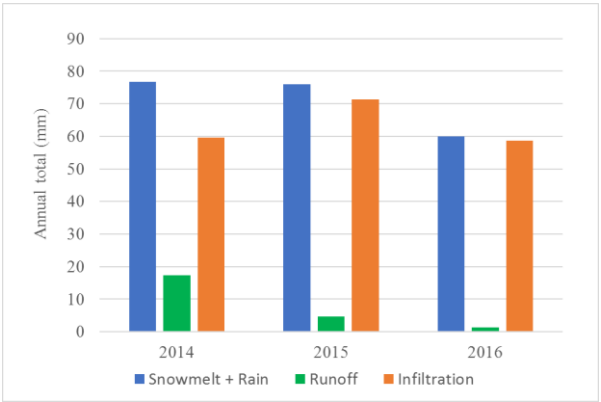

(c)

Figure 4-37(a) Snowmelt partitioning inferred from observation (b) Snowmelt partitioning based on SFSIM (c) Snowmelt partitioning based on FroSIn

Comparing the snowmelt partitioning from the SFSIM and the observations from pond 50, it was noticed that in the model runoff was over predicted compared to infiltration, whilst from the observation, it was determined that infiltration dominated over runoff during the snowmelt period. The overestimating of runoff from the SFSIM was because of the inability to incorporate unfrozen air-filled pores, which provides significant infiltration capacity, even during frozen conditions. It was also believed that this is a significant and generic limitation of most of the snowmelt infiltration models which deals with the frozen soils.

However, the snowmelt partitioning results from the FroSIn and the observation were quite comparable with each other for simulating the infiltration value. The FroSIn was useful in predicting significant amount of infiltration into the frozen soil.

It is also worthwhile noting that both the models (the SFSIM and the FroSIn) does not account for evapotranspiration flux for the overall surface water balance which might have some biases in the overall simulated results and needs further model development.

4.3.8 Additional FroSIn model insight from Brightwater creek (BWC)

The FroSIn model was also set up for BWC with the soil parameter values from Table 4-4. The initial condition was taken as the prescribed pressure head values of October and the saturated hydraulic conductivity was considered similar to that at St Denis (i.e. 0.01 m/d) as both of them represents the prairies with similar soil type as clay and also because BWC lack the measurement of saturated hydraulic conductivity data.

Figure 4-38 and Table 4-6, shows the driving data (snowmelt, rain and soil temperature) and initial condition data from P1 profile at BWC respectively.

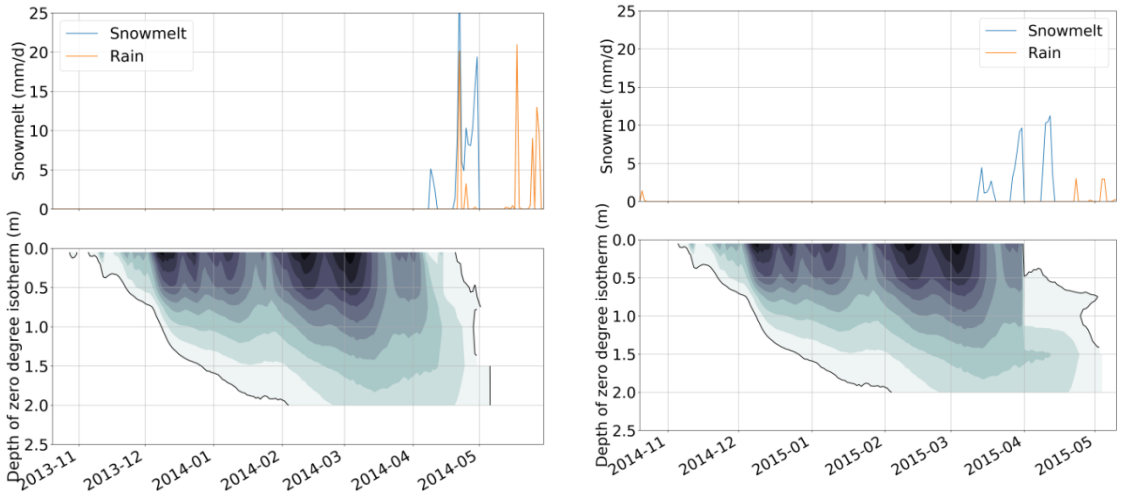

(a)

(b)

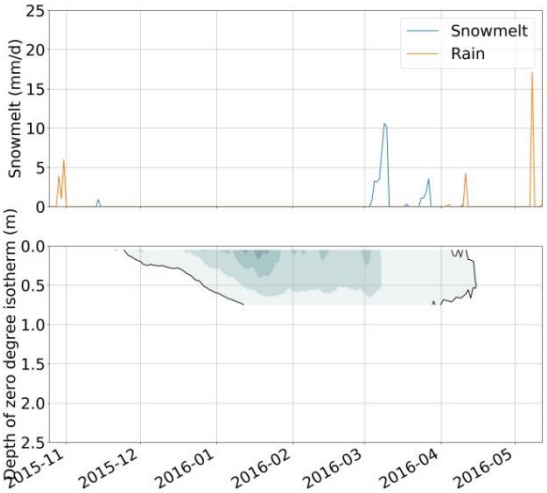

(c)

Figure 4-38 Driving data for P1 profile at BWC

Table 4-6 Initial condition data for P1 profile at BWC

Year	2014	2015	2016
Initial condition date	2013-10-31	2014-10-31	2015-10-31
Depth (cm)	Pressure (ψ) (m)	Pressure (ψ) (m)	Pressure (ψ) (m)
20 cm	-6.99	-118.96	-1.25
50 cm	-153.62	-17.04	-6.8

The analysis was performed from the October till May for different years (2014, 2015 and 2016).

Figure 4-39, shows the modelling results using FroSIn. From the overall surface water balance, it was also noticed that there was more infiltration compared to runoff in all the years (2014, 2015 and 2016). The modelling results from FroSIn for other profiles (P2 and P3 profiles) are in the Appendix E (Figure E.5 and E.6).

P1 Profile -2014	2015	2016
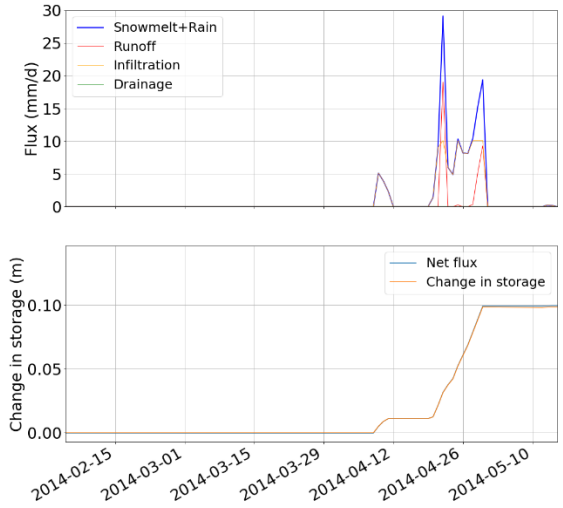	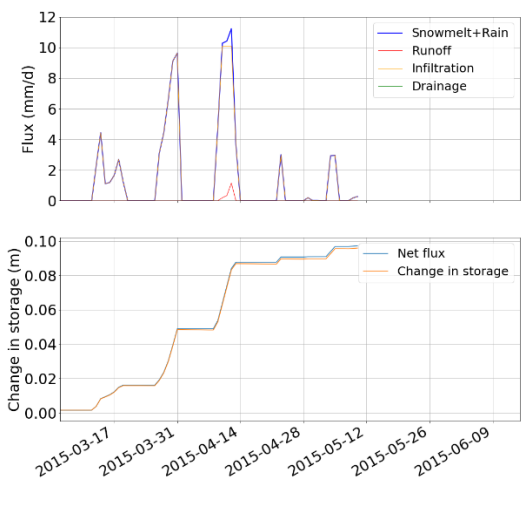	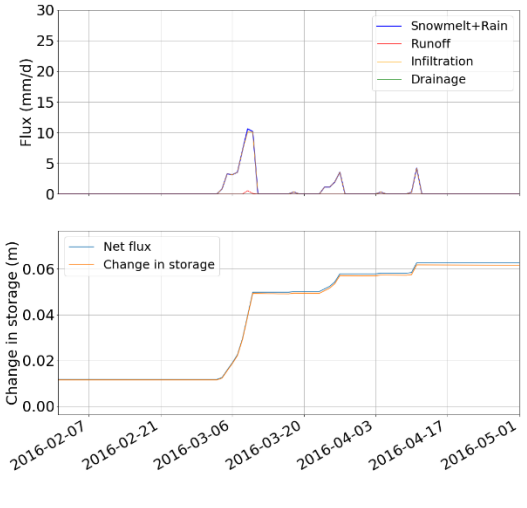
- Water balance (All in mm) ---------- SURFACE Snowmelt + Rain: 187.570 Runoff: 47.824 Infiltration: 139.746 Surface balance: 0.000 (0.000%) SUBSURFACE Infiltration: 139.746 Drainage: 0.075 Net flux: 139.671 Change in storage: 138.226 Subsurface balance: -1.445 (-1.046%)	Water balance (All in mm) ---------- SURFACE Snowmelt + Rain: 97.028 Runoff: 1.676 Infiltration: 95.352 Surface balance: -0.000 (-0.000%) SUBSURFACE Infiltration: 95.352 Drainage: 0.026 Net flux: 95.326 Change in storage: 93.995 Subsurface balance: -1.331 (-1.416%)	Water balance (All in mm) ---------- SURFACE Snowmelt + Rain: 68.919 Runoff: 7.629 Infiltration: 61.290 Surface balance: 0.000 (0.000%) SUBSURFACE Infiltration: 61.290 Drainage: 0.029 Net flux: 61.261 Change in storage: 60.412 Subsurface balance: -0.849 (-1.406%)

Figure 4-39 Simulated results for P1 profile using FroSIn at BWC

CHAPTER 5

CONCLUSIONS

In this thesis, field data and models were combined to obtain insights into how snowmelt and spring rainfall is partitioned between infiltration and runoff. Empirical estimates of the partitioning of snowmelt were obtained by comparing the volume of snowmelt over the catchment area of a terminal pond with the increased volume in the pond during the spring melt period. Whilst the numbers are uncertain, the results consistently showed that the infiltration volumes were larger than runoff volumes.

The characterization of the soil hydraulic properties was performed using Log Normal Pore Size Distribution (LNPSD) model. The LNPSD model was validated with the equivalent van Genuchten model (VGM). It was observed that the parameters from LNPSD were well fitted with the VGM for various soil types except clay. It was further observed that the residual water content for the clay in VGM did not converge to zero even after rescaling the water content to zero at higher matric potential, which might be an essential area for future research. The LNPSD model was then applied to fit the observed soil water and freezing characteristic curves at St Denis and BWC to determine the soil pore size parameters in log scale (the porosity, the mean radius and the standard deviation).

Two different models, SFSIM and FroSIn were used to model the snowmelt infiltrations at St Denis and BWC. The SFSIM uses a conventional approach of determining the hydraulic properties linking to temperature alone and does not allow for infiltration into the air-filled larger pores. The simulations from SFSIM resulted in high runoff values compared to infiltration during the snowmelt period of 2014, 2015 and 2016. However, the model results from the FroSIn showed higher infiltration than the runoff, which is comparable to the ground observation at pond 50 at St Denis. FroSIn explains a unique relationship between the water content, temperature and pressure and incorporates snowmelt infiltration into the larger unfrozen air-filled pores which might have improved the results.

Both the models were found to be sensitive to the initial soil water condition and the saturated hydraulic conductivity for the model runs. The initial conditions were provided from the prescribed pressure head data before freeze-up (October) and sensitivity analyses were performed to determine the saturated hydraulic conductivity for St Denis and found to be 0.01 m/day. For further validation, FroSIn model was used at BWC which also showed higher rates of infiltration than runoff.

The findings of this research have important implications in understanding general vadose zone hydrology of the prairie environment and to recognize the importance of unfrozen air-filled pores during spring snowmelt. The modelling results might also be useful to know the antecedent water content after the spring snowmelt to determine the saturation level of the soil. This saturation level of the soil is useful to understand the soil water storage and runoff rates and further assist in forecasting flooding in the prairies. In overall, the algorithm in FroSIn model was helpful to simulate reasonable infiltration volumes during spring snowmelt, which is comparable to the observation at St Denis. Further steps would be to integrate FroSIn into the heat and mass transport model to incorporate changes in thermal properties of frozen soil to accurately quantify snowmelt into infiltration and runoff.

REFERENCES

Abudu, S., Cui, C., Saydi, M., & King, J. P. (2012). Application of snowmelt runoff model (SRM) in mountainous watersheds: A review. *Water Science and Engineering*, *5*(2), 123–136.

Anderson, D. M., & Tice, A. R. (1973). Predicting unfrozen water contents in frozen soils from surface area measurements. *J. Terramechanics*, (393).

Anderson, E. (1973). *National Weather Service river forecast system: Snow accumulation and ablation model*. US Department of Commerce, National Oceanic and Atmospheric Administration, National Weather Service.

Anderson, E. A. (1968). Development and testing of snow pack energy balance equations. *Water Resources Research*, *4*(1), 19–37.

Baldocchi. (1988). Measuring Biosphere-Atmosphere Exchanges of Biologically Related Gases with Micrometeorological Methods, *69*(5), 1331–1340.

Barrow, E. (2009). *Climate Scenarios for Saskatchewan (No. 09-01)*. Prairie Adaptation Research Collaborative (PARC), Regina, Canada.

Bear, J., & Cheng, A. (2010). Modeling groundwater flow and contaminant transport. In *Springer Science & Business Media* (Vol. 23).

Bergstrom, S. (1976). *Development and application of a conceptual runoff model for Scandinavian catchments*. RH07, SMHI, Norrkoumlping, Sweden.

Bøggild, C., Reeh, N., & Oerter, H. (1994). Modelling ablation and mass-balance sensitivity to climate change of Storstrømmen, northeast Greenland. *Global and Planetary Change*, *9*(1), 79–90.

Brannen, R. E. (2015). *Controls on connectivity and streamflow generation in a Canadian Prairie landscape (Master's thesis)*. University of Saskatchewan, Saskatoon, Canada. Retrieved from https://ecommons.usask.ca/xmlui/bitstream/handle/10388/ETD-2015-04-2013/BRANNEN-THESIS.pdf?sequence=3&isAllowed=y

Brannen, R., Spence, C., & Ireson, A. (2015). Influence of shallow groundwater-surface water interactions on the hydrological connectivity and water budget of a wetland complex. *Hydrological Processes*, *29*(18), 3862–3877.

Brutsaert, W. (1968). The permeability of a porous medium determined from certain probability laws for pore size distribution. *Water Resources Research*, *4*(2), 425–434.

C.W. Fetter. (1994). *Applied Hydrogeology*. Upper Saddle River, New Jersey: Prentice-Hall, Inc.

Carey, S. K., & Pomeroy, J. W. (2009). Progress in Canadian Snow and Frozen Ground Hydrology, 2003-2007. *Canadian Water Resources Journal*, *34*(2), 127–138.

Carey, S., & Woo, M. (1998). Snowmelt hydrology of two subarctic slopes, southern Yukon, Canada. *Hydrology Research*, *29*(4–5), 331–346.

Childs and Collis George. (1950). The permeability of porous material. In *Proceedings of the Royal Society of London A: Mathematical, Physical and Engineering Sciences* (pp. 392–405). The Royal Society.

Corey, A. T., & Brooks, R. H. (1966). Properties of porous media affecting fluid flow. *Journal of the Irrigation and Drainage Division*, *92*(2), 61–90.

Corominas, J., van Westen, C., Frattini, P., Cascini, L., Malet, J.-P., Fotopoulou, S., … Smith, J. T. (2013). Recommendations for the quantitative analysis of landslide risk. *Bulletin of Engineering Geology and the Environment*, *73*(2), 209–263.

Dall'Amico, M., Endrizzi, S., Gruber, S., & Rigon, R. (2011). A robust and energy-conserving model of freezing variably-saturated soil. *Cryosphere*, *5*(2), 469–484.

Daniel, J. A., & Staricka, J. A. (2000). Frozen soil impact on ground water- surface water interaction. *The American Resources Association*, *36*(1), 51–60.

Darcy. (1856). *Les fontaines publiques de la ville de Dijon (The water supply of Dijon) :* Paris, Victor Dalmont.

Devia, G. K., Ganasri, B. P., & Dwarakish, G. S. (2015). A Review on Hydrological Models. *Aquatic Procedia*, *4*, 1001–1007.

Dingman, S. L. (2015). *Physical Hydrology* (Third). Long Grove, IL: Waveland Press, Inc.

Edlefsen, N. E., & Anderson, A. B. C. (1943). Thermodynamics of soil moisture. *Hilgardia*, *15*, 31–298.

Ehsanzadeh, E., Spence, C., van der Kamp, G., & McConkey, B. (2012). On the behaviour of dynamic contributing areas and flood frequency curves in North American Prairie watersheds. *Journal of Hydrology*, *414*, 364–373.

Ellis, C. R., Pomeroy, J. W., Brown, T., & MacDonald, J. (2010). Simulation of snow accumulation and melt in needleleaf forest environments. *Hydrology and Earth System Sciences*, *14*(6), 925–940.

Fang, X., & Pomeroy, J. (2007). Snowmelt runoff sensitivity analysis to drought on the Canadian prairies. *Hydrological Processes*, *21*, 2594–2609.

Flerchinger, G. N., & Saxton, K. E. (1989). Snow-Residue-Soil System I . Theory and Development. *Soil and Water Division ASAE*, *32*(2), 565–567.

Fredlund, D. G., & Xing, A. (1994). Equations for the soil-water characteristic curve. *Canadian Geotechnical Journal*, *31*, 521–532.

Fredlund, D. G., Xing, A., & Huang, S. (1994). Predicting the permeability function for unsaturated soils using the soil-water characteristic curve. *Canadian Geotechnical Journal*, *31*(4), 533–546.

Gelfan, a. N., Pomeroy, J. W., & Kuchment, L. S. (2004). Modeling forest cover influences on snow accumulation, sublimation, and melt. *Journal of Hydrometeorology*, *5*(5), 785–803.

Granger, R. J., Gray, D. M., & Dyck, G. E. (1984). Snowmelt infiltration to frozen Prairie soils. *Canadian Journal of Earth Sciences*, *21*(6), 669–677.

Gray, D., Granger, R., & Nicholaichuk, W. (1985). Snowmelt infiltration to uncracked, cracked and subsoiled frozen soils. In *Snow Management for Agriculture Workshop*. Swift Current, Saskatchewan.

Gray, D., Landine, P. G., & Granger, R. J. (1984). Simulating infiltration into frozen prairie soils

in streamflow models. *Canadian Journal of Earth Sciences*, *22*, 464–472.

Gray, D. M., & Landine, P. G. (1988). An energy-budget snowmelt model for the Canadian Prairies. *Canadian Journal of Earth Sciences*, *25*(8), 1292–1303.

Gray, D. M., Pomeroy, J. W., & Landine, P. G. (1986). *Development and Performance Evaluahon of Energy Balance Snowmelt Models*. *Division of Hydrology, University of Saskatchewan*. Saskatoon, Saskatchewan.

Gray, D. M., Toth, B., Zhao, L., Pomeroy, J. W., & Granger, R. J. (2001). Estimating areal snowmelt infiltration into frozen soils. *Hydrological Processes*, *15*(16), 3095–3111.

Gray, & Landine, P. G. (1988). An energy-budget snowmelt model for the Canadian Prairies. *Canadian Journal of Earth Sciences*, *25*(8), 1292–1303.

Hansson, K., Šimůnek, J., Mizoguchi, M., Lundin, L., & Van Genuchten, M. (2004). Water flow and heat transport in frozen soil. *Vadose Zone*, *3*, 693–704.

Harlan, R. L. (1973). Analysis of coupled heat-fluid transport in partially frozen soil. *Water Resources Research*, *9*(5), 1314–1323.

Hayashi, M. (2013). The Cold Vadose Zone: Hydrological and Ecological Significance of Frozen-Soil Processes. *Vadose Zone Journal*, *12*, 2136.

Hayashi, M., & Van Der Kamp, G. (2000). Simple equations to represent the volume-area-depth relations of shallow wetlands in small topographic depressions. *Journal of Hydrology*, *237*(1–2), 74–85.

Hayashi, M., van der Kamp, G., & Rosenberry, D. O. (2016). Hydrology of Prairie Wetlands: Understanding the Integrated Surface-Water and Groundwater Processes. *Wetlands*, *36*(2), 237–254.

Hayashi, M., Van Der Kamp, G., & Rudolph, D. L. (1998). Water and solute transfer between a prairie wetland and adjacent uplands, 2. Chloride cycle. *Journal of Hydrology*, *207*(1–2), 56–67.

Hayashi, M., Van Der Kamp, G., & Schmidt, R. (2003). Focused infiltration of snowmelt water

in partially frozen soil under small depressions. *Journal of Hydrology*, *270*(3–4), 214–229.

Hedstrom, N. R., & Pomeroy, J. W. (1998). Measurements and modeling of snow interception in the boreal forest. *Hydrological Processes*, *12*(10), 1611–1625.

Helgason, W., & Pomeroy, J. W. (2012). Problems Closing the Energy Balance over a Homogeneous Snow Cover during Midwinter. *Journal of Hydrometeorology*, *13*(2), 557–572.

Hillel, D. (1998). *Environmental soil physics: Fundamentals, applications, and environmental considerations*. Academic press.

Ho, C. L. I. (2002). *Urban Snow Hydrology and Modelling (Master's Thesis)*. University of Calgary, Alberta, Canada.

Hock, R. (2003). Temperature index melt modelling in mountain areas. *Journal of Hydrology*, *282*(1–4), 104–115.

Horst, T. W. (1997). A simple formula for attenuation of eddy fluxes measured with first-order-response scalar sensors. *Boundary-Layer Meteorology*, *82*, 219–233.

Horton, R. E. (1933). The Role of infiltration in the hydrologic cycle. *Eos, Transactions, American Geophysical Union*, *14*(1), 446.

Ireson, A. (2014). *Modelling infiltration processes in frozen soils, Oral presentation*. San Francisco: American Geophysical Union Meeting. Retrieved from http://homepage.usask.ca/~ani378/Talks/AIreson AGU2014 FreezingSoils_H083.pdf

Ireson, van der Kamp, G., Ferguson, G., Nachshon, U., & Wheater, H. S. (2012). Hydrogeological processes in seasonally frozen northern latitudes: understanding, gaps and challenges. *Hydrogeology Journal*, *21*(1), 53–66.

Islam, Z. (2011). *A Review on Physically Based Hydrologic Modeling*. University of Alberta.

Iwata, Y., Hayashi, M., & Hirota, T. (2008). Comparison of Snowmelt Infiltration under Different Soil-Freezing Conditions Influenced by Snow Cover. *Vadose Zone Journal*, *7*(1), 79.

Iwata, Y., Hayashi, M., Suzuki, S., Hirota, T., & Hasegawa, S. (2010). Effects of snow cover on soil freezing, water movement, and snowmelt infiltration: A paired plot experiment. *Water Resources Research*, *46*(9), 1–12.

Johnson, W. C., Werner, B., Guntenspergen, G. R., Voldseth, R. a., Millett, B., Naugle, D. E., … Olawsky, C. (2010). Prairie Wetland Complexes as Landscape Functional Units in a Changing Climate. *BioScience*, *60*(2), 128–140.

Jordan, R. (1991). *A one-dimensional temperature model for a snow cover: Technical documentation for SNTHERM. 89.* COLD REGIONS RESEARCH AND ENGINEERING LAB HANOVER NH.

Kane, D. L. (1980). Snowmelt infiltration into seasonally frozen soils. *Cold Regions Science and Technology*, *3*(2–3), 153–161.

King, J. C., Pomeroy, J. W., Gray, D. M., Fierz, C., Paul, M. B. F., Harding, R. J., … Pluss, C. (2008). *Snow – atmosphere energy and mass balance*. *Snow and Climate: Physical Processes, Surface Energy Exchange and Modeling*.

Koopmans, R. W. R., & Miller, R. D. (1966). Soil Freezing and Soil Water Characteristic Curves. *Soil Science Society of America Journal*, *30*(6), 680.

Kosugi, K. (1994). Three-parameter lognormal distribution model for soil water retention. *Water Resources Research*, *30*(4), 891–901.

Kosugi, K. (1996). Lognormal distribution model for unsaturated soil hydraulic properties. *Water Resources Research*, *32*(9), 2697–2703.

Kurylyk, B. L., & Watanabe, K. (2013). The mathematical representation of freezing and thawing processes in variably-saturated, non-deformable soils. *Advances in Water Resources*, *60*, 160–177.

Kustas, W. P., Rango, A., & Uijlenhoet, R. (1994). A simple energy budget algorithm for the snowmelt runoff model. *Water Resources Research*, *30*(5), 1515–1527.

Leong, D. N. S., & Donner, S. D. (2015). Climate change impacts on streamflow availability for

the Athabasca Oil Sands. *Climatic Change*, *133*(4), 651–663.

Liu, Z., Zhang, B., Yu, X., & Tao, J. (2012). A new method for soil water characteristic curve measurement based on similarities between soil freezing and drying. *Geotechnical Testing Journal*, *35*(1), 2–10.

Lundin, L. (1990). Hydraulic Properties in an Operational Model of Frozen Soil. *Journal of Hydrology*, *118*, 289–310.

Male, D. H., & Granger, R. J. (1981). Snow surface energy exchange. *Water Resources Research*, *17*(3), 609–627.

Mango, L. M., Melesse, A. M., McClain, M. E., Gann, D., & Setegn, S. G. (2011). Land use and climate change impacts on the hydrology of the upper Mara River Basin, Kenya: Results of a modeling study to support better resource management. *Hydrology and Earth System Sciences*, *15*(7), 2245–2258.

Marks, D., Domingo, J., Susong, D., Link, T., & Garen, D. (1999). A spatially distributed energy balance snowmelt model for application in mountain basins. *Hydrological Processes*, *13*(12–13), 1935–1959.

Marsh, P., & Pomeroy, J. W. (1996). Meltwater fluxes at an arctic forest-tundra site. *Hydrological Processes*, *10*(10), 1383–1400.

Martinec, J., & Rango, A. (1986). Parameter values for snowmelt runoff modelling. *Journal of Hydrology*, *84*(3–4), 197–219.

Massman, W. J. (2000). A simple method for estimating frequency response corrections for eddy covariance systems. *Agricultural and Forest Meteorology*, *104*(3), 185–198.

Miller, K., & Yates, D. (2006). *Climate change and water resources: a primer for municipal water providers*. *Awwa Research Foundation* (Vol. 37).

Miller, R. (1980). *Freezing phenomena in soils*. *Applications of soil physics*. Academic Press, San Diego, pg. 254-299.

Nachshon, U., Ireson, A., van der Kamp, G., & Wheater, H. (2013). Sulfate salt dynamics in the

glaciated plains of North America. *Journal of Hydrology*, *499*, 188–199.

Pan, X., Helgason, W., Ireson, A., & Wheater, H. (2017). Field-scale water balance closure in seasonally frozen conditions. *Hydrology and Earth System Sciences*, *21*(11), 5401–5413.

Pomeroy, J., & Brun, E. (2001). Physical properties of snow. *Snow Ecology: An Interdisciplinary Examination of Snow-Covered Ecosystems*, 45–126.

Pomeroy, J., & Dumanski, S. (2017, March). Floods , droughts and climate change – what will the future hold ?, (March 16, 2017), 1–4.

Pomeroy, J., Fang, X., Westbrook, C., Minke, A., Guo, X., & Brown, T. (2010). *Prairie Hydrological Model Study Final Report*. Saskatoon, Saskatchewan.

Pomeroy, J., & Gray, D. (1995). Snowcover accumulation, relocation and management. *Bulletin of the International Society of Soil Science*, *88*(2).

Pomeroy, J. W., Fang, X., & Williams, B. (2009). *Impacts of Climate Change on Saskatchewan ' s Water Resources*. Saskatoon, Saskatchewan.

Pomeroy, J. W., Gray, D. M., Brown, T., Hedstrom, N. R., Quinton, W. L., Granger, R. J., & Carey, S. K. (2007). The cold regions hydrological model: a platform for basing process representation and model structure on physical evidence. *Hydrological Processes*, *21*(19), 2650–2667.

Pomeroy, J. W., Gray, D. M., Hedstrom, N. R., & Janowicz, J. R. (2002). Prediction of seasonal snow accumulation in cold climate forests. *Hydrological Processes*, *16*(18), 3543–3558.

Pomeroy, J. W., Toth, B., Granger, R. J., Hedstrom, N. R., & Essery, R. L. H. (2003). Variation in Surface Energetics during Snowmelt in a Subarctic Mountain Catchment. *Journal of Hydrometeorology*, *4*(4), 702–719.

Prudhomme, C., & Davies, H. (2009). Assessing uncertainties in climate change impact analyses on the river flow regimes in the UK. Part 2: Future climate. *Climatic Change*, *93*(1–2), 197–222.

Richards, L. A. (1931). Capillary conduction of liquids through porous mediums. *Journal of*

Applied Physics, *1*(5), 318–333.

Rott, H., Yueh, S. H., Cline, D. W., Duguay, C., Essery, R., Haas, C., … Thompson, A. (2010). Cold Regions Hydrology High-Resolution Observatory for Snow and Cold Land Processes. *Proceedings of the IEEE*, *98*(5), 752–765.

Rutter, N., Essery, R., Pomeroy, J., Altimir, N., Andreadis, K., Baker, I., … Yamazaki, T. (2009). Evaluation of forest snow processes models (SnowMIP2). *Journal of Geophysical Research*, *114*(D6), D06111.

Salinger, J. (2005). Climate Variability and Change: Past, Present and Future - An Overview'. *Climate Change*, *70*(1–2), 9–30.

Schindler, D. W., & Smol, J. P. (2006). Cumulative effects of climate warming and other human activities on freshwaters of Arctic and subarctic North America. *AMBIO: A Journal of the Human Environment*, *35*(4), 160–168.

Seyfried, M. S., Grant, L. E., Du, E., & Humes, K. (2005). Dielectric Loss and Calibration of the Hydra Probe Soil Water Sensor. *Vadose Zone Journal*, *4*(4), 1070.

Shaw, D. a., Vanderkamp, G., Conly, F. M., Pietroniro, A., & Martz, L. (2012). The Fill-Spill Hydrology of Prairie Wetland Complexes during Drought and Deluge. *Hydrological Processes*, *26*(20), 3147–3156.

Shirazi, M. A., & Boersma, L. (1984). A Unifying Quantitative Analysis of Soil Texture1. *Soil Science Society of America Journal*, *48*(1), 142.

Shook, K., Pomeroy, J. W., Spence, C., & Boychuk, L. (2013). Storage dynamics simulations in prairie wetland hydrology models: Evaluation and parameterization. *Hydrological Processes*, *27*(13), 1875–1889.

Smith, C. D. (2007). Correcting the wind bias in snowfall measurements made with a Geonor T-200B 16 precipitation gauge and Alter wind shield. *In: Proceedings of the 14th SMOI, San Antonio*.

Spaans, E. J. A., & Baker, J. M. (1996). The soil freezing characteristic: Its measurement and

similarity to the soil moisture characteristic. *Soil Science Society of America Journal*, *60*(1), 13–19.

Spaans, E. J. a, & Baker, J. M. (1995). Examining the use of time domain refiectometry for measuring liquid water content in frozen soil TDR Calibration : Hypothesis. *Water Resources Research*, *31*(12), 2917–2925.

Stähli, M., Jansson, P.-E., & Lundin, L.-C. (1996). Preferential water flow in a frozen soil - a two-domain model approach. *Hydrological Processes*, *10*(10), 1305–1316.

Stähli, M., Jansson, P. E., & Lundin, L. C. (1999). Soil moisture redistribution and infiltration in frozen sandy soils. *Water Resour. Res.*, *35*(1), 95–103.

Stevens Water Monitoring Systems Inc. (2007). The Hydra Probe ® Soil Sensor Users Manual, (July), 1–63.

Suzuki, K. (2013). Estimation of Snowmelt Infiltration into Frozen Ground and Snowmelt Runoff in the Mogot Experimental Watershed in East Siberia. *International Journal of Geosciences*, *4*(10), 1346–1354.

Tangborn, W. (1984). Prediction of glacier derived runoff for hydroelectric development. *Geografiska Annaler. Series A. Physical Geography*, 257–265.

Tao, Y., & Gray, D. (1994). Prediction of snowmelt infiltration into frozen soils. *Numerical Heat Transfer*, *26*(6), 643–665.

Tarboton, D., & Luce, C. (1996). *Utah energy balance snow accumulation and melt model (UEB) (p.63)*. Utah Water Research Laboratory.

U.S. Army Corps of Engineers. (1956). *Snow hydrology - Summary report of the snow investigations, North Pacific Division.*

van der Kamp, G., & Hayashi, M. (2009). Groundwater-wetland ecosystem interaction in the semiarid glaciated plains of North America. *Hydrogeology Journal*, *17*(1), 203–214.

van der Kamp, G., Hayashi, M., & Gallén, D. (2003). Comparing the hydrology of grassed and cultivated catchments in the semi-arid Canadian prairies. *Hydrological Processes*, *17*(3),

559–575.

van Genuchten, M. T. (1980). A Closed-form Equation for Predicting the Hydraulic Conductivity of Unsaturated Soils. *Soil Science Society of America Journal*, *44*(5), 892.

Vincent, L. A., Wang, X. L., Milewska, E. J., Wan, H., Yang, F., & Swail, V. (2012). A second generation of homogenized Canadian monthly surface air temperature for climate trend analysis. *Journal of Geophysical Research Atmospheres*, *117*(17), 1–13.

Viterbo, P., & Betts, A. K. (1999). Impact on ECMWF forecasts of changes to the albedo of the boreal forests in the presence of snow. *Journal of Geophysical Research: Atmospheres*, *104*(D22), 27803–27810.

Watanabe, K., & Flury, M. (2008). Capillary bundle model of hydraulic conductivity for frozen soil. *Water Resources Research*, *44*(12).

Watanabe, K., Kito, T., Dun, S., Wu, J. Q., Greer, R. C., & Flury, M. (2013). Water Infiltration into a Frozen Soil with Simultaneous Melting of the Frozen Layer. *Vadose Zone Journal*, *12*(1).

Wheaton, E. (2011). *What effects do droughts have in Canada? Highlights of the repercussions of a major multi-year drought*. *The 1999-2005 Canadian Prairies Drought: Science, Impacts and Lessons*. University of Manitoba,Winnipeg, The Drought Research Initiative.

Williams, P. J. (1964). Unfrozen water content of frozen soils and soil moisture suction. *Geotechnique*, *14*(3), 231–246.

Williams, P., & Smith, M. (1989). The Frozen Ground, Fundamentals of Geocryology. In *Studies of Polar Research*. Cambridge University Press Cambridge.

Woo, M. K., & Marsh, P. (2005). Snow, frozen soils and permafrost hydrology in Canada, 1999-2002. *Hydrological Processes*, *19*(1), 215–229.

X. Fang and J. W. Pomeroy. (2009). Modelling blowing snow redistribution to prairie wetlands. *Hydrological Processes*, *23*(18), 2557–2569.

X. Fang and J. W. Pomeroy. (2010). Drought impacts on Canadian prairie wetland snow

hydrology. *Hydrological Processes*, *22*(15), 2267–2274.

Zhang, Heginbottom, J. A., Barry, R. ., & J, B. (2003). Distribution of seasonally and perennially frozen ground in the Northern Hemisphere. In *Proceedings of the 8th International Conference on Permafrost* (pp. 1289–1294). AA Balkema Publishers.

Zhao, L., & Gray, D. M. (1999). Estimating snowmelt infiltration into frozen soils. *Hydrological Processes*, *13*(12–13), 1827–1842.

Zhao, L., Gray, D., & Male, D. (1997). Numerical analysis of simultaneous heat and mass transfer during infiltration into frozen ground. *Journal of Hydrology*, *200*, 345–363.

Zhou, J., Pomeroy, J. W., Zhang, W., Cheng, G., Wang, G., & Chen, C. (2013). Simulating cold regions hydrological processes using a modular model in the west of China. *Journal of Hydrology*, *509*, 13–24.

LIST OF APPENDICES

The writings and equations for the model descriptions in Appendix A, Appendix B and Appendix C, are contributed by Dr. Andrew Ireson.

Appendix A: Model for flow processes in unfrozen soil

Flow processes in soils, including infiltration at the upper boundary, are described by Richards' equation. The solution to Richards' equation requires relationships between water content, matric potential and hydraulic conductivity. These are typically described using parametric equations, which might be considered entirely empirical, but some of which have a theoretical basis. The series-parallel conceptual model was put forward by Childs and Collis George, (1950) and further described by Brutsaert, (1968), and is based on the idea that a control volume of soil is analogous to two random arrangements of capillary tubes, aligned in series, and parallel to the direction of flow (i.e. vertical in this case), as illustrated in Figure A-1. The capillary tubes individually transmit water according to Poiseuille's Law (Childs and Collis George, 1950), and flow is also restricted at the interface between the two collections of tubes based on their interconnectivity, which is function of the random arrangement, and can be quantified statistically. On this basis, discrete pore size distributions can be used to generate $\theta(\psi)$ and $K(\psi)$ relationships, as was originally done by Childs and Collis George, (1950). Subsequently, the same conceptual ideas were implemented in a continuous manner, using integration to derive parametric forms for these same curves (Brutsaert, 1968; Fredlund and Xing, 1994). This latter approach is more accurate and more elegant, but in this case, as will be shown in the following sections, the discrete approach makes it simple to experiment with how ice develops within pores and restricts the hydraulic conductivity.

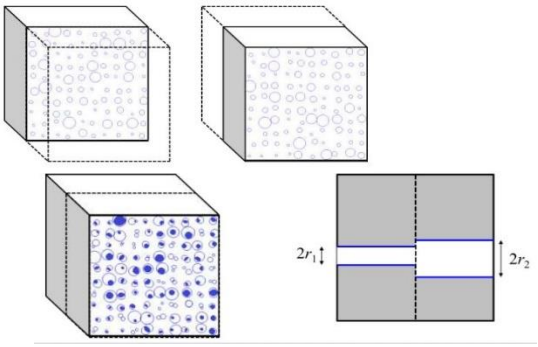

Figure A-1 Series-parallel concept (modified after Childs and Collis George, 1950)

A.1 Characterizing the hydraulic properties

Consider a control volume of soil, V_{CV} (m^3), of depth, Δz (m) and with a regular cross-sectional area, A (m^2). We assume that this control volume contains a discrete number of soil pores of varying radii. All the pores are considered to be parallel in the vertical direction (i.e.z). The pore size distribution may be assumed to be log-normally distributed (Fredlund et al., 1994; Kosugi, 1996) though this is not an essential assumption. We assume that the actual pore size distribution can be adequately approximated by a discrete distribution with m number of pore size bins, each of which has equal bin width in log space. Considering the minimum (r_{min}) and maximum (r_{max}) pore radius, the bin-width (r_{bin}) is given as,

$$r_{bin} = \frac{log10(r_{max}) - log10(r_{max})}{m} \quad \text{(A.1)}$$

The radius r_i (m) representing the midpoint of bin i, where i= 1,2, 3….m, is given by:

$$\log10\,(r_i) = \log 10\,(r_{min}) + (i - {}^{1}/_{2})\, r_{bin} \quad \text{(A.2)}$$

A particular soil is considered to contain N_i pores within the bin centred at radius r_i. The volume V_i of an individual pore of radius r_i is given by $V_i = \pi . r_i^2 . \Delta z$. The volume of all pores within the bin centred at radius r_i is given as,

$$V_i . N_i = \pi . r_i^2 . \Delta z . N_i \quad \text{(A.3)}$$

The soil porosity, n, is given as

$$n = \sum_{i=1}^{m} \frac{V_i . N_i}{V_{CV}} = \sum_{i=1}^{m} \frac{\pi . r_i^2 . \Delta z . N_i}{V_{CV}} = \sum_{i=1}^{m} \frac{\pi . r_i^2 . N_i}{A} \quad \text{(A.4)}$$

This is valid for any imaginable pore size distribution, i.e. any distribution of N_i values, subject to the constraint that the porosity cannot exceed 1. For practical purposes a single porous material is often well described by a log-normal pore size distribution. In this case, the distribution of N_i can be described by three parameters: the porosity, n; the log mean pore radius, lr_m; and the log standard deviation of the pore radii, lr_s. First an unscaled arbitrary distribution U_i is given by the standard lognormal distribution function

$$U_i = \frac{1}{r_i lr_s \sqrt{2\pi}} \exp\left(- \frac{(\ln(\mathrm{r_i}) - \mathrm{lr_m})^2}{2 lr_s^2} \right) \quad \text{(A.5)}$$

which is then scaled to give the correct porosity, to the correct distribution function

$$N_i = R_i \frac{n}{\sum_{i=1}^{m} \pi . r_i^2 . R_i / A} \quad \text{(A.6)}$$

It is noted that any distribution function (parametric or not) may be scaled in this way to match the desired porosity.

A.2 Water retention curve

The pores are assumed to be either water filled or air filled based on capillarity theory. A pore of radius, r (m) is considered to have an air entry pressure, ψ_a (m) given by

$$\psi_a = \frac{2\gamma \cos(\alpha)}{\rho g r} = -\frac{C}{r} \quad \text{(A.7)}$$

Where, γ is the surface tension of the fluid (kg s^{-1}), α is the contact angle of the meniscus (degrees), ρ is the density of fluid (kg m^{-3}), g is acceleration due to gravity (m s^{-2}). Within the control volume the matric potential, ψ (m) is assumed to be uniform within all water filled pores. This can be used to define the threshold pore radius, r_t, given by

$$r_t = -\frac{C}{\psi} \quad \text{(A.8)}$$

such that pores with a radius greater than r_t will be air filled, and pores with a radius less than or equal to r_t will be water filled. Now the volumetric water content ($m^3\ m^{-3}$) at this value of matric potential is obtained from

$$\theta(\psi) = \sum_{i=1}^{M} \pi . r_i^2 . N_i / A \tag{A.9}$$

where M is an index which corresponds to the largest water filled pore, for given value of suction pressure (ψ), i.e the maximum i where $r_i \leq r_t$.

A.3 Hydraulic Conductivity Curve

Hydraulic conductivity, K ($m\ d^{-1}$), is simply the constant of proportionality that relates flow to the hydraulic head gradient and cross-sectional area, i.e.

$$Q = -KA\frac{dh}{dz} \tag{A.10}$$

Poiseuille's Law describes laminar flow, Q, in a circular tube of radius r, (Childs and Collis George, 1950),

$$Q = -\frac{\pi r^4 \rho g}{8\mu}\frac{dh}{dz} \tag{A.11}$$

where ρ is the density of water (taken as $1000\ kg\ m^{-3}$) and μ is the dynamic viscosity of water (taken as $8.9 \times 10^{-4}\ kg\ m^{-1}\ s^{-1}$). By comparison of equation A.10 and A.11, we find that for a single tube the hydraulic conductivity, K_T, is

$$K_T = \frac{\pi r^2}{A}\frac{r^2 \rho g}{8\mu} \tag{A.12}$$

where $\frac{\pi r^2}{A}$ is equivalent to the porosity, n. In complete isolation, this tube has a cross-sectional area πr^2, and a porosity of 1. However, if we consider a control volume that is a cuboid of dimensions $\Delta x, \Delta y, \Delta z$, with a single vertical tube running through it, the cross-sectional area we must consider

is $\Delta x \Delta y$ and the porosity is $\pi r^2/(\Delta x \Delta y)$. Since we here consider flow in the vertical, z, dimension only, we can consider a unit cross-sectional area. Now consider a collection of parallel and non-interacting capillary tubes within this control volume, with a discrete pore size distribution N_i (as described above). The total flow is given by the sum of flow through each tube, and hence the saturated hydraulic conductivity, K_{BS} (here B refers to "bundle" and S to "saturated"), is given by,

$$K_{BS} = \sum_{i=1}^{m} N_i \pi r_i^2 \frac{r_i^2 \rho g}{8\mu} \tag{A.13}$$

The unsaturated hydraulic conductivity is calculated, like the water content, as the sum to the limit of saturation, i.e.

$$K_B(\psi) = \sum_{i=1}^{M} N_i \pi r_i^2 \frac{r_i^2 \rho g}{8\mu} \tag{A.14}$$

The model above could be described as the "parallel model", but we are after the "series-parallel model". The series part comes from having two independent bundles in series which randomly interconnect at their interface, and flow occurs only where two tubes connect. For one of these bundles, the probability of intersecting a pore of radius r_i at any random point on the face of the cross-section is,

$$p_i = \frac{N_i \pi r_i^2}{\Delta x \Delta y} = N_i \pi r_i^2 \tag{A.15}$$

and likewise, the probability of intersecting a pore of radius r_j is

$$p_j = \frac{N_j \pi r_j^2}{\Delta x \Delta y} = N_j \pi r_j^2 \tag{A.16}$$

Now, taking two bundles in series, the probability that a pore of radius r_i in block 1 intersects a pore of radius r_j in block 2 is the product $p_i.p_j$. We can assume then that the relative area of the cross-section where pores of radius r_i intersect pores of radius r_j is equal to this probability, i.e.

$$f_{ij} = p_i . p_j \tag{A.17}$$

We assume that the flow in each combination is limited by the smallest pore radius of the two. If in this demonstration case we have $r_i < r_j$, then the contribution to the bulk flow from pores of radius r_i (again assuming for now that the soil is saturated) is $f_{ij} \frac{r_i^2 \rho g}{8\mu}$. In this simple manner, we can loop through every combination of pore sizes in each block, and find the frequency that that pore combination occurs. The saturated hydraulic conductivity is now given by K_{SPS} (where SP refers "series-parallel" and S to saturated condition),

$$K_{SPS} = \sum_{i=1}^{m} \sum_{j=1}^{m} f_{ij} . \frac{\min(r_i, r_j)^2 \rho g}{8\mu} \tag{A.18}$$

For variably saturated conditions, again pores with a radius $r > r_M$ are air filled and do not conduct water, thus can be excluded from the double sum, such that the unsaturated hydraulic conductivity,

$$K_{SP}(\psi) = \sum_{i=1}^{M} \sum_{j=1}^{M} f_{ij} . \frac{\min(r_i, r_j)^2 \rho g}{8\mu} \tag{A.19}$$

This is the series-parallel model for hydraulic conductivity (Brutsaert, 1968; Childs and Collis George, 1950). This idealized model provides a reasonable model for the relative hydraulic conductivity, that is the shape of the $K(\psi)$ curve, but not it's absolute magnitude, according to Brutsaert (1968). Due to the fact that pores are tortuous (i.e. not straight) and geometrically more complex that tubes, additional resistance to flow is encountered in real soils, affecting the Saturated hydraulic conductivity, i.e. the absolute magnitude of the $K(\psi)$ curve. Childs and Collis-George accounted for this with an empirical matching coefficient, which we also do here, such that our $K(\psi)$ model is finally given by,

$$K(\psi) = K_F \sum_{i=1}^{M} \sum_{j=1}^{M} f_{ij} . \frac{\min(r_i, r_j)^2 \rho g}{8\mu} \tag{A.20}$$

A.4 Implementation within Richards' Equation

The above approach provides us with tabulated $\theta(\psi)$ and $K(\psi)$ relationships, which for a single porous medium comprising a lognormal pore size distribution is defined by four parameters: lr_m, lr_s, n and K_F (all defined above). In practical implementation for unfrozen soils, these curves are calculated once, and then linear interpolation (in linear space for θ and in log space for K) is used to calculate the continuous properties $\theta(\psi)$ and $K(\psi)$. The final properties, the specific storage $C(\psi) = d\theta/d\psi$ is obtained by finite difference approximation based on the tabulated values of θ.

Appendix B: Standard Frozen Soil Infiltration Model (SFSIM)

Various snowmelt infiltration models are available which uses the concept of coupled heat transport and variably saturated water flow using the Richards' equation. These models here are referred to as a Standard Frozen Soil Infiltration Model (SFSIM) for modelling the water flow into the frozen soil pores. Watanabe and Flury, (2008) in particular conceptualized the frozen soil into a series of capillary tubes where the infiltration into the frozen soil pores are based on series-parallel concept (Childs and Collis George, 1950) as described in Appendix A. They accounted relationship between unsaturated hydraulic conductivity and geometry of the soil pores. Dall'Amico et al., (2011) and Hansson et al., (2004) introduced a model for heat and mass transport accounting for water flow due to gravity, pressure gradient and temperature gradient into the frozen soil.

The series-parallel model assumes that the soil comprises pore that are either water filled and transmit flow, or air filled and do not. For frozen soils, we need to consider a third phase – frozen water, or ice, in the pore space. However, soils do not instantly freeze at 0^o C – water within the pores is subject to freezing point depression (Williams and Smith, 1989). This is universally dealt within the literature by adopting the freezing curve (Spaans and Baker, 1996; Watanabe et al., 2013). Here, we simply assume that as a soil is subjected to sub-zero temperatures, the pores freeze progressively, starting from the larger pores which freeze at the highest sub-zero temperatures, through to the smaller pores, which freeze at even lower temperatures. In this, freezing (displacement of unfrozen water with ice) is exactly analogous to drying (displacement of unfrozen water with air) and many workers have made this connection (Spaans and Baker, 1996). The Generalized Clausius-Clapeyron Equation describes the change in pressure with temperature of a substance during phase change. We adopt here the simplified formulation of this equation by Edlefsen and Anderson, (1943) which relates matric potential to temperature for sub-zero conditions as,

$$\psi(T) = \frac{L_f}{g} * \frac{T - T_m}{T_m} \tag{B.1}$$

From capillary theory, we can define the minimum freezing radius, r_F, as

$$r_F = -\frac{C}{\psi(T)} = -\frac{CgT_m}{L_F(T_m - T)} \tag{B.2}$$

where, L_f is the Latent heat of fusion (taken as 3.34×10^5 J kg^{-1}), T_m is the freezing point temperature of pure water (taken as 273.15 K), and T is the temperature of the soil, assumed to be uniform within the control volume (K).

Likewise, the pore is ice filled when $r_a \geq r \geq r_f$, where,

$$r_f = -\frac{C}{\psi} \tag{B.3}$$

The unfrozen and frozen water content are found by summing the relative volumes of water filled and ice filled pores, respectively. The variables Li, Fi and Ai define the proportion of the pores within a certain bin (i), that are liquid, ice and air filled respectively. Each of these variables will take the value of 1 when all pores in that bin are filled with a particular phase, and 0 when all pores in that bin are empty with respect to that phase. Applying this in a simple binary manner either full or empty results in a stepped water retention curve. In order to better approximate a continuous function linear interpolation is used. The variables for each pore radius bin (i) is defined as,

$$Li = \max\left(0, \min\left(1, \frac{log10(r_a) - lr_{i-\frac{1}{2}}}{lr_{i+\frac{1}{2}} - lr_{i-\frac{1}{2}}}\right)\right) \tag{B.4}$$

$$Fi = \max\left(0, \min\left(1, \frac{lr_{i+\frac{1}{2}} - log10(r_f)}{lr_{i+\frac{1}{2}} - lr_{i-\frac{1}{2}}}\right)\right) \tag{B.5}$$

$$\text{Ai} = 1\text{-Li-Fi} \tag{B.6}$$

Where, $lr_{i+\frac{1}{2}}$ and $lr_{i-\frac{1}{2}}$ represent the lower and upper boundaries of the bin r_i. It is noticed that for all the bins the sum of Li + Fi +Ai=1

Now, the unfrozen (θ) and frozen water content (θ_f) (m^3/m^3) is given as,

$$\theta(\psi) = \sum_{i=1}^{m} L_i . \pi . r_i^2 . N_i / A \tag{B.7}$$

$$\theta_f(\psi) = \sum_{i=1}^{m} F_i . \pi . r_i^2 . N_i / A \tag{B.8}$$

Water content (θ) is given by,

$$\theta(\psi) = \sum_{i=1}^{x} \pi . r_i^2 . N_i / A \tag{B.9}$$

where x is an index which corresponds to the largest water filled pore, for given value of suction pressure (ψ), i.e the maximum i where $r_i \leq -\frac{C}{\psi}$

$$\theta(\psi) = \frac{1}{\Delta x \Delta y} \int_{r=0}^{-C/\psi} f(r) \pi r^2 dr = \frac{1}{\Delta x \Delta y} \int_{\psi=-\infty}^{\psi} f(\psi) \pi (-C/\psi)^2 d\psi \tag{B.10}$$

where f(r) and f(ψ) are the distribution functions which can be both discrete and continuous.

In most of the standard infiltration model, during the freezing conditions, the unfrozen water content is dependent on the temperature, which just considers the freezing threshold. The models do not account the wetting threshold, which might result in infiltration into the frozen soil. This is also a reason why it does not allow for infiltration into the air-filled larger pores.

Appendix C: Frozen Soil Infiltration Model (FroSIn)

Frozen Soil Infiltration Model (FroSIn) is an algorithm to simulate snowmelt infiltration into unfrozen air-filled pores of a frozen soil. The soil pores in the unsaturated zone are conceptualized as the capillary tubes as discussed in Appendix A, where the water is subjected to series-parallel flow (Childs and Collis George, 1950; Watanabe and Flury, 2008) in the capillary tube. The model uses a finite difference method to address the problem of water movement into frozen soil and assumes the soil pores to be either frozen, water filled or unfrozen as described in Appendix B.

Figure C-1 shows the conceptual model of freezing soil in FroSIn consisting a discrete pore size distribution. In a particular pore size distribution; there is a pressure, which defines the wetting threshold (W_T) and temperature, which define the freezing threshold (F_T) of the soil. These threshold positions the soil into water, ice and air in the particular control volume.

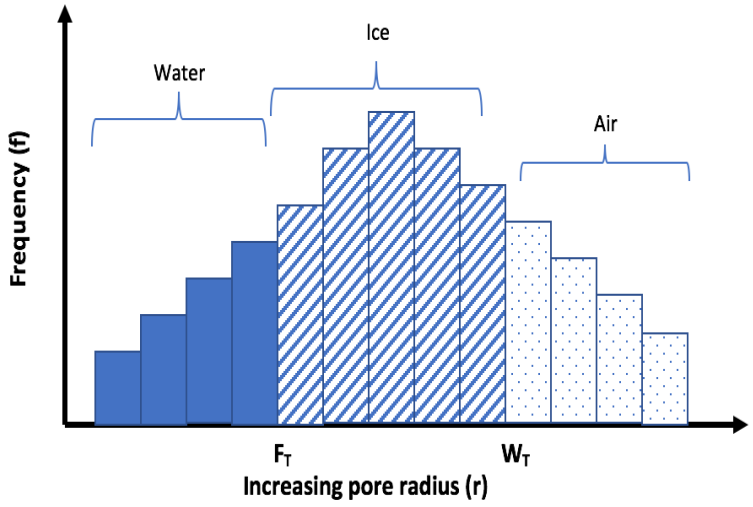

Figure C-1 Conceptual model of freezing soil in FroSIn

The soil water characteristics ($\theta(\psi)$) curve is based on the log normal distribution law (Kosugi, 1994) of the soil pores and the direct relationship between the soil pore radius and the capillary pressure. At a given instant in time, the pressure determines which pores are water filled and which

are air filled. At this instant, the temperature determines the frozen water filled pores and the K(ψ) curve is recalculated based on the frozen pores having zero hydraulic conductivity (K). The hydraulic properties are determined by interpolation from the distribution functions.

Both the models (SFSIM and FroSIn) has the possibility accounting for the upper and lower boundary conditions along with the initial conditions. The model outputs snowmelt runoff and infiltration fluxes along with reporting the overall surface and sub-surface water balance of the study area.

Appendix D: Tables

Table D.1: Data type from St Denis

SN	Type of Data Set	Data Characteristics		Period of Record	Common Application
		Spatial	Temporal		
1	Precipitation	n/a	30 min	Oct 1996 to present	For boundary condition in the model
2	Wind speed	2 m, 10 m	30 min	Oct 1996 to present	For data analysis
3	Surface air temperature	1.5 m, 10 m	30 min	Oct 1996 to present	For data analysis
4	Net radiation	n/a	30 min	Oct 1996 to present	For data analysis
5	Relative humidity	1.5 m, 10 m	30 min	Oct 1996 to present	For data analysis
6	Snow depth	n/a	Daily	Oct 1996 to present	For data analysis
7	Soil temperature	5 cm, 20 cm, 50 cm, 100 cm, 200 cm, 300 cm	1 hour	July 2013 to present	To determine soil freezing curve and driving data for model
8	Soil volumetric water content	5 cm, 20 cm, 50 cm, 100 cm, 200 cm, 300 cm	1 hour	July 2013 to present	To determine soil water characteristic curve
9	Soil matric potential	5 cm, 20 cm, 50 cm, 100 cm, 200 cm, 300 cm	1 hour	July 2013 to present	To determine soil water content/ freezing curve
10	Piezometer data /level logger	Deep/shallow	30 min	Oct, 2013 to present	To determine ground water table level

Table D.2: Data type from Brightwater Creek

SN	Type of Data Set	Data Characteristics		Period of Record	Common Application
		Spatial	Temporal		
1	Precipitation	n/a	30 min	May 2007 to present	For boundary condition in the model
2	Wind Speed	2m, 4m, 8m	30 min	May 2007 to present	For data analysis
3	Surface air temperature	2m, 4m, 8m	30 min	May 2007 to Present	For data analysis
4	Net Radiation	n/a	30 min	May 2007	For data analysis
5	Relative humidity	2m, 4m, 8m	30 min	May 2007	For data analysis
6	Snow depth	n/a	Daily	2007 to present	For data analysis
7	Soil temperature	20 cm, 50 cm,100 cm, 160 cm	30 min	July 2013 to present	To determine soil freezing curve and driving data for model
8	Soil volumetric water content	20 cm, 50 cm,100 cm, 160 cm	30 min	July 2013 to present	To determine soil water characteristic curve
9	Soil matric potential	20 cm, 50 cm,100 cm, 160 cm	30 min	July 2013 to present	To determine soil water content/ freezing curve
10	Piezometer data /level logger	Deep (6 m)	30 min	Oct 2013 to present	To determine ground water table level

Appendix E: Figures

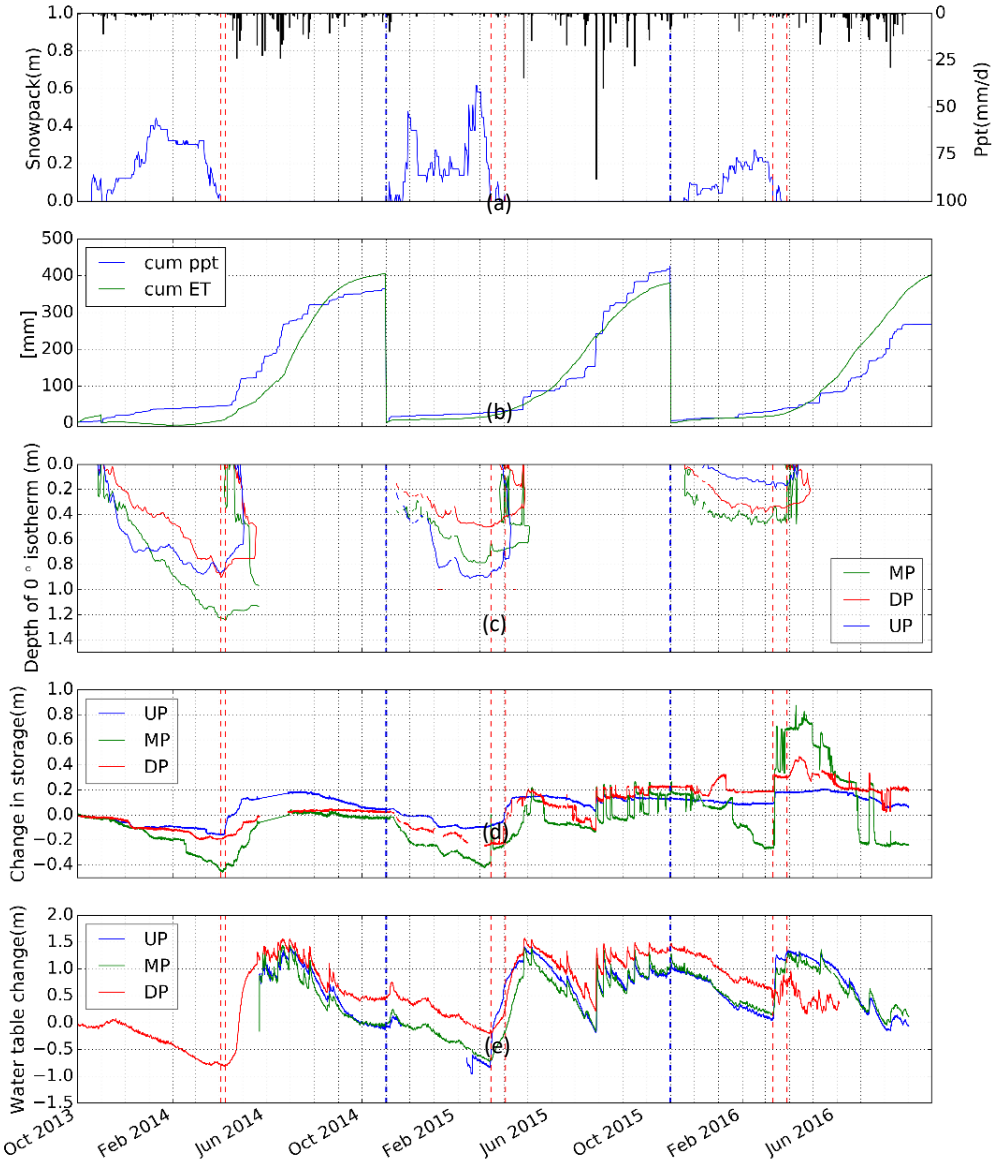

Figure E.1: The figure summaries the fluctuations of the major variables in vadose zone hydrology during the hydrological years of 2014, 2015 and 2016 at St Denis. (a) Precipitation and snowpack depth measurement at the flux tower, (b) Cumulative annual change of evapotranspiration (ET) and precipitation (ppt), (c) Soil freezing depth above groundwater table at Uri transect, (d) Change in unfrozen soil water storage in shallow vadose zone and (e) Change in groundwater table. UP, MP and DP are the Upslope Profile, Midslope Profile and Downslope Profile respectively. The red dotted lines are the start and end of the snowmelt period and the blue dotted line is the start of the hydrological year (November).

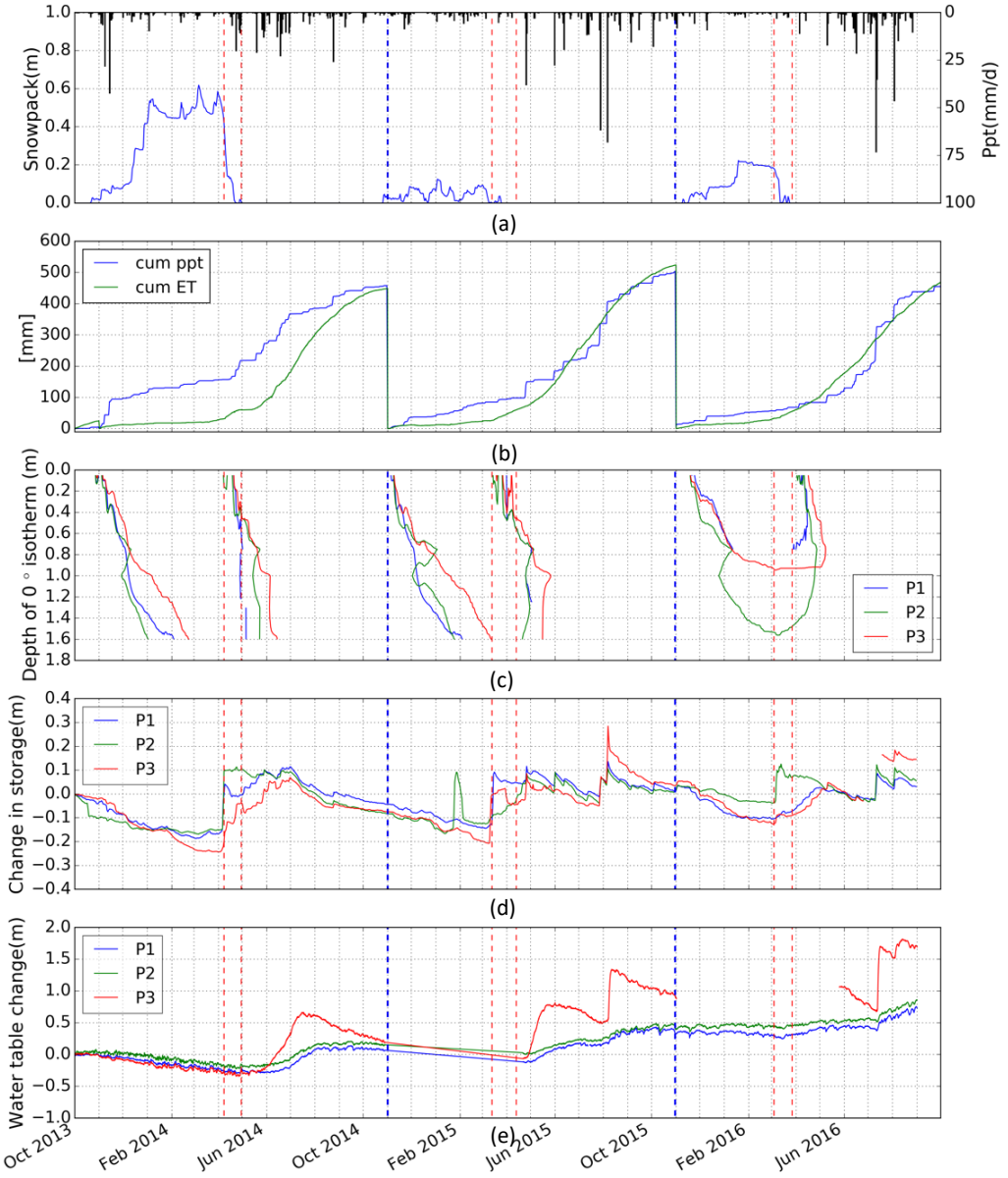

Figure E.2: The figure summaries the fluctuations of the major variables in vadose zone hydrology during the hydrological years of 2014, 2015 and 2016 at Brightwater Creek (BWC). (a) Precipitation and snowpack depth measurement at the flux tower, (b) Cumulative annual change of evapotranspiration (ET) and precipitation (ppt), (c) Soil freezing depth above groundwater table at Uri transect, (d) Change in unfrozen soil water storage in shallow vadose zone and (e) Change in groundwater table. P1, P2 and P3 are the soil profiles along the transect. The red dotted lines are the start and end of the snowmelt period and the blue dotted line is the start of the hydrological year (November).

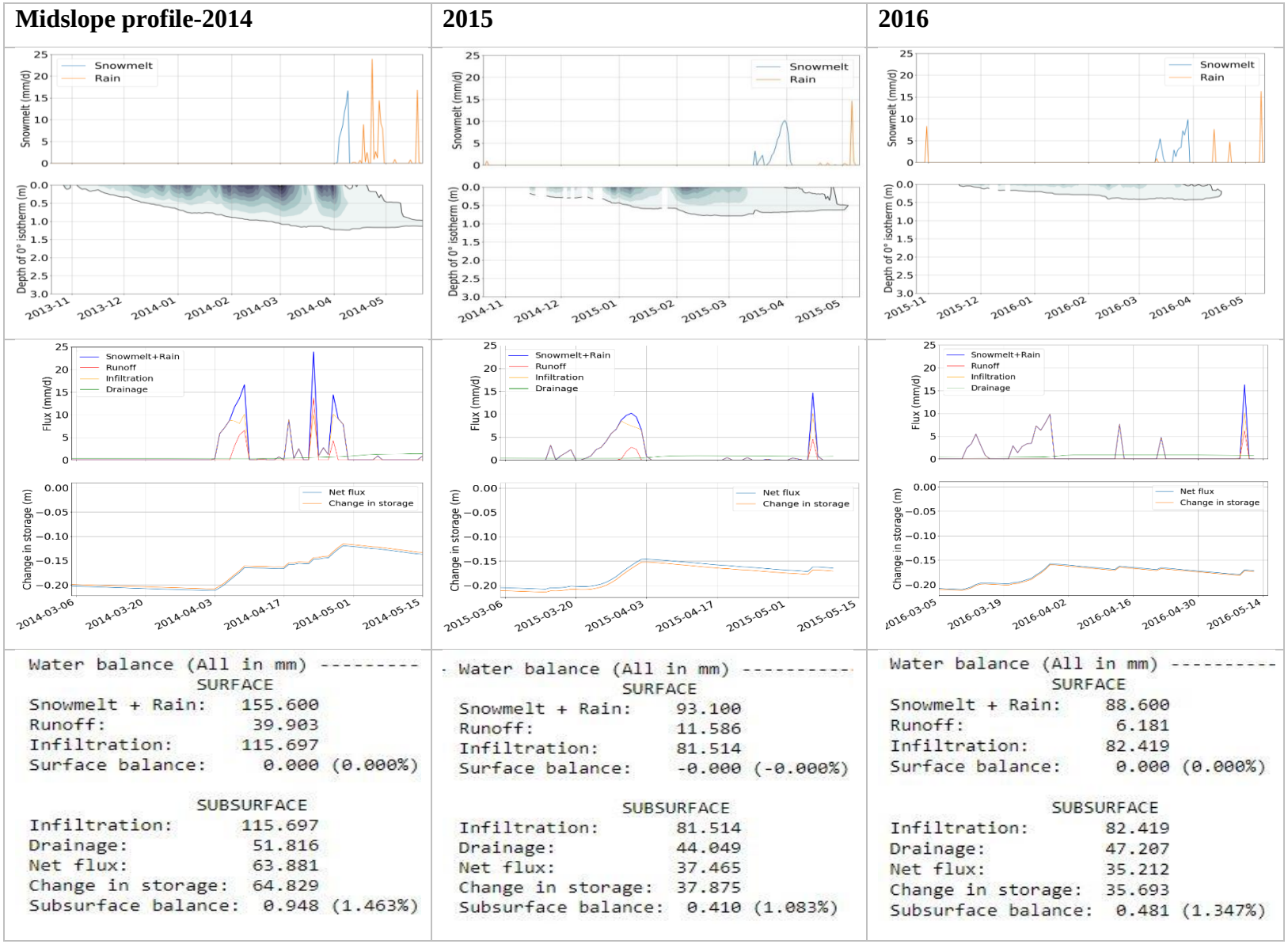

Figure E.3: Driving data and simulated results using FroSIn for midslope profile at St Denis

Downslope profile-2014	2015	2016
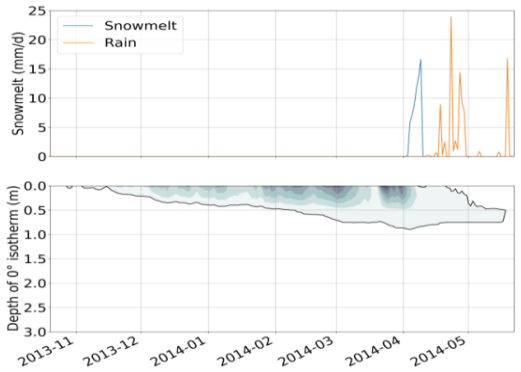	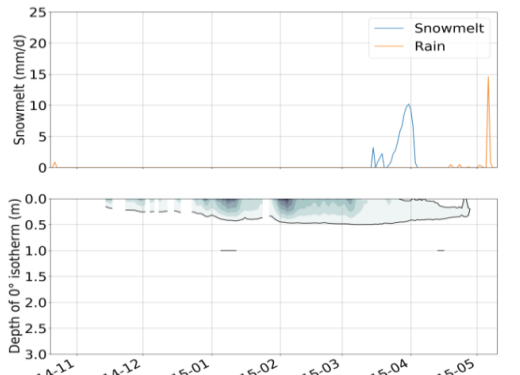	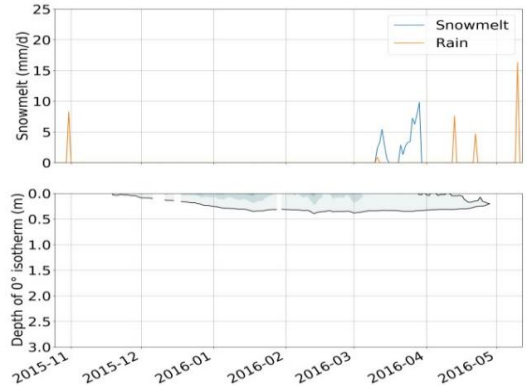
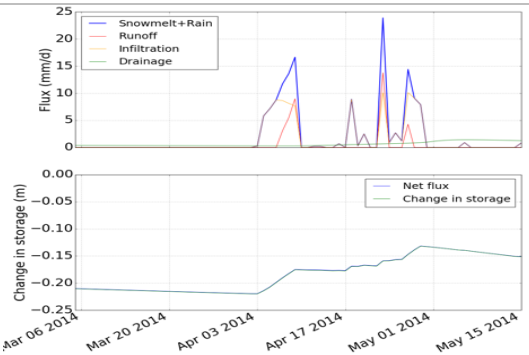	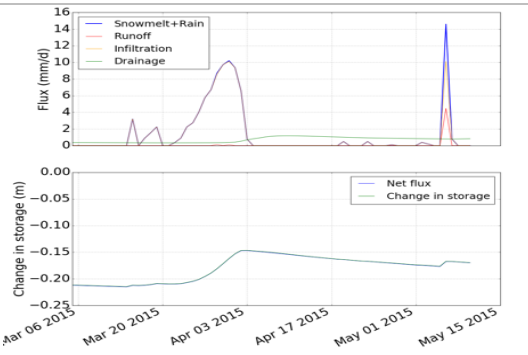	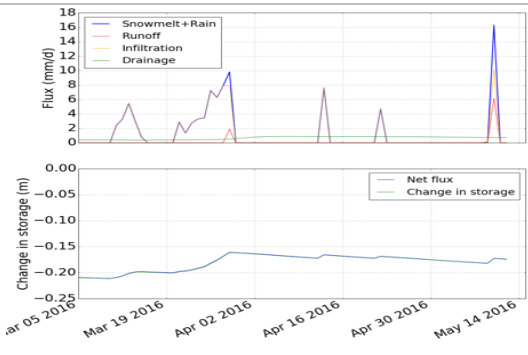
- Water balance (All in mm) ---------- SURFACE Snowmelt + Rain: 155.600 Runoff: 42.266 Infiltration: 113.334 Surface balance: 0.000 (0.000%) SUBSURFACE Infiltration: 113.334 Drainage: 55.107 Net flux: 58.227 Change in storage: 58.950 Subsurface balance: 0.723 (1.227%)	- Water balance (All in mm) ---------- SURFACE Snowmelt + Rain: 93.100 Runoff: 4.671 Infiltration: 88.429 Surface balance: 0.000 (0.000%) SUBSURFACE Infiltration: 88.429 Drainage: 49.177 Net flux: 39.252 Change in storage: 39.621 Subsurface balance: 0.369 (0.932%)	- Water balance (All in mm) ---------- SURFACE Snowmelt + Rain: 88.600 Runoff: 8.082 Infiltration: 80.518 Surface balance: -0.000 (-0.000%) SUBSURFACE Infiltration: 80.518 Drainage: 46.468 Net flux: 34.050 Change in storage: 34.558 Subsurface balance: 0.508 (1.470%)

Figure E.4: Driving data and simulated results using FroSIn for downslope profile at St Denis

P2 profile-2014	2015	2016
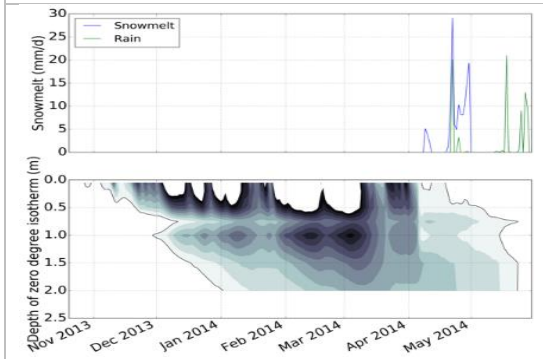	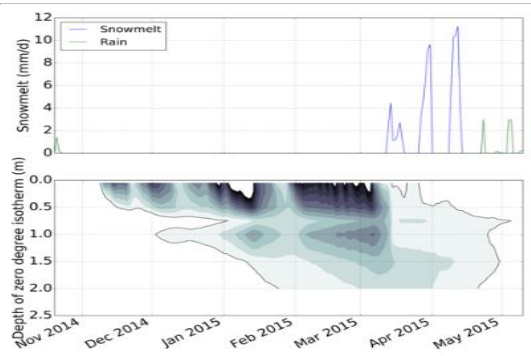	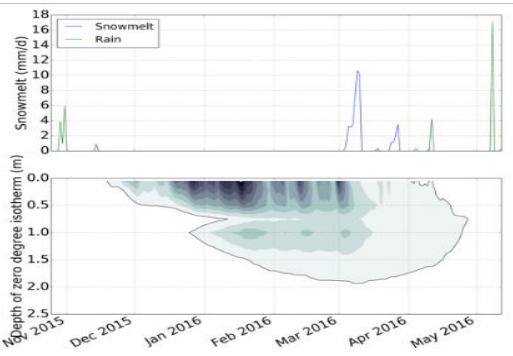
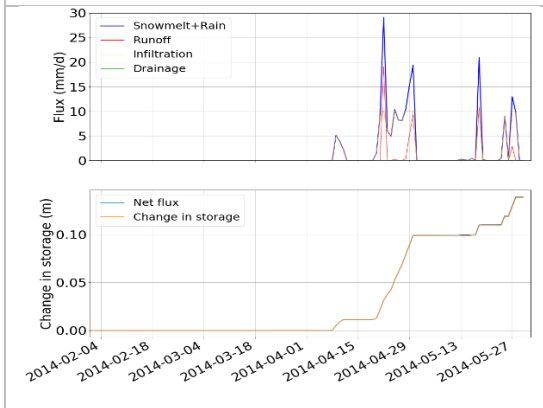	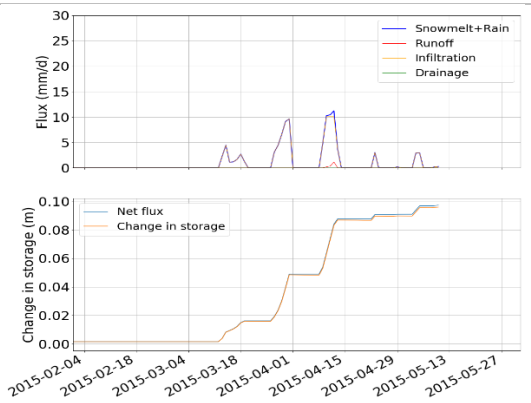	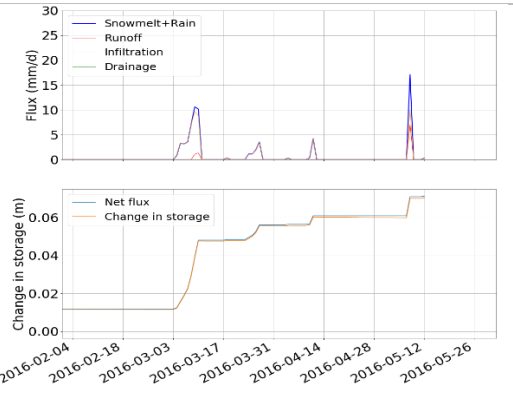
Water balance (All in mm) ---------- SURFACE Snowmelt + Rain: 187.570 Runoff: 47.824 Infiltration: 139.746 Surface balance: 0.000 (0.000%) SUBSURFACE Infiltration: 139.746 Drainage: 0.046 Net flux: 139.700 Change in storage: 138.339 Subsurface balance: -1.361 (-0.984%)	- Water balance (All in mm) ---------- SURFACE Snowmelt + Rain: 97.481 Runoff: 1.676 Infiltration: 95.804 Surface balance: 0.000 (0.000%) SUBSURFACE Infiltration: 95.804 Drainage: 0.012 Net flux: 95.793 Change in storage: 94.527 Subsurface balance: -1.265 (-1.338%)	- Water balance (All in mm) ---------- SURFACE Snowmelt + Rain: 68.919 Runoff: 9.395 Infiltration: 59.524 Surface balance: 0.000 (0.000%) SUBSURFACE Infiltration: 59.524 Drainage: 0.028 Net flux: 59.496 Change in storage: 58.801 Subsurface balance: -0.695 (-1.182%)

Figure E.5: Driving data and simulated results using FroSIn for P2 profile at BWC

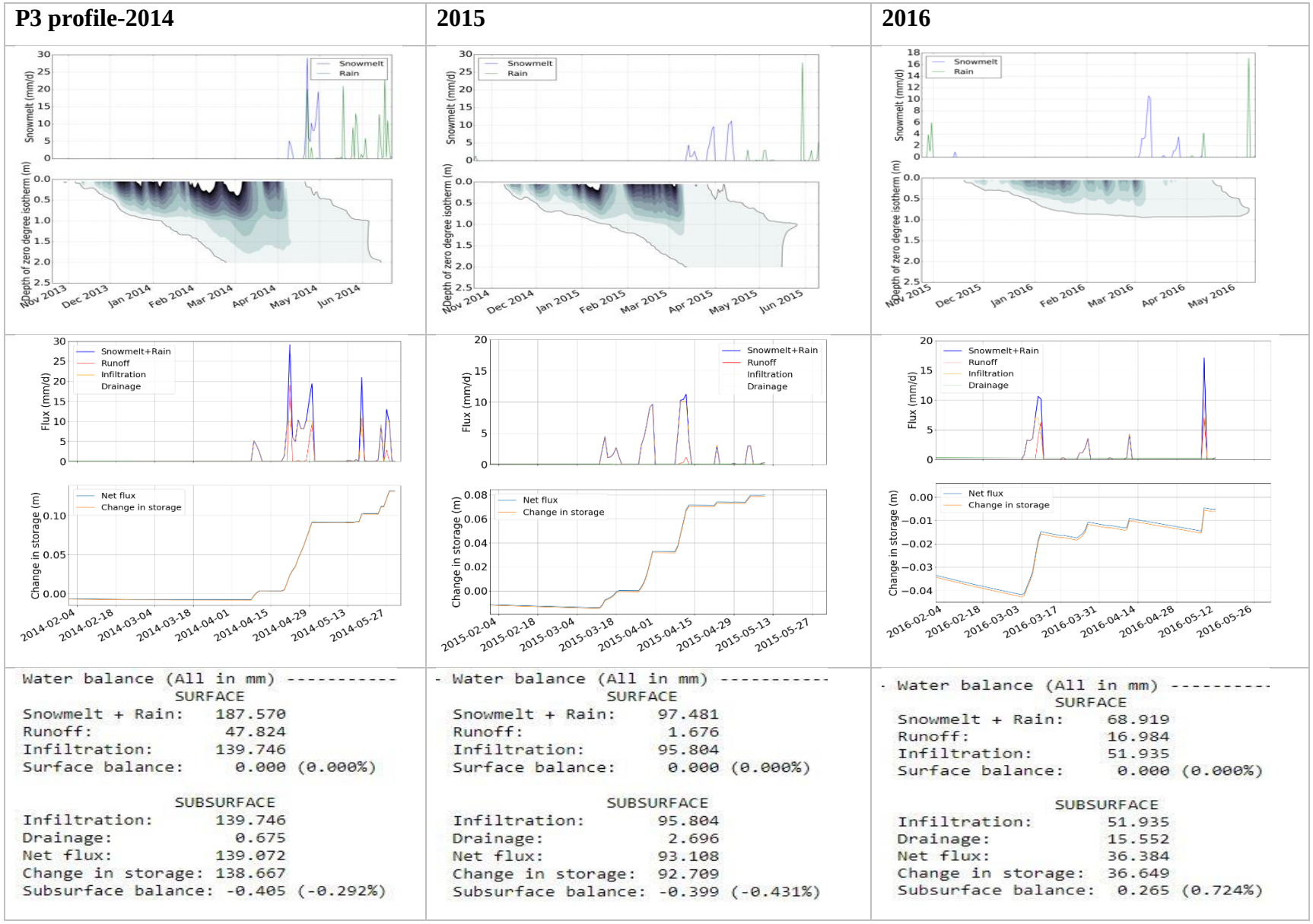

Figure E.6: Driving data and simulated results using FroSIn for P3 profile at BWC